Published in final edited form as:
Q Rev Biophys. 2006 February ; 39(1): 57–116.

Computational biology in the study of cardiac ion channels and cell electrophysiology

Yoram Rudy* and **Jonathan R. Silva**
Cardiac Bioelectricity & Arrhythmia Center and the Department of Biomedical Engineering, Washington University in St. Louis, MO, USA

Abstract

The cardiac cell is a complex biological system where various processes interact to generate electrical excitation (the action potential, AP) and contraction. During AP generation, membrane ion channels interact nonlinearly with dynamically changing ionic concentrations and varying transmembrane voltage, and are subject to regulatory processes. In recent years, a large body of knowledge has accumulated on the molecular structure of cardiac ion channels, their function, and their modification by genetic mutations that are associated with cardiac arrhythmias and sudden death. However, ion channels are typically studied in isolation (in expression systems or isolated membrane patches), away from the physiological environment of the cell where they interact to generate the AP. A major challenge remains the integration of ion-channel properties into the functioning, complex and highly interactive cell system, with the objective to relate molecular-level processes and their modification by disease to whole-cell function and clinical phenotype. In this article we describe how computational biology can be used to achieve such integration. We explain how mathematical (Markov) models of ion-channel kinetics are incorporated into integrated models of cardiac cells to compute the AP. We provide examples of mathematical (computer) simulations of physiological and pathological phenomena, including AP adaptation to changes in heart rate, genetic mutations in *SCN5A* and *HERG* genes that are associated with fatal cardiac arrhythmias, and effects of the CaMKII regulatory pathway and β-adrenergic cascade on the cell electrophysiological function.

1. Prologue

> ‘Things should be made as simple as possible, but not any simpler.’
>
> Albert Einstein

Cardiac muscle can generate propagating electrical impulses (action potentials), a property that classifies it as an excitable tissue similar to skeletal muscle and nerve. At the single-cell level, the electrical action potential (AP) triggers mechanical contraction by inducing a transient rise of intracellular calcium which, in turn, carries the contraction message to the contractile proteins of the cell. This process that couples electrical excitation to mechanical function is termed excitation-contraction coupling. APs are generated by individual cells and are conducted from cell to cell through intercellular gap junctions, forming waves of excitation that activate and synchronize the blood pumping action of the heart. Similar to nerve and skeletal muscle, AP initiation and conduction in cardiac ventricular tissue rely mostly on a single membrane process, namely the flow of sodium ions through sodium-specific ion channels. However, unlike the short-duration APs of skeletal muscle and nerve, the cardiac ventricular AP is characterized by long plateau and repolarization phases that prevent premature arrhythmogenic excitation and provide control of mechanical contraction. In

* Author for correspondence: Dr Y. Rudy, Cardiac Bioelectricity & Arrhythmia Center and the Department of Biomedical Engineering, Washington University in St. Louis, Whitaker Hall, 1 Brookings Dr., St. Louis, MO, 63130-4899, USA. Tel.: (314) 935-8160; Fax: (314) 935-8168; E-mail: rudy@wustl.edu

contrast to the 'single-current mechanism' of AP initiation, the plateau and repolarization phases rely on multiple ionic processes that provide precise control of the AP time-course and duration. In the cell, membrane ion channels interact with dynamically changing ionic concentrations and varying transmembrane voltage, and are subject to various regulatory processes. These interactions are nonlinear, making the single cardiac cell a complex interactive system where a high degree of synthesis and integration occurs. Because our intuition is mostly 'linear', our ability to predict the outcome of these multiple nonlinear processes and to elucidate the underlying mechanisms is very limited. Analysis and synthesis of such complex nonlinear systems require mathematical approaches similar to those applied in other fields of science, notably physics and engineering.

In the last decade major advances were made in our ability to identify genetic mutations and link them to clinical disease phenotypes. A large body of knowledge has accumulated on the molecular structure of cardiac ion channels, their kinetic properties as related to this structure, and the modification of the structure/function by genetic defects that are associated with cardiac arrhythmias (Schwartz *et al*. 1995;Keating & Sanguinetti, 1996;Brugada *et al*. 1998;Priori *et al*. 1999a,b;Clancy & Kass, 2005;Nerbonne & Kass, 2005). Most of these data were obtained in expression systems (e.g. *Xenopus* oocyte, HEK cells) and isolated membrane patches, away from the physiological environment of the cardiac cell where the ion channels interact to generate the AP. A major challenge for the next decade and beyond is the integration of this information into the functioning cardiac cell and tissue in order to relate molecular-level processes and their modification by disease to whole-cell function and cardiac excitation.

In this review, we describe how computational biology approaches can be used to achieve this goal. Specifically, we use mathematical models of cardiac ion channels and cells to link molecular processes that underlie ion-channel function to the electrical activity of the whole cell. Simulations include normal functioning of cardiac cells in response to changes in heart rate (AP rate-adaptation) and altered cellular phenotypes due to ion-channel mutations. Simulating mutations and molecular interactions requires the formulation of single-channel models that represent specific channel states (e.g. open, closed, inactivated) and their interdependencies, and incorporation of these models into the model of the whole cell. This single-channel-based approach constitutes a major departure from the Hodgkin–Huxley scheme developed for the squid axon (Hodgkin & Huxley, 1952) and adopted in many cardiac cell models, where the starting point for computing the AP is macroscopic ionic currents through large ensembles of ion channels. Finally, two recent examples are described, demonstrating how regulatory pathways (the CaMKII pathway and the β-adrenergic cascade) can be incorporated into integrative mathematical models of the whole cell.

2. The Hodgkin–Huxley formalism for computing the action potential

2.1 The axon action potential model

The first computational model of the AP was formulated by Hodgkin and Huxley for the axon. Their circuit model of the cell membrane remains the basis for many modern neuronal and cardiac AP models, so we begin with a brief description of their work. In collaboration with Katz, Hodgkin and Huxley made a fundamental stride in characterizing voltage-dependent conductance changes in excitable cells by applying the voltage-clamp technique to the nerve axon (Hodgkin *et al*. 1952). These experiments suggested that inward movement of Na^+ is responsible for the strong positive deflection observed in intracellular recordings of the membrane potential, V_m, upon depolarization (Hodgkin & Huxley, 1939), while outward flow of K^+ causes repolarization to the resting, hyperpolarized state. Intrigued by these results, Hodgkin and Huxley constructed a mathematical model to test whether these fluxes could generate the AP morphology that they had recorded (Hodgkin & Huxley, 1952).

The framework for this model is described by the circuit diagram in Fig. 1*a*. Represented by the circuit are Na^+, K^+ and leakage currents as well as the capacitive effect of the membrane, which is a result of its hydrophobic nature that makes it impermeable to charged ions. This capacitance provides charge separation so that changes in V_m are due to charge displacement caused by the ionic currents and can be described by the following equation:

$$\frac{dV_m}{dt} = -\frac{1}{C_m} \cdot I_{ion},$$

where C_m is the membrane capacitance ($\mu F/cm^2$) and I_{ion} is the total transmembrane ionic current ($\mu A/cm^2$).

This equation assumes space-clamp conditions and absence of external stimulus. Cell capacitance per unit area of membrane and current densities are typically used to calculate V_m, to normalize for variability in cell size.

For the axon model I_{ion} is the sum of three currents: I_{Na}, which represents the depolarizing sodium current, I_K that accounts for the repolarizing K^+ current and I_L, a leakage current. The driving force for I_{Na} and I_K is generated by transmembrane Na^+ and K^+ concentration gradients, and its magnitude is the difference between V_m and the equilibrium potential, which is computed using the Nernst equation (Plonsey & Barr, 2000). For example, the Na^+ equilibrium potential, E_{Na}, is found with the following Nernst equation:

$$E_{Na} = \frac{R \cdot T}{F} \cdot \ln\left(\frac{[Na^+]_o}{[Na^+]_i}\right),$$

where E_{Na} is the equilibrium potential for Na^+ (mV), R is the gas constant [$J \cdot (kmol \cdot K)^{-1}$], T is the temperature (K), F is Faraday's constant ($C \cdot mol^{-1}$), and $[Na^+]_i$ and $[Na^+]_o$ are the intracellular and extracellular Na^+ concentrations (mM).

Once the driving force is known, the current is calculated using Ohm's law. For example, the equation for I_{Na} is

$$I_{Na} = g_{Na} \cdot (V_m - E_{Na}),$$

where I_{Na} is the transmembrane Na^+ current ($\mu A/cm^2$) and g_{Na} is the Na^+ conductance (mS/cm^2).

Hodgkin and Huxley computed the conductance for each current as a function of the open probability of a series of hypothetical gates and the maximum conductance of the membrane for each ion species. The gates provide the voltage and time dependence of the conductance, and the maximum conductance is simply the conductance when all gates are open. Each gate can go through a first-order voltage-dependent transition from a closed to an open position or from an open to a closed position at a rate that is independent of the positions of all other gates. An ion can pass through the gate only in its open position.

Na^+ current activation (increasing conductance) is accurately modeled by three identical activation gates that move from closed to open positions at depolarized V_m. The open probability of the activation gate is typically assigned the variable m that ranges from 0 (all gates closed) to 1 (all gates open), and the time-dependent change in m is described by the following first-order differential equation:

$$\frac{dm}{dt} = \alpha \cdot (1 - m) - \beta \cdot m,$$

where m and $(1-m)$ are the gate open and closed probabilities, t is time (ms), and α and β are V_m-dependent opening and closing transition rates (ms^{-1}).

Since the transitions are assumed to be independent, the probability that all three gates are open is m^3. At positive V_m all three gates transition rapidly (within milliseconds even at 6–7 °C, Fig. 1*b*) to the open state, providing the depolarizing current necessary for the AP upstroke.

The voltage-clamp recordings (Fig. 1*b*) also show a decrease in current shortly after activation. This process was termed inactivation, and was modeled by using a single first-order inactivation gate with open probability h. At hyperpolarized potentials, h is fully open. When the membrane is depolarized, the inactivation gate closes to cause the monoexponential decrease observed in I_{Na}. Since h operates independently of m, the open probability for the Na^+ gates is $m^3 \cdot h$, and the conductance is

$$g_{Na} = \overline{g_{Na}} \cdot m^3 \cdot h,$$

where $\overline{g_{Na}}$ is the maximum conductance (mS/μF).

The equations that describe I_K are similar, with the driving force dependent on the transmembrane K^+ gradient, which causes the current to be outward. The other significant difference is in the gating; no inactivation is observed and activation is more sigmoidal (Fig. 1*c*). Fitting this behavior requires four identical independent gates, n, and the open probability is n^4:

$$I_K = \overline{g_K} \cdot n^4 \cdot (V_m - E_K),$$

where I_K is current ($\mu A/cm^2$), $\overline{g_K}$ is the maximum K^+ conductance (mS/cm^2), and $E_K = (R \cdot T/F) \cdot \ln([K^+]_o/[K^+]_i)$.

For completeness, there is also a leakage conductance, which was incorporated to account for current not carried by I_{Na} or I_K. This conductance is assumed constant and does not vary with time or V_m. The leakage current, I_L, has the following formulation:

$$I_L = \overline{g_L} \cdot (V_m - E_L),$$

where $\overline{g_L}$ is its constant conductance and E_L its equilibrium potential.

Hodgkin and Huxley were successful in reproducing the axonal AP morphology under a variety of conditions with this surprisingly simple and elegant model. However, the actual mechanism that produced the voltage- and time-dependent gating in the axon still remained undiscovered. Over the following decades, the ion channel was established as the protein structure that provides the pathway for ion flow across the membrane, and detailed genetic, structural and electrophysiological description of ion channels has been published (for review see Hille, 2001).

2.2 Cardiac action potential models

The first cardiac AP models were formulated by McAllister *et al*. (1975), of the Purkinje fiber, and Beeler & Reuter (1977), of the ventricular myocyte. These models relied on the Hodgkin–Huxley formalism to describe the ionic currents, and similar to the Hodgkin–Huxley model

assumed that intracellular ion concentrations ($[Na^+]_i$, $[K^+]_i$) remain constant during the AP. However, in cardiac myocytes, entry of Ca^{2+} through $I_{Ca(L)}$, the L-type calcium channel, causes a dramatic change in its intracellular concentration, mostly by triggering Ca^{2+} release from the sarcoplasmic reticulum (SR) via the calcium-induced calcium-release (CICR) process (Fabiato, 1992). Incorporation of dynamic changes in $[Ca^{2+}]_i$ was necessary to reproduce AP morphology even in the earliest ventricular cell models (e.g. the Beeler–Reuter model) (Beeler & Reuter, 1977).

Changes in $[Na^+]_i$ and $[K^+]_i$ can also influence AP morphology over time if cells are paced at fast rate. The first model to incorporate detailed information regarding dynamic concentration changes of these ions during the AP was the DiFrancesco–Noble model of the Purkinje fiber AP (DiFrancesco & Noble, 1985). Rasmusson *et al*. (1990) developed a similar model for a bullfrog atrial cell. The Luo–Rudy dynamic (LRd) model of the guinea pig ventricular AP formulated these processes for the ventricular myocyte (Luo & Rudy, 1994a) (Fig. 2*a*). These models were founding members in a new class of 'second-generation' models that account for dynamic ion concentration changes. Several such models of the ventricular and atrial AP in different species have been published since that time (Rasmusson *et al*. 1990;Courtemanche *et al*. 1998;Noble *et al*. 1998;Priebe & Beuckelmann, 1998;Nygren *et al*. 1998;Ramirez *et al*. 2000;Rice *et al*. 2000;Puglisi & Bers, 2001;Fox *et al*. 2002;Matsuoka *et al*. 2003;Pandit *et al*. 2003;Bondarenko *et al*. 2004;Hund & Rudy, 2004;Iyer *et al*. 2004;Shannon *et al*. 2004).

Simulation of changes in intracellular ion concentrations requires incorporation of the pumps and exchangers that maintain resting levels (Fig. 2*a*). The primary pump is the Na^+/K^+ ATPase (NaK) that converts energy produced by the metabolic system into potential energy (in the form of transmembrane ion concentration gradients) that is used to generate the AP. Extrusion of Na^+ and accumulation of intracellular K^+ by NaK generates a high $[K^+]_i$ and maintains a low $[Na^+]_i$ relative to the extracellular space. The Na^+/Ca^{2+} exchanger, NCX, uses the sodium gradient created by NaK to extrude Ca^{2+} and together with uptake into the SR, maintain a very low resting intracellular concentration $[Ca^{2+}]_i$. Under certain pathological conditions (e.g. reduced NaK capacity), during continual fast pacing, these gradients can become depleted, because the cumulative amount of ions carried by transmembrane current during repetitive APs surpasses the ability of pumps and exchangers to maintain resting concentrations. These changes can have important physiological consequences. Under pathological conditions of $[Na^+]_i$ overload, for example, depolarization slows, the AP duration (APD) shortens, and the inducibility of arrhythmia increases (Faber & Rudy, 2000).

Recently, there have been reports that the values of intracellular ion concentrations in second-generation AP models that account for dynamic concentration changes do not reach a steady state when paced over a long period of time, but drift until their values leave the physiological range (Guan *et al.* 1997;Yehia *et al.* 1999;Endresen *et al.* 2000;Krogh-Madsen *et al.* 2005). In the LRd model, drift is only observed when ions (usually K^+) that carry the stimulus current are not accounted for. If the stimulus is properly implemented and the ions that it carries are included in computing concentrations, no drift is observed even at fast pacing for long intervals [Fig. 2(*b*)–(*e*)] (Hund *et al*. 2001).

Figure 2 also shows a comparison between two methods solving the equation that describes transmembrane voltage, V_m, in the LRd model. The first 'differential' method, which has traditionally been used, describes changes in V_m as a function of the transmembrane ionic current using the differential equation:

$$\frac{dV_m}{dt} = -\frac{1}{C_m} \cdot I_{ion}.$$

When dynamic intracellular ion concentrations are accounted for, V_m can also be computed directly from the concentrations by integrating the differential equation for voltage (see Varghese & Sell, 1997;Endresen *et al*. 2000;Dokos & Lovell, 2001;Hund *et al*. 2001 for details) to formulate the 'algebraic' method:

$$V_m = \frac{V_{myo}F}{A_{cap}C_m}\left(\sum_X (z_X \cdot [X]_i) + \frac{2 \cdot V_{JSR}}{V_{myo}} \cdot [Ca^{2+}]_{JSR} + \frac{2 \cdot V_{NSR}}{V_{myo}} \cdot [Ca^{2+}]_{NSR} - C_0\right),$$

V_{myo} is the volume of the myoplasm (μL); F is Faraday's constant (C/mol); V_{JSR} and V_{NSR} are volumes of the junctional and network SR compartments; A_{cap} and C_m are the capacitive area (cm^2) and capacitance ($\mu F/cm^2$) of the membrane; $[X]_i$ and z_x are the myoplasmic concentration and valence of each ion; $[Ca^{2+}]_{JSR}$ and $[Ca^{2+}]_{NSR}$ are Ca^{2+} concentrations in JSR and NSR; C_0 is a constant of integration.

The algebraic equation is based on a charge conservation principle and the charge–voltage relationship of a capacitor, $V = q/C$ (where q is the charge, C the capacitance and V the voltage).

The constant C_0 is determined by substituting the initial values of the ion concentrations into the algebraic equation. With this choice, C_0 is consistent with the initial conditions used for simulations using the differential formulation. A comparison between simulations using the differential or algebraic formulation [Fig. 2(*b*)–(*e*)] demonstrates that when C_0 is chosen accordingly, both methods produce identical results (Hund *et al*. 2001;Kurata *et al*. 2005).

3. Ion-channel-based formulation of the action potential

3.1 Ion-channel structure

Ion channels are typically composed of one or more α-subunits that can be modulated by accessory subunits. In heart, the sodium channel is formed by a single α-subunit that has four domains (DI–DIV) (Fig. 3*a*). Each domain is composed of six transmembrane spanning segments (S1–S6) that have been identified based on the hydrophobicity of their amino acids. Differently from the Na^+ channel, cardiac K^+ channels are tetrameric with four identical α-subunits, each with six transmembrane-spanning segments (Fig. 3*b*).

The domains in the Na^+-channel α-subunit and the K^+-channel α-subunits have similar structures that confer voltage dependence and ion selectivity. The S5–S6 linker, or P-loop, enters the membrane as a hairpin to form the pore through which the ion enters or leaves. A stretch of amino acids within the P-loop determines channel selectivity. Voltage-dependent activation is caused by movement of the voltage sensor, S4, which contains positive charges that cause the segment to shift when V_m changes. This shift changes the channel conformation to an open configuration that allows the passage of ions.

One astounding aspect of the Hodgkin–Huxley K^+ channel model is the correspondence between the four hypothetical activation gates, n, and the four α-subunits that form the tetrameric channel. Each subunit contains a voltage sensor, and all four sensors must be in the activated position for the channel to open. Therefore, each activation gate can be thought of as simulating the activation of an individual subunit. Of course, the channel structure and the correspondence between abstract model 'gates' and movement of voltage sensors of the channel protein were completely unknown to Hodgkin and Huxley when they constructed their model.

3.2 Markov models of ion-channel kinetics

As more information about ion-channel gating has been obtained, it has become clear that models with explicit representation of single ion-channel states are required. In the Hodgkin–

Huxley formulation, the gating parameters (e.g. *n*, *m*, *h*) do not represent specific kinetic states of ion channels. It has also become apparent that the Hodgkin–Huxley formulation is not sufficient to describe various aspects of channel behavior. One such aspect is the inactivation of the Na^+ channel, which has a greater probability of occurring when the channel is open (Armstrong & Bezanilla, 1977;Bezanilla & Armstrong, 1977). If this is the case, then inactivation depends on activation and the assumption of independent gating that allows us to multiply m^3 and *h* to compute conductance no longer holds. What we require is a class of models that can accurately represent the dependence of a given transition on the occupancy of different states of the channel. For sodium channel inactivation, the model must account for the dependence of the inactivation transition on the probability that the channel occupies the open state. Markov-type models fit this profile, and are based on the assumption that transitions between channel states depend on the present conformation of the channel, but not on previous behavior. Because the molecular interactions of channels are often state dependent, Markov model transitions typically represent specific channel movements that have been characterized experimentally. This section describes the application of Markov-type models to simulate such interactions.

We begin by describing a simple hypothetical channel with a single open (O) and a single closed (C) state (Fig. 4*a*). The following first-order equations describe the rate of change of occupancy in the closed and open states:

$$\frac{dC}{dt} = -\alpha \cdot C + \beta \cdot O,$$
$$\frac{dO}{dt} = \alpha \cdot C - \beta \cdot O,$$

where O and C are the probabilities that the channel resides in the open or closed state; α and β are voltage dependent transition rates (ms^{-1}) between these states.

In addition to activation, many channels undergo inactivation. A hypothetical four-state model (closed, open, and two inactivated states) with two sets of forward and reverse transition rates is shown in Fig. 4*b*. One set of rates, α and β, describes movement between states where the channel is open (O) or closed (C) (states that are not inactivated), and between the two inactivated states I_O and I_C. In the Markov scheme of Fig. 4*b*, these are horizontal transitions. The second set, γ and δ, describes vertical transitions to and from the inactivated states. Channels are only open when the channel is both activated and not inactivated, in state O. If differential equations are used to compute the occupancy of each state they take the following form:

$$\frac{dC}{dt} = \beta \cdot O + \delta \cdot I_C - (\alpha + \gamma) \cdot C,$$
$$\frac{dO}{dt} = \alpha \cdot C + \delta \cdot I_O - (\beta + \gamma) \cdot O,$$
$$\frac{dI_C}{dt} = \beta \cdot I_O + \gamma \cdot C - (\alpha + \delta) \cdot I_C,$$
$$\frac{dI_O}{dt} = \alpha \cdot I_C + \gamma \cdot O - (\beta + \delta) \cdot I_O,$$

where α, β, γ, and δ are transition rates, as shown in Figure 4*b*.

Because each state represents a channel conformation, calculating the occupancies of these states can provide mechanistic insight into how transitions within the channel itself govern its behavior and participation in the AP. For example, channels that move during depolarization from C to I_C to I_O are not available to conduct current and do not participate in the AP. In

contrast, channels that arrive at I_O through O are available to conduct current while occupying the open state and have an effect on the AP. Thus, the Markov formulation can be used to relate AP morphology and properties to specific kinetic states of ion channels and the transitions between them during the different AP phases.

When using Hodgkin–Huxley type formulations, the occupancy for each state is not explicitly calculated. Instead, these models assume independent gating, an assumption that improves computational efficiency, which was certainly necessary in 1952 when the Hodgkin–Huxley model was published. In the Markov model of Fig. 4*b* the vertical transitions (C to I_C and O to I_O) have identical transition rates (α, β). This implies that channel inactivation can be represented by a single gate. Similarly, the horizontal transition rates between I_C and I_O are identical to the transition rates between C and O, and can be represented by a single gate. Horizontal movement from [C, I_C] to [O, I_O] represents channel activation; we can assign an activation gate *m* to describe these transitions. Similarly, we assign a second gate, *h*, to the inactivation process. Because the rates of inactivation transitions from C or O are identical, inactivation does not depend on the position of the activation gate (i.e. whether it is in the C or O position). The probability that the channel is in C or in O is *h*, and the probability that the channel is in O or in I_O is *m*. Because the gates are independent, the open probability (O) is calculated as their product ($m \cdot h$). This expression is the same as would have been derived for the Hodgkin–Huxley formulation. Thus, under the assumption of independent gating the Markov formalism and the Hodgkin–Huxley formalism are interchangeable.

However, experiments have shown that typically channel activation and inactivation processes are not independent, but coupled. A simple version of activation and inactivation coupling, in a hypothetical channel, is shown in Fig. 4*c*. In this scheme, channel inactivation can only occur from the open state, and channel activation and inactivation do not involve independent transitions (such as the independent movement of several voltage sensors, see example in Fig. 4*d* and related discussion). Therefore, the state-to-state transitions are dependent, the assumption of independent gating is no longer valid, and the Hodgkin–Huxley formalism in terms of gating variables can not be applied; each state must be described individually by a differential equation:

$$\frac{dC}{dt} = \alpha \cdot C - \beta \cdot O,$$

$$\frac{dO}{dt} = \alpha \cdot C + \delta \cdot I - (\beta + \gamma) \cdot O,$$

$$\frac{dI}{dt} = \gamma \cdot O - \delta \cdot I,$$

where α, β, γ, and δ are transition rates, as shown in Fig. 4*c*.

So far, we have only described activation that involves a single transition. However, since most channels are tetrameric and the voltage sensor in each subunit must activate, more than one transition is normally needed to describe activation. A state diagram for a Markov model that represents each of the voltage sensor transitions in a tetrameric channel with identical subunits is shown in Fig. 4*d*. Each closed state represents a permutation of the positions of the voltage sensors. For example, the first closed state is the permutation where all four sensors are in the resting position, the second where one voltage sensor is activated and the other three are resting. The final state, open, is where all four subunits have a voltage sensor in the activated conformation. The transition rates reflect these permutations, e.g. the rate from C_1 to C_2 is $4 \cdot \alpha$, because all of the four voltage sensors are in the resting position and can move independently to the activated position. Analogously, the rate from C_2 to C_1 is β because only a single voltage sensor has yet to return to the resting state. The occupancy of each state can be computed with a differential equation as for the above models.

Since each subunit in Fig. 4*d* activates independently, channel activation can be represented with a gate assigned to each subunit, to form an analogous Hodgkin–Huxley-type model. All subunits in this channel are identical, so they can be represented by identical gates, to which we assign the gating variable *n*. Because the four gates are independent, the open probability of the channel is n^4.

Just as channel activation and inactivation are not typically independent, channel activation itself may also contain dependent transitions. A model containing such dependent transitions has been proposed for *Shaker* K^+ channel activation to account for a delay observed before activation (Zagotta *et al*. 1994a,b). This model represents four subunits with identical activation rates, but supposes that each of those subunits goes through two conformational transitions, R1 and R2, before reaching the activated state, A. A state diagram for one of the four subunits is shown in Fig. 4*e*. As can be seen from the state diagram, no subunit can reach the activated state without first traversing an intermediate state (R_2).

Until recently these two transitions were hypothetical voltage sensor conformations that were needed to account for the macroscopic channel behavior of delayed activation. Silverman and colleagues have published experimental evidence in *Shaker* K^+ channels that arginine residues in the voltage sensor (S4) interact with acidic residues in S2 sequentially (Silverman *et al*. 2003), providing a mechanism for two-stage voltage sensor activation, as suggested by Zagotta *et al*. (1994b) (Fig. 5*a*). These experiments suggest the model shown in Fig. 5*a* (upper panel), which has resting (R_1), intermediate (R_2) and activated (A) positions. The amino acids involved in this interaction are conserved in many K^+ channels, suggesting that this activation mechanism is also likely to be operational in cardiac K^+ channels.

The voltage-sensor activation model can be extended to represent each of the channel's four subunits (Fig. 5*b*), with a final cooperative transition to the open state. The corresponding Markov state diagram is shown in Fig. 5*c*. Each left–right transition represents movement of one voltage sensor from R_1 to its intermediate position R_2; such transitions are slow ($\alpha = 4 \cdot 4\ s^{-1}$ for cardiac slow delayed rectifier, I_{Ks}). Each top-down transition represents movement of a voltage sensor from R_2 to its activated position, A; such transitions are typically fast (for I_{Ks}, $\gamma = 44 \cdot 7\ s^{-1}$). Thus, each closed state corresponds to an experimentally indicated conformation of the channel with a unique combination of voltage-sensor positions (e.g. C_3 has two sensors in R_1 and 2 in R_2; C_7 has two sensors in R_1, one in R2 and one in A; C_{10} has two in R_1 and two in A, etc.). The 15 closed states represent all such possible combinations. When all voltage sensors are activated (C_{15}), a cooperative transition can occur to the open state O. For I_{Ks}, this last transition is voltage independent (Loussouarn *et al*. 2003;Silva & Rudy, 2005).

The Markov models compute occupancy of the channel in its various kinetic states as a function of voltage and time (and possibly other factors such as ligand binding). The channel conducts ions when it occupies its open state (or, in some cases, multiple open states). Therefore, the macroscopic current density through an ensemble of such channels is described by the following equation:

$$I_X = \overline{g_{sc,x}} \cdot n \cdot O \cdot (V_m - E_X),$$

where for an arbitrary channel X, $\overline{g_{sc,x}}$ is the single channel conductance, *n* is the number of channels per unit membrane area, O is the probability that a channel occupies the open state, and $(V_m - E_X)$ is the driving force.

This equation specifically accounts for the fact that current is generated by a population of ion channels that reside in the open state with a probability that depends on time and voltage.

This single-channel based formulation of the current density can be incorporated into a model of the AP. Because in this scheme discrete channel states (i.e. open, closed, inactivated) are represented explicitly, the model can be used to describe not only the macroscopic current during the AP, but also the occupancies and transitions of channel states. This approach provides a mechanistic link between the whole-cell AP and the structure/function of ion channels. An example of such an approach, describing state occupancies and transitions of selected ion channels during the AP at slow and fast pacing, is provided in the next section.

3.3 Role of selected ion channels in rate dependence of the cardiac action potential

Increased heart rate and elevated force of contraction are essential for increasing cardiac output. However, if APD does not shorten at fast rates ventricular relaxation during the diastolic interval (DI) cannot take place, resulting in reduced filling and decreased cardiac function. In response to rate increase, myocytes have the intrinsic ability to adapt, shortening APD to allow a sufficient DI for filling. This rate-dependent adaptation relies on complex interdependence between the ion channels that determine the AP, and on the molecular interactions that determine channel opening, closing and inactivation. By inserting detailed Markov models of the main depolarizing (I_{Na}) (Clancy & Rudy, 1999,2002) and repolarizing [I_{Kr} (Clancy & Rudy, 2001) and I_{Ks} (Silva & Rudy, 2005)] currents into an AP model (Fig. 2*a*), the cellular-level effects can be studied. Because molecular interactions are usually dependent on the conformation of the channel, Markov-type models have been helpful in simulating this behavior (in the LRd model, Hodgkin–Huxley or Markov representations of currents can be used interchangeably).

I_{Na}, the fast inward Na^+ current, does not seem a likely candidate to play a major role in AP changes with rate, primarily because of its very large density that is necessary to ensure AP generation and conduction with a large margin of safety (Shaw & Rudy, 1997b). However, at fast rate channels can accumulate in an inactivated state that has a slow exit rate. This accumulation inhibits a sufficient number of channels to reduce I_{Na}, the maximum V_m and the maximum rate of depolarization, dV_m/dt_{max}. This effect was accounted for in earlier AP models using the Hodgkin–Huxley formalism [Beeler–Reuter (Beeler & Reuter, 1977), LR1 (Luo & Rudy, 1991)] and was studied in detail. However, it was not until recently that specific molecular level interactions have been identified as candidates for this and other regulatory processes of I_{Na}.

In the heart, I_{Na} is generated primarily by channels formed with the α-subunit $Na_v1.5$, which is genetically encoded by *SCN5A* (George *et al*. 1995). Additionally, expression of multiple modulatory β-subunits (β_1 –β_4) is detected. $Na_v1.5$ (Fig. 3*a*) has four homologous domains (DI–DIV), each with six transmembrane-spanning segments (S1–S6) and a pore-forming P-loop between S5 and S6. Positively charged residues in S4 of each domain link channel activation to changes in V_m (Grant, 2001). A conserved phenylalanine residue in the III–IV linker of heart and brain I_{Na} channels has been linked to fast inactivation (Hartmann *et al*. 1994;Moorman *et al*. 1990), and is part of three hydrophobic amino acids [isoleucine-phenylalanine-methionine (IFM)] that have been shown to block the open pore (McPhee *et al*. 1994,1995,1998). Docking sites for this inactivation gate have been identified on the S4–S5 linkers in domains III and IV (Balser, 1999). Recently, the C-terminus has been shown to participate in fast inactivation by interacting with the III–IV linker and stabilizing the inactivated state (Motoike *et al*. 2004).

Each of these processes has been accounted for in the Markov model shown in Fig. 6*a* (Clancy & Rudy, 2002). Since I_{Na} activation is a cooperative process (Chanda *et al*. 2004) (activation of a voltage sensor in one domain influences activation in the other domains), three closed states, each representing a putative channel conformation are used, rather than modeling the activation of voltage sensors in each domain separately. Fast inactivation takes place

preferentially from the open state reflecting its dependence on channel activation (Armstrong & Bezanilla, 1977;Bezanilla & Armstrong, 1977). Inactivation can then be stabilized by a transition from IF to an intermediate inactivated state IM_1, which reflects participation of the C-terminus (Veldkamp *et al*. 2000), and channels that are slowly inactivated reside in IM_2. Finally, closed-state inactivation has been included by movement from C_3 and C_2 into the inactivated tier (IC_3 and IC_2) to correctly simulate channel availability (Clancy & Rudy, 2002).

While I_{Na} participates only in the first few ms of the AP, its rate-dependence is highly dependent on APD and DI. During the initial AP upstroke I_{Na} can generate as much as 300 μA/μF of inward current (Fig. 6*b*). This current is generated by rapid closed to open transitions followed by fast inactivation. Throughout the rest of the AP, channels continue to transition to stable inactivated states IM_1 and IM_2. The number of channels that remain in these states between beats determines channel availability for the subsequent AP. At slow rates, there is practically no accumulation of channels in IM_1 and IM_2 (Fig. 6*b*). Because V_m is depolarized for a higher percentage of time at fast rate, more channels transition to IM_1 and IM_2 with less time to recover. At cycle length (CL) = 300 ms 20% of channels remain in these unavailable states between beats, and I_{Na} magnitude is noticeably reduced (Fig. 6*c*). This reduced depolarizing current results in a lower peak V_m, which affects the activation of other channels that are important determinants of APD, such as I_{Kr}, I_{Ks}, and $I_{Ca(L)}$.

Like I_{Na}, guinea-pig I_{Kr} activation and onset of fast inactivation are relatively rapid. Activation dependence on V_m is also a result of displacement of positive charges in S4. However, instead of four domains in a single α-subunit, I_{Kr} is a tetrameric channel formed by four identical subunits that are genetically encoded by *HERG*. Several different auxiliary β-subunits have been shown to interact with the homomeric *HERG* channel including the MinK-related peptide (MiRP1, aka KCNE2) (Abbott *et al*. 1999) and MinK (aka KCNE1) (Yang *et al*. 1995;Ohyama *et al*. 2001). Voltage-dependent inactivation is caused by conformational changes in the outer mouth of the channel that mechanistically resembles C-type inactivation in *Shaker* (Smith *et al*. 1996). While it is plausible that charges in S4 could determine voltage dependence, mutation of these charges does not affect the amount of gating charge transfer during inactivation (Zhang *et al*. 2004). An alternate possibility is that voltage-dependence is conferred by the P-helix (positions 614–621 of the NH_2 -terminal half of the P-loop) (Zhang *et al*. 2004), however, this hypothesis has not been tested.

As with I_{Na}, I_{Kr} activation is modeled using cooperative transitions (Clancy & Rudy, 2001), and inactivation occurs preferentially from the open state (Fig. 7*a*) (Clancy & Rudy, 2001;Silva & Rudy, 2005). Some inactivation can also occur from the closed state nearest to the open state (C_1) as demonstrated by single-channel recordings (Kiehn *et al*. 1999). During most of the AP, the balance between I_{Kr} activation and inactivation favors inactivation (Fig. 7*b*, *c*), preventing the development of a large current. As V_m repolarizes and reaches levels where significant channel recovery from inactivation occurs, open-state occupancy rises to a maximum and I_{Kr} intensifies, reaching a peak late during the AP (Fig. 7*b*, *c*). Consequently, I_{Kr} participates mostly late during the AP, where it can influence repolarization significantly due to the delicate balance between inward and outward currents at this stage. Because voltage dependence of recovery is much stronger than time dependence during the AP, peak I_{Kr} is similar at slow and fast rates (cf. Fig. 7*b*, *c*), making I_{Kr} secondary to I_{Ks} in underlying rate-dependent adaptation of APD in guinea pig ventricular myocytes.

The primary repolarizing current in guinea pig is I_{Ks}, and it is composed of four KCNQ1 α-subunits as well as a modulatory β-subunit, KCNE1. While the ratio of KCNE1 to KCNQ1 in native channels has been probed using several different methods (Cui *et al*. 1994;Sesti & Goldstein, 1998;Wang *et al*. 1998;Chen *et al*. 2003), a consensus remains elusive. A recent

study (Chen *et al*. 2003) concluded that each I_{Ks} channel contains four KCNQ1 subunits and two KCNE1 subunits and that other subunit stoichiometries are not naturally assembled. Noise variance analysis has shown that KCNE1 increases single-channel I_{Ks} conductance as well as channel expression relative to KCNQ1 alone (Pusch, 1998;Sesti & Goldstein, 1998;Yang & Sigworth, 1998). It also removes inactivation and slows channel activation kinetics (Tristani-Firouzi & Sanguinetti, 1998), creating a significant delay before activation. Biophysical analysis of the delay in *Shaker* channels suggests that two-stage voltage sensor activation, as described in Section 3 · 2 above, is necessary to reproduce the activation kinetics (Zagotta *et al*. 1994b). We used a similar model, where each closed state represents a possible combination of voltage sensor positions (see Fig. 5) to represent I_{Ks} (Fig. 8*a*) (Silva & Rudy, 2005). We added a cooperative, voltage-independent transition before opening, to reproduce steady-state activation measurements (Lu *et al*. 2001). Application of phosphatidylinositol- 4,5-bisphosphate (PIP_2) to excised patches containing I_{Ks} channels strongly affects their open probability, but does not change the voltage-dependent properties of the channel (Loussouarn *et al*. 2003) indicating that PIP_2 interaction is with this voltage-independent transition [observed in *Shaker* K^+ channels as well (Koren *et al*. 1990)]. A second open state, also included in the model, is evident when the channel is probed with rubidium and is responsible for two exponential components of deactivation observed experimentally (Pusch *et al*. 2000). The complete I_{Ks} model is shown in Fig. 8*a* (details can be found in Silva & Rudy, 2005).

Closed states in the model are divided into two zones, zone 2 (green) contains channels where at least one subunit still has to make a first transition to the intermediate state R_2 (see Fig. 5*a*), zone 1 (blue) contains channels with voltage sensors that only need to make more rapid second transitions into the activated state A. As shown in Fig. 8*b*, at the slow rate (CL = 1000 ms) 60% of I_{Ks} channels reside in zone 2 before AP depolarization and must make a slow transition into zone 1 before opening. At this rate, only 40% of channels reside in zone 1 before AP onset. In contrast, at the fast rate (CL = 300 ms) nearly 75% of channels accumulate in zone 1 before AP onset, leading to a rapid rise in current during the AP (Fig. 8*c*). At this rate, there is not sufficient time between beats for channels to transition back to zone 2 before the next AP. Note that there is minimal open-state accumulation, rather, accumulation takes place in zone 1 of closed states that are near the open state. This result, a consequence of two-stage voltage-sensor activation, is confirmed by AP-clamp experiments showing a rapid increase in I_{Ks} at fast rate, but no instantaneous current at AP initiation (Rocchetti *et al.* 2001) that would have been indicative of open-state accumulation. Thus, at fast rate there is a build-up of channels in zone 1 of closed states. These channels can open quickly ‘on demand’ to cause fast I_{Ks} increase towards the repolarization phase of the AP, when the current can effectively shorten the APD. We termed the channels that accumulate in zone 1 ‘available reserve’ (AR). This novel mechanism of APD shortening at fast rate differs from the accepted mechanism which relies on channel accumulation in the open state to generate instantaneous current upon AP depolarization.

3.4 Physiological implications of I_{Ks} subunit interaction

As noted above, KCNE1 interaction with KCNQ1 to form I_{Ks} increases channel conductance and expression, and removes inactivation. It also acts to decrease activation rate and accelerate deactivation. These effects clearly oppose each other; the conductance increase and removal of inactivation augment the current, while the activation/deactivation kinetic changes reduce the current. Moreover, in human myocytes slowing of activation and increased rate of deactivation are much more pronounced than in other species (Virag *et al*. 2001). The co-existence of opposing effects would seem to prohibit I_{Ks} participation in AP repolarization and in determining APD. In particular, fast deactivation prevents channel accumulation in the open state at fast rate, a property that has been considered necessary for participation in rate-adaptation of APD. However, mutations to both KCNQ1 (Wang *et al*. 1996) and KCNE1

(Splawski *et al*. 1997) (LQT1 and LQT5 mutations respectively) can prolong the QT interval and predispose patients to cardiac arrhythmias and sudden death. Adenosine 3′,5′-monophosphate (cAMP)-dependent protein kinase A (PKA) and protein phosphatase 1 (PP1) co-immunoprecipitate with human KCNQ1, implying an I_{Ks} role in APD modulation during β-adrenergic stimulation (Terrenoire *et al*. 2005). Heterogeneity in I_{Ks} channel density, in particular its low density in mid-myocardial cells (M-cells) is responsible for differences in APD across the ventricular wall in many species (Liu & Antzelevitch, 1995;Antzelevitch & Fish, 2001;Antzelevitch & Dumaine, 2002). It has also been suggested that I_{Ks} serves as a repolarization reserve (RR) that can compensate for reductions in I_{Kr} by mutations or drugs (Roden, 2004). These observations suggest that I_{Ks} does play an important role in AP repolarization in human heart.

To explore the KCNQ1–KCNE1 subunit interaction in the context of AP repolarization, we constructed two Markov-type models, the first of the homomeric human KCNQ1 channel and the second of the human heteromeric I_{Ks} channel (KCNQ1 with KCNE1) (Kupershmidt *et al*. 2002). The KCNQ1 model (not shown) has a similar 15 closed-state structure to that of I_{Ks} (Fig. 8*a*) but differs in several significant aspects (Silva & Rudy, 2005). It includes an inactivation process, detected as a hook in the tail current (Tristani-Firouzi & Sanguinetti, 1998); the hook is only observed after a delay, implying multiple open states (five in the model) (Pusch *et al*. 2001). Deactivation is slower and activation transitions are more rapid resulting in more channels residing in closed states near the open state even at slow rates (Silva & Rudy, 2005). Two-stage voltage-sensor activation is still used to model channel opening because of an experimentally observed delay of several ms before KCNQ1 activation (Tristani-Firouzi & Sanguinetti, 1998).

Each model is inserted into the LRd model of the guinea pig ventricular myocyte to create a virtual chimeric myocyte. This environment is interesting because, as discussed above, the guinea pig relies heavily on I_{Ks} for repolarization, while minimizing the role of I_{Kr} during the AP plateau. Such conditions are observed in human ventricular myocytes when I_{Kr} is reduced, and are suitable for testing the ability of I_{Ks} to participate in the RR when I_{Kr} is compromised by mutations or drugs.

Figure 9 shows APs at fast and slow rates, with I_{Ks} [panels (*a*) and (*c*)] and with KCNQ1 [panels (*b*) and (*d*)]. Densities were adjusted to produce similar APDs for both channels, with duration of ~200 ms at CL = 1000 ms. APs with I_{Ks} shorten substantially more at the fast rate (CL = 250 ms) than those with KCNQ1 (Fig. 9*a*, *b*). The KCNQ1 and I_{Ks} currents underlying V_m are plotted below the respective APs. At fast rates, KCNQ1 generates a large instantaneous current at the AP onset (Fig. 9*d*, arrow), which does not increase any further during the AP. The instantaneous current is generated by channel accumulation in the open state between beats. In contrast, at the fast rate little open state accumulation is observed for I_{Ks} (Fig. 9*c*, arrow), but the current rises more rapidly by relying on the fast opening of channels that accumulate in zone 1 to build up an ‘AR’. Minimizing the current at the beginning of the AP conserves current and allows I_{Ks} to peak at the end of the AP, where it is most efficient in causing repolarization.

The difference observed between KCNQ1 and I_{Ks} participation in the AP is a result of different levels of channel accumulation in zone 1. I_{Ks} channels increase zone 1 occupancy by 25% as rate changes from slow to fast (Fig. 9*e*). In contrast, KCNQ1 occupancy in zone 1 remains practically constant (only 4% increase) regardless of rate (Fig. 9*e*). This enhanced capacity to build an AR, a consequence of the kinetic changes conferred by the interaction with KCNE1, results in superior ability of I_{Ks} to cause rate adaptation of APD in comparison to KCNQ1 (steeper adaptation curve in Fig. 9*f*). We conclude that the kinetic changes conferred by

KCNE1 complement its effect of increasing channel conductance by enabling I_{Ks} channels to participate in repolarization late during the AP when they are most effective.

3.5 Mechanism of cardiac action potential rate-adaptation is species dependent

While the mechanisms that regulate APD adaptation to changes in rate are similar across mammalian species, the degree of participation of a given channel varies widely. Moreover, because of differences in channel kinetics and expression levels, AP morphology is also species specific. For example, canine ventricular epicardial APs display a notch during the early plateau phase (Fig. 10*a*, left) that is caused by the transient outward K^+ current, $I_{to,1}$ (Liu *et al*. 1993;Hund & Rudy, 2004). This notch is absent in guinea pig APs (Fig. 10*a*, right), as $I_{to,1}$ is not detected in guinea pig ventricular myocytes.

The presence of $I_{to,1}$ in canine epicardial myocytes indirectly influences, through its effects on other currents, rate-dependent AP changes and APD adaptation. At slow rate, a large $I_{to,1}$ creates a deep notch in V_m (Fig. 10*a*, left) that is greatly reduced or absent at fast rate because of reduced $I_{to,1}$ (a consequence of its slow recovery from inactivation). The reduction in V_m due to the notch at slow rate increases the driving force for $I_{Ca(L)}$ and enhances its voltage-dependent activation during the AP plateau (Fig. 10*b*, left, arrow). The increase of plateau $I_{Ca(L)}$ leads to APD prolongation and formation of the prominent dome that characterizes the canine ventricular epicardial AP (Liu *et al*. 1993). The transient reduction of V_m also inhibits the reverse mode of I_{NaCa} (not shown). In this mode, I_{NaCa} brings Ca^{2+} into the cell and extrudes Na^+ with a 1:3 stoichiometry, generating a net outward (repolarizing) current. Inhibition of this current by the notch contributes to APD prolongation. Finally, the magnitude of I_{Kr} during the AP is determined primarily by the fraction of channels that recover from inactivation (see Fig. 7). At lower V_m, fewer channels activate and inactivate, reducing the number of channels that are available to recover from inactivation during the AP. The resulting reduction of I_{Kr} also contributes to APD prolongation.

Figure 10 provides a comparison of rate-dependent AP changes and APD adaptation in the canine (left panels) and the guinea pig (right panels). Reduced plateau $I_{Ca(L)}$ (Fig. 10*b*, left) is the primary mechanism of canine AP shortening at fast rate (elimination of the $I_{Ca(L)}$ effect in the model reduces adaptation by 71% for a CL range of 8000 ms to 300 ms) (Hund & Rudy, 2004). In contrast, $I_{Ca(L)}$ in the guinea pig shows only minimal dependence on rate (Fig. 10*b*, right). The major determinant of APD adaptation in the guinea pig is I_{Ks}. In this species, I_{Ks} is a relatively large current which is slow to deactivate. At fast rate, slow deactivation results in some I_{Ks} accumulation between beats (Fig. 10*c*, right, arrow) and there is faster increase of current during the AP plateau, resulting in APD shortening. Faster increase of I_{Kr} at fast rate also contributes to APD adaptation in the guinea pig (Fig. 10*d*, right). In the canine, I_{Ks} and I_{Kr} are much smaller than in the guinea pig and I_{Ks} accumulation does not occur between beats due to its faster deactivation (Fig. 10*c*, left). However, as discussed in Section 3.4, I_{Ks} is able to develop an AR of deactivated channels at fast rate, and its role in repolarization is augmented under conditions of β-adrenergic stimulation (Marx *et al*. 2002;Stengl *et al*. 2003;Volders *et al*. 2003). I_{Kr} in the canine decreases at fast rates, an effect that actually opposes APD shortening. The decrease of I_{Kr} is a result of two opposing effects : (1) reduced $I_{to,1}$ acting to increase V_m (reduced notch) and increase I_{Kr}; (2) reduced plateau $I_{Ca(L)}$ acting to decrease V_m and reduce I_{Kr}. The net result is I_{Kr} reduction at fast rate (Fig. 10*d*, left).

The simulations in this section serve to underscore an important property of the cardiac AP. Under most conditions, the AP upstroke is generated by a very large I_{Na} with a large margin of safety (major reduction of I_{Na} is required to affect the upstroke). The dependence on a single, large current is consistent with the requirement that AP generation should be a robust ‘all or none’ process. In contrast, the AP plateau and repolarization phases are controlled by a delicate balance between much smaller inward and outward currents, and by their interplay via the

membrane potential. Such delicate balance between multiple currents provides multiple 'control points' for precise control of APD and its rate dependence. The need to accommodate more APs per unit time when rate increases dictates such 'system design'. Unfortunately, this delicate balance can be easily perturbed by undesired changes in the properties of any of the component currents. Such changes can be caused by genetic mutations of ion-channel proteins, by pathology-induced remodeling, or by drugs. In the next section, we provide examples of simulations that examine the cellular electrophysiological consequences of ion-channel mutations.

4. Simulating ion-channel mutations and their electrophysiological consequences

Abnormal repolarization of the AP provides a substrate for life-threatening cardiac arrhythmias. As stated in the conclusion of the previous section, the dependence of repolarization on a delicate balance between various currents makes it vulnerable to perturbation by disease or drugs. Mutations in genes that encode cardiac ion channels can lead to abnormal channel function ('channelopathy') which perturbs the AP to cause arrhythmias (Keating & Sanguinetti, 1996;Priori *et al*. 1999a,b). Mutation-induced alterations in ion channel function are studied in expression systems (e.g. *Xenopus* oocyte) in isolation from the physiological environment of the cardiac cell where the channels interact to generate the AP. In this section we demonstrate how computational biology can be used to integrate this information into the functioning cardiac cell in order to relate these molecular-level findings to whole-cell function and to the clinical phenotype. We provide examples from the hereditary Long QT syndrome (LQT) that presents clinically as prolongation of the QT interval on the electrocardiogram and the occurrence of life-threatening arrhythmias and sudden cardiac death. Specifically, we simulate LQT type 3 (LQT3) and LQT type 2 (LQT2) that are associated with mutations in *SCN5A* (the gene that encodes I_{Na}) and in *HERG* (I_{Kr}), respectively. We also simulate the Brugada syndrome (Brugada *et al*. 1998) that presents clinically as ST segment elevation in the right precordial leads of the electrocardiogram and is also associated with severe arrhythmias and sudden death. Because mutations affect specific structural elements and kinetic states of the model and their interdependencies, single-channel-based Markov models are required to conduct these simulations. We also show how the molecular structure of an ion channel (I_{Ks}) underlies its ability to compensate for reduced repolarizing current when I_{Kr} is compromised by mutation (LQT2) or drugs ('acquired LQT'), a property that identifies the role of I_{Ks} as repolarization reserve (RR) under pathological conditions.

4.1 Mutations in *SCN5A*, the gene that encodes the cardiac sodium channel

4.1.1 The ΔKPQ mutation and LQT3—ΔKPQ is a mutation in the *SCN5A* gene that encodes I_{Na}. It causes a deletion of three amino acids from a highly conserved region of the III–IV linker, a portion of the I_{Na} channel protein that is involved in fast inactivation (Fig. 11, inset). It was observed experimentally in expression systems that this structural defect leads to two modifications of channel function: (1) faster activation and recovery from inactivation, and (2) transient complete failure of inactivation in some of the channels (Bennett *et al*. 1995;Dumaine *et al*. 1996;Chandra *et al*. 1998;Nuyens *et al*. 2001).

During its excitatory cycle (Fig. 11) an ion channel awaits excitation in a closed configuration (*a*). Upon excitation, it permits the passage of ions through the channel pore (*b*). Based on the 'hinged-lid' model of inactivation (West *et al*. 1992), the open configuration of the channel allows a portion of the protein (in the III–IV linker) to plug the channel pore, a process termed inactivation (*c*). To complete the cycle, the hinged-lid structure leaves the channel pore allowing the channel to close (a process termed recovery) and return to its rest state (*a*), ready for the next excitatory cycle. Because of the structural defect in the inactivation gate, ΔKPQ

mutant channels experience a transient failure of inactivation as shown schematically in (*e*), where the hinged-lid structure fails to plug the channel pore. As stated above, ΔKPQ channels that do inactivate recover from inactivation faster than wild-type (WT) normal channels.

The modifications of channel gating by the ΔKPQ mutation were simulated in the Markov model of I_{Na} shown in Fig. 12*a* (Clancy & Rudy, 1999). The WT channel model includes three closed states (C3, C2, C1), an open state (O) which is the only conducting state of the channel, and fast (IF) and slow (IS) inactivation states. The mutant channel contains two modes of gating, the upper 'background mode' and the lower 'burst mode'. The background mode is similar in structure to the WT model, except for altered voltage dependence of activation, inactivation, and recovery from inactivation that results in faster transitions between these states, reflecting the experimentally observed kinetic changes. The burst mode does not include an inactivation state, simulating the transient failure of inactivation of ΔKPQ channels.

Figure 12(*b*,*c*) compares single-channel gating of WT [panel (*b*)] and ΔKPQ [panel (*c*)] as recorded experimentally (right tracings) or simulated by the model of panel (*a*) (left tracings). In both experiments and simulations, WT channels open and inactivate in response to a depolarizing pulse, showing only a single opening event on each tracing (Fig. 12*b*). ΔKPQ channels in the background mode open and recover from inactivation faster than WT. Because of the strong coupling between states O and IF, faster opening results in an increased population of channels in the IF state. Faster recovery of these channels from IF into the open state increases the probability of channel reopenings after the first opening during a depolarizing pulse. Such secondary openings are clearly evident in the recorded and simulated three top traces of Fig. 12*c*. Most mutant channels (>99%) reside in the background mode. However, there is a small, but finite, probability of channel entry into the burst mode, where channels are 'trapped' because of even smaller probability of return to the background mode. The burst-mode model does not include the inactivation states IF and IS, representing the transient failure of channels to inactivate. In this mode, channels fluctuate between closed and open states and display frequent opening events ('bursting') as seen in the simulated and recorded bottom two traces of Fig. 12*c*.

The observation that ΔKPQ channels reopen and burst at depolarized potentials leads to the hypothesis that together these modes generate a significant late I_{Na} current during the AP plateau and that this current is sufficient to delay AP repolarization and prolong the APD. The prolonged APD is reflected as QT interval prolongation on the ECG, the Long QT syndrome phenotype. To examine this possibility, the Markov models of Fig. 12 were introduced into the LRd ventricular cell model (Fig. 2*a*) paced at various rates (Clancy & Rudy, 1999). Figure 13 shows simulated APs (top) and corresponding macroscopic transmembrane I_{Na} through an ensemble of Na channels for : (I) WT paced at CL of 400 ms; (II) ΔKPQ at the same CL; and (III) ΔKPQ at a slower rate (CL = 600 ms). ΔKPQ experimental data are included for comparison in (IV), showing close resemblance of the measured I_{Na} trace with that simulated in (II). During a WT AP, I_{Na} displays an early large peak ('spike') that generates the AP upstroke; it decays quickly, reflecting the absence of late openings at the single-channel level. In contrast, the additive effects of channel reopenings in the background mode and bursting in the burst mode of ΔKPQ result in a late component of macroscopic current during the AP plateau. Despite its small magnitude (3·0 μA/μF; only 1% of the early peak I_{Na}), this current is sufficient to shift the delicate balance between inward and outward currents in the inward (depolarizing) direction and prolong the APD. In the simulation presented here APD of the mutant cell is markedly prolonged, by 62·3 ms, relative to WT at CL = 400 ms. With slowing of the pacing rate to CL = 600 ms, a secondary depolarization develops during the late plateau phase of the AP. This after-depolarization is classified as early after-depolarization (EAD) because it occurs during the AP, before complete AP repolarization. In the context of arrhythmogenesis, regional delays of the repolarization process by AP prolongation and/or

EADs can create spatial non-uniformities of excitability ('dispersion of repolarization') that provide a substrate for the development of unidirectional block and re-entry. Moreover, under certain conditions EADs can elicit an excitatory response that provides the trigger for arrhythmic activity. Note that in the simulation of Fig. 13, EADs develop at a relatively short CL (600 ms). In the congenital LQT3, arrhythmias occur at slow heart rates (bradycardia), usually during sleep or relaxation (Schwartz *et al*. 1995). The simulation assumes that all (100%) Na channels in the cell are ΔKPQ mutant channels. Typically, affected individuals are heterozygous for the mutation, so that only 50% of channels are ΔKPQ. Repeating the simulation with 50% WT and 50% ΔKPQ Na channels (Fig. 14), slowing the rate to CL of 1200 ms (a typical heart rate of clinical bradycardia) is required for EAD generation.

The late (sustained) component of ΔKPQ I_{Na} arises mostly from bursting channels caught in the burst mode of gating. These channels experience a transient failure of inactivation. A different kinetic mechanism has been suggested by computer simulations to underlie LQT3 associated with the SCN5A I1768V mutation (Clancy *et al*. 2003). For this mutation, I_{Na} mutant channels recover from inactivation at a faster rate than WT and reopen during the repolarization phase of the AP, when the membrane voltage is decreasing (non-equilibrium conditions). The I_{Na} current generated by channel reopenings tilts the balance of currents during repolarization in the depolarizing direction, thus prolonging repolarization and APD, and leading to formation of EADs.

The EAD in Fig. 13 (III) depolarizes from plateau potentials and is therefore termed a plateau EAD. The simulation of Fig. 15 provides insight into the ionic mechanism that underlies depolarization of such EADs (January *et al*. 1988;January & Riddle, 1989;Rosen, 1990;Luo & Rudy, 1994b;Zeng & Rudy, 1995;Viswanathan & Rudy, 2000). APs (Fig. 15*a*) and corresponding $I_{Ca(L)}$ (Fig. 15*b*) are shown for the last paced beat of a train of 40 beats (CL = 500 ms) and for an additional beat that follows a 1500 ms pause (onset of clinical arrhythmias in LQT syndrome often follows a pause). We overlay the pre-pause and post-pause data in Fig. 15 to facilitate comparison. Three EADs are generated during the post-pause AP plateau. Inspection of the $I_{Ca(L)}$ tracing shows that the upstroke of each EAD corresponds to an increase of inward $I_{Ca(L)}$. In contrast, in the pre-pause AP, $I_{Ca(L)}$ decreases monotonically to the baseline and EADs are not generated. If $I_{Ca(L)}$ during the post-pause AP is clamped to follow the monotonic decline that it traces during the pre-pause AP, the EADs are abolished (not shown). These simulations identify $I_{Ca(L)}$ as the depolarizing charge carrier that generates the EAD upstroke. Thus, $I_{Ca(L)}$ provides the primary ionic mechanism of plateau EAD generation. In the different types of the LQT syndrome, mutations in different ion channels lead to APD prolongation. In LQT3 the mutations are in SCN5A, leading to a late I_{Na} current that prolongs the APD, as shown for the ΔKPQ mutation in Fig. 13. The prolonged plateau provides sufficient time at the appropriate potential range for $I_{Ca(L)}$ recovery from inactivation and reactivation. The inward $I_{Ca(L)}$ current generated by reactivation carries a depolarizing charge that depolarizes the membrane to form the EAD. It is important to recognize that in the LQT3 example of Fig. 13, the defective mutant channels do not generate the arrhythmogenic EAD. By prolonging the plateau phase of the AP they provide conditions for $I_{Ca(L)}$ recovery and reactivation, setting the stage for EAD generation by L-type Ca channels that are 'innocent bystanders', completely normal and unaffected by the mutation. This illustrates an important principle regarding the electrophysiological responses of the cell; being a highly interactive nonlinear system, the cellular response to a particular perturbation (e.g. altered I_{Na}) is determined by complex interactions between the various components of the cell. Considering that human intuition is mostly linear, computational biology provides a useful tool for elucidating mechanisms and predicting cellular responses, as demonstrated by the simulations presented here.

4.1.2 SCN5A mutation that underlies a dual phenotype—1795insD is a mutation that involves insertion of an aspartic acid in the C terminus of the cardiac Na channel (Fig. 16*a*). This single mutation causes two distinct clinical syndromes in affected individuals; LQT at slow heart rate and Brugada syndrome at fast heart rate, that can lead to life-threatening cardiac arrhythmias and sudden death (Bezzina *et al*. 1999;Veldkamp *et al*. 2000). LQT is reflected in the ECG as prolongation of the QT interval; Brugada manifests as ST segment elevation in the right precordial leads (Fig. 17). Coexistence of these syndromes in the same individual is seemingly paradoxical because LQT is associated with enhanced I_{Na} (generation of a late component of current, as shown in the previous section), whereas Brugada is associated with reduced I_{Na}. Using computational biology, we attempted to explain how a single Na-channel mutation can cause these two distinct ECG phenotypes.

Similar to the ΔKPQ simulations of the previous section, our starting point is the development of Markov models for WT and 1795insD Na channels (Fig. 16*b*) (Clancy & Rudy, 2002). To account for all experimental observations, two intermediate inactivation states IM1 and IM2 (with slower kinetics than IF) and closed-inactivation states IC2 and IC3 (accounting for channel inactivation directly from the closed states) are included in the model (Veldkamp *et al*. 2000;Wang *et al*. 2000;Wehrens *et al*. 2000;Abriel *et al*. 2001). The mutant channel displays bursting kinetics, represented in the model as a burst mode. Transitions into the burst mode can occur from the closed and open states of the model, but not from the inactivated states. In mutant channels, transitions into IM1 and IM2 are faster than in WT, whereas recovery from these inactivation states is slower, making these states more ‘absorbing’. Similarly, transition out of IC2 and IC3 are also slower than WT, increasing the absorbency of these states. As shown in Fig. 18, the greater absorbency reduces channel availability (leftward shift of the availability curve, middle column) and, importantly, slows significantly its recovery from inactivation (left column). A plot on a logarithmic timescale (left column, insets) reveals that mutant channels may require more than 100 ms to recover from inactivation, a time that is of the order of the AP duration. As a result, there is loss of I_{Na} current that is cumulative between beats at fast rates of pacing (Fig. 19).

To examine how this single mutation can cause the two distinct ECG abnormalities associated with LQT and Brugada, we simulated its effects on the AP of different myocardial cell types from the epicardium (epicardial cells) and from the mid-myocardium (M cells) (Clancy & Rudy, 2002). Epicardial cells, especially from the right ventricular outflow tract (RVOT) are characterized by high levels of I_{to} (the transient outward current) and I_{Ks} expression (Antzelevitch *et al*. 1999;Dumaine *et al*. 1999;Yan & Antzelevitch, 1999). The AP of such cells has a characteristic ‘spike and dome’ morphology (Fig. 20) with an early spike (formed by I_{Na}-supported depolarization) and a plateau-phase dome (formed by $I_{Ca(L)}$-supported depolarization) separated by an early plateau notch (formed by I_{to}-supported repolarization). When mutant RVOT epicardial cells are paced at fast rate of CL = 300 ms (Fig. 21), AP alternates between two morphologies : ‘coved dome’ with a marked and greatly prolonged notch, and ‘loss of dome’ due to premature repolarization from the notch without formation of the dome. These morphology changes occur only in epicardial cells at fast rate; they do not occur at slow rate in any cell type and, importantly, they do not occur in endocardial or M cells even at fast rate. As a result, at fast rate a transmural gradient in transmembrane potential is established during the AP plateau and repolarization phases. As will be shown below, this gradient is reflected in ST segment changes on the ECG.

The mechanism underlying the AP morphology changes of RVOT epicardial cells at fast rate is as follows (Fig. 22) : mutant peak I_{Na} is reduced because of incomplete recovery between beats as a consequence of the high absorbency of inactivation states of mutant channels. On the background of large outward I_{to} and I_{Ks} in these cells, the reduction of I_{Na} tilts the balance of currents in the outward direction, causing premature repolarization before significant

activation of plateau $I_{Ca(L)}$ and loss of the AP dome. On alternate beats, I_{Na} may recover more completely during the prolonged recovery time (diastolic interval) that follows the short 'loss of dome' AP. For such beats I_{Na} may be sufficient to overcome the large I_{to}, $I_{Ca(L)}$ activation does occur and the dome is generated following a prolonged notch ('coved-dome' AP). In M cells I_{to} and I_{Ks} are smaller than in epicardial cells, and in endocardial cells I_{to} is absent. Consequently, the suppressed mutant I_{Na} is capable of maintaining a balance of currents that is sufficiently depolarizing, and loss of the dome or a very prolonged notch do not occur in these cells.

The AP changes described above occur only at fast pacing rates. At slow rates, mutant channels have sufficient recovery time between beats and severe cumulative suppression of I_{Na} does not occur. Consequently, the effect of the mutation on epicardial AP at slow rate is minimal (Fig. 21). In contrast, as shown in Fig. 23, the mutation affects the M-cell AP preferentially at slow rate. During the long diastolic interval, channels recover from the absorbing inactivated states and populate the closed states (see Markov I_{Na} model in Fig. 16*b*), from which they can enter the burst mode. Similar to the ΔKPQ mutation, the burst mode generates a late I_{Na} current during the AP plateau that prolongs the APD (Fig. 24). In M cells, I_{Ks} is smaller than in the other cell types and the late I_{Na} is opposed by a smaller repolarizing current. Therefore, the mutation causes preferential prolongation of M-cell APD at slow rate. In the simulation of Fig. 23, M-cell APD is unaffected at CL = 300 ms; it is prolonged by ~60 ms at CL = 850 ms, and at CL = 1000 ms APD is markedly prolonged and EADs develop.

The longest myocardial APD determines the QT interval on the ECG. Therefore, prolongation of the M-cell APD at slow rate explains the QT interval prolongation and LQT ECG phenotype of patients with the 1795insD mutation at slow rate (Fig. 25). At fast rate, the preferential suppression of RVOT epicardial plateau potentials creates a potential gradient ∇V_m from the epicardial to the M region during the AP plateau (the phase that corresponds to the ST segment of the ECG; Fig. 25). Because ECG potentials are proportional to $-\nabla V_m$, this gradient generates ST segment elevation on the ECG, the Brugada phenotype. The ST-segment elevation is prominent in the right precordial leads because of their proximity to the RVOT, the location of epicardial cells with a large I_{to} that lose the dome or experience a prolonged notch. Figure 26 shows simulated ECG waveforms in a multicellular model that contains the epicardial/M/endocardial heterogeneity (Gima & Rudy, 2002). Incorporation of late I_{Na} prolongs the QT interval and broadens the T wave, as observed clinically in LQT3 patients. Reduction of I_{Na} through increased inactivation generates ST-segment elevation in the computed ECG waveforms with morphological changes that reflect the severity of I_{Na} suppression, in agreement with clinical observations in Brugada patients (Antzelevitch, 2001).

The 1795insD simulations demonstrate an important principle, namely that even a simple mutation (an insertion of a single amino acid) can cause multiple different (and even opposite) phenotypes with different pathological and clinical manifestations. This ability stems from the fact that the mutation interacts with a heterogeneous substrate, in this case the heterogeneous myocardium that contains different cell types with different electrophysiological properties. Through rate-dependent processes, the I_{Na} mutation affects differently epicardial, endocardial, and M cells in a rate-dependent fashion to produce multiple clinical phenotypes. The observation that the phenotypes are determined by complex interactions between the mutant channel and its physiological environment highlights the need for integrative computational models for establishing a mechanistic link between abnormal channel function and its arrhythmogenic consequences.

4.2 Mutations in *HERG*, the gene that encodes I_{Kr} : re-examination of the 'gain of function/ loss of function' concept

Various mutations in HERG, the major subunit of I_{Kr}, underlie type 2 of the congenital long-QT syndrome, LQT2 (Roden & Balser, 1999). Many of these mutations cause trafficking abnormalities that prevent transport of the channel protein to the cell membrane (Zhou *et al*. 1998). The resulting complete absence of I_{Kr} constitutes a total 'loss of function' of this current. The reduction of total repolarizing current due to loss of I_{Kr}, causes AP prolongation which is reflected on the ECG as prolongation of the QT interval (the LQT phenotype). Other mutations do not cause complete loss of I_{Kr} current, but alter the channel kinetic properties. The mechanisms through which such mutations cause AP prolongation are not so obvious and require careful investigation. As with the SCN5A mutations of the previous sections, we use computational biology to study the effects of selected HERG mutations on the AP (Clancy & Rudy, 2001).

Three mutations are selected as examples (Fig. 27). The T474I point mutation in the S2–S3 linker shifts the activation curve to more negative potentials (as determined experimentally, mutant $V_{½}$ is shifted by −27.3 mV relative to WT) (Zhou *et al*. 1998). Such shift causes earlier activation during the AP, a property that constitutes 'gain of function'. However, experiments also show reduction of macroscopic current density (Nakajima *et al*. 1998;Zhou *et al*. 1998). To simulate the negative shift of activation, we alter the voltage dependence of activation transition rates (from C3 to C2 and C1 to O; see Markov model of I_{Kr}, Fig. 7*a*). The observed reduction in macroscopic current is simulated by reducing G_{Kr}, the maximum membrane conductance for I_{Kr}, by 35%.

R56Q is a point mutation in the Per–Arnt–Sim (PAS) domain in the N-terminus of HERG, which in the WT interacts with the channel to reduce its deactivation rate (Chen *et al*. 1999). Mutations in this region appear to alter the interaction of the N-terminus with the channel, thereby accelerating channel deactivation. In the Markov model of I_{Kr}, this effect is simulated by increasing the rate of transition from the open state to the closest closed state (O to C1; the process of deactivation) and into deeper closed states (from C2 to C3). With faster deactivation,the channel resides for a shorter time in its open, conducting state. This constitutes ' loss of channel function ' and results in reduced I_{Kr} current.

The N629D mutation results in two alterations of channel properties : (1) loss of C-type inactivation, and (2) loss of K^+ selectivity (mutant channels can conduct other monovalent cations) (Lees-Miller *et al*. 2000). These changes constitute ' gain of function' because the channel does not inactivate and can rely on Na^+, in addition to K^+, as charge carrier. Based on the ' loss of function/gain of function' classification, a gain of I_{Kr} function is expected to generate a greater repolarizing current and shorten the AP. Yet, this mutation is associated with LQT, a seemingly paradoxical observation. We simulate the changes in I_{Kr} function by eliminating inactivation (O to I transition rate is set to zero) and by permitting Na^+ to be conducted through the channel with relative selectivity P_{Na}/P_K=0.65.

The effect of the above three mutations on the cellular AP are simulated by inserting the mutant I_{Kr} channels into the LRd model cell. A comparison of APs from the mutations and from WT is shown in Fig. 28. I_{Kr} current and occupancies of channel states during the AP are also shown. For WT (left column) upon AP depolarization channels move from C3 to C2 to C1 (see Fig. 27*b* for Markov I_{Kr} model) from which they can open to O or inactivate to I. Channels that open, inactivate rapidly from O to I. The balance between inactivation from the open state (O to I) and recovery from inactivation to the open state (I to O) shifts progressively to favor recovery during AP plateau repolarization. Consequently, a pronounced peak of occupancy in the open state (O) is generated late during the plateau (Fig. 28*f*, arrow) causing I_{Kr} to peak at this time (Fig. 28*b*), when it is most effective in influencing repolarization and APD (at this

phase, a very delicate balance between inward and outward currents determines the AP time-course which is easily modulated) (Clancy & Rudy, 2001).

For the T474I mutant, there is only minor prolongation of APD relative to WT, caused by the G_{Kr} reduction. The kinetic alteration caused by the mutation (negative shift of activation) accelerates activation and influences I_{Kr} early during the AP (Fig. 28*b*), when it has minimal effect on AP repolarization and APD. Note that the late peak of open-state occupancy is preserved in mutant channels (Fig. 28*f*), ensuring that mutant I_{Kr} reaches its peak late in the AP (similar to WT) when it has a strong influence on AP repolarization and APD.

The R56Q mutation causes a large prolongation of APD (at pacing CL of 750 ms, APD is prolonged by 33 ms relative to WT). In contrast to the T474I mutation that alters I_{Kr} early during the AP, R56Q exerts its effect during the late AP plateau and repolarization phase. The mutation accelerates deactivation (transitions from O to C1), which removes the late peak of open-state occupancy (Fig. 28*f*, arrow) and of I_{Kr} (Fig. 28*b*). The resulting reduction of I_{Kr} current late in the AP, when I_{Kr} normally plays a major role in repolarization, causes major prolongation of APD.

As stated earlier, N629D is a ‘ gain of function’ mutation; its effects on the AP of epicardial and M cells are shown in Fig. 29. The mutation-induced alteration of ion selectivity elevates the reversal potential of I_{Kr} to −13 mV, in the range of the AP plateau potentials. Consequently, I_{Kr} reverses direction during the AP plateau and becomes an inward current when the membrane repolarizes below −13 mV. This late depolarizing current (Fig. 29, arrows), carried by Na^+ ions, causes major prolongation of epicardial APD (by 80 ms). In the M cell, on the background of the smaller I_{Ks} in such cells, the inward I_{Kr} current is sufficient to cause the generation of EADs. Interestingly, the mechanism of APD prolongation is a late inward current carried by Na^+ ions. In this aspect, it resembles the mechanism of APD prolongation associated with the SCN5A mutations described in Sections 5.1. and 5.2. above, where a late Na^+ current is carried by the mutant I_{Na} channels.

The HERG simulations in this section demonstrate an important principle: the consequence of a mutation that alters channel kinetics depends on the details of the kinetic change and when during the AP it exerts its effect. In the examples of this section, accelerated activation (T474I) had only minor effect on repolarization because its effect was early during the AP. In contrast, accelerated deactivation (R56Q) had a large effect on APD because it had an effect during the late AP plateau. Moreover, a ‘ gain of function ’ mutation (N629D) in HERG, normally a repolarizing channel, caused APD prolongation. These observations challenge the widely accepted concept that the effect of an ion-channel alteration on the APD can be simply classified in terms of ‘ loss or gain of function’; that is, gain (loss) of a depolarizing channel function causes prolongation (shortening) of APD respectively, and gain (loss) of a repolarizing channel function causes shortening (prolongation) of APD respectively. In general, such classification is too simplistic and, as demonstrated here, could lead to erroneous predictions of effects on the AP and of the resulting cellular electrophysiological phenotype.

4.3 Role of I_{Ks} as 'repolarization reserve'

In Sections 3.3 and 3.4, the role of I_{Ks} in rate-dependent repolarization and APD adaptation was discussed. Mutations in the α-subunit of I_{Ks} lead to type 1 long QT syndrome (LQT1) which is the most common of the LQT types and generates cardiac arrhythmias at high levels of β-adrenergic tone (during exercise or stress) (Duggal *et al.* 1998;Schwarz *et al.* 1977). The effects of reduced I_{Ks} on the AP have been simulated for different cell types (epicardial, M, and endocardial) and at different rates (Viswanathan & Rudy, 2000). A simulation of a mutation that interrupts β-adrenergic regulation of I_{Ks} (KCNQ1-G589D) has predicted APD prolongation and transient after-depolarizations during β-adrenergic stimulation (Saucerman

et al. 2004). This mutation has been linked to LQT syndrome in Finnish patients and associated with exercise induced arrhythmias (Piippo *et al*. 2001;Fodstad *et al*. 2004).

Here, we examine the role played by I_{Ks} when I_{Kr} is reduced. I_{Kr} can be compromised by mutations that cause the congenital LQT2 (Section 4.2) More common is I_{Kr} blockade by drugs, including certain antibiotics and antipsychotic agents, that leads to the acquired form of LQT (Roden, 2004). It has been hypothesized that I_{Ks} can supply a RR current that can compensate for the reduction in I_{Kr} under such conditions (Roden, 2004). This possibility is examined in the simulations of Fig. 30.

Figure 30*a* shows mean I_{Ks} (black) and mean KCNQ1 current (gray) during the first and 40th AP for pacing at CL of 500 ms. Comparison of the two beats shows that I_{Ks} increased by~50% during the period of pacing, while KCNQ1 remained almost unchanged. In the presence of I_{Kr} blockade, the increase of I_{Ks} from beat 1 to beat 40 is even greater, while KCNQ1 shows only a limited change. The ability of I_{Ks} to supply a greater current when I_{Kr} is blockaded results from its build up of an AR in zone 1 of closed states (Sections 3.3 and 3.4). In the presence of I_{Kr} blockade, the AP plateau is maintained at a higher potential and for a longer time. This facilitates transitions of I_{Ks} channels into zone 1 that constitutes the AR. In contrast, KCNQ1 channels accumulate in the open state between beats (Sections 3.3 and 3.4) and open on every beat, preventing significant build up of AR. In this respect, KCNQ1 is a ‘wasteful ’ channel.

It is important to evaluate whether I_{Ks} can provide the RR needed to prevent development of EADs when I_{Kr} is compromised. Many clinical arrhythmias due to reduced I_{Kr} occur following a pause (Kay *et al.* 1983;Viswanathan & Rudy, 1999). A pause protocol in presence of I_{Kr} block is simulated in Fig. 30*b*, with a pause inserted after 40 beats. The post-pause AP with KCNQ1 (gray) develops an EAD as a consequence of insufficient KCNQ1 current during the late AP. In contrast, the AP with I_{Ks} (black) repolarizes normally because I_{Ks} provides current late during the AP plateau, where it can affect repolarization significantly and prevent formation of the EAD.

Thus, I_{Ks} can provide RR and prevent arrhythmogenic EADs when I_{Kr} is compromised by disease or drugs. Its ability to do so results from its kinetic properties that maximize the current late, rather than early, during the AP. These kinetic properties are conferred by the interaction between the molecular subunits of the channel, KCNQ1 and KCNE1.

5. Modeling cell signaling in electrophysiology

Traditionally, cellular models have focused on simulating electrical activity under control conditions, where adrenergic and other cell stimuli are at basal levels. Various regulatory pathways have a strong modulatory effect on cell electrophysiology. This effect can be achieved through direct interaction with ion channel proteins [e.g. β-adrenergic modulation of I_{Ks} (Marx *et al.* 2002)] or indirectly by modifying cellular Ca^{2+} cycling and the Ca^{2+} transient which, in turn, interacts with various electrogenic processes (e.g. Na^{+}–Ca^{2+} exchange) to modulate the AP. The participation of regulatory processes in cell electrophysiology is essential for normal cardiac function. However, such processes can also tilt the delicate electrophysiological balance in the direction of arrhythmogenesis, as observed in LQT1 patients (Priori *et al*. 2003) or in patients with catecholaminergic polymorphic ventricular arrhythmias due to abnormal Ca^{2+} cycling (Lahat *et al*. 2003;Francis *et al*. 2005), where arrhythmias are triggered under high β-adrenergic tone.

The dynamic interactions between regulatory pathways, cellular Ca^{2+} cycling, and cell electrophysiology add a high level of complexity to cell behavior. Without the guidance of mathematical models, it is impossible to predict the cellular responses to modification of any

of the cell components (by disease, drugs or other interventions) or to identify the underlying mechanism with any degree of certainty. In this section we provide examples of models that integrate the effects of cell signaling and regulatory pathways into the electrophysiological behavior of cardiac cells.

5.1 CaMKII regulation of the Ca^{2+} transient

The heart enhances its output in response to elevated cardiovascular demand by increasing its rate which is concurrent with a greater force of contraction. This force-frequency dependence arises even in the absence of β-adrenergic stimulation, as evidenced by the observation that in isolated myocytes fast pacing leads to a greater calcium transient (CaT) amplitude and increased force of contraction (Wang *et al*. 1988). The CaMKII signaling cascade is likely to be involved in this process, because it has been shown to interact with the cell machinery that generates the CaT (Maier & Bers, 2002;Hund & Rudy, 2004,2006;Zhang *et al*. 2005). Specifically, CaMKII substrates include $I_{Ca(L)}$, the ryanodine receptor (RyR), the SR Ca^{2+}-uptake pump (SERCA2a) and phospholamban (PLB) (Le Peuch *et al*. 1979;Wegener *et al*. 1989;Witcher *et al*. 1991;Toyofuku *et al*. 1994;Yuan & Bers, 1994;Odermatt *et al*. 1996;Hagemann *et al*. 2000). CaMKII also phosphorylates neighboring CaMKII subunits (autophosphorylation) (Hanson *et al.* 1994), enabling it to detect Ca^{2+} spike frequency, which links its effects to the rate of pacing and of AP generation (Fig. 31).

The rate-dependent activity of CaMKII and its effects on the above substrates were simulated in a model of the canine ventricular cell (Hund & Rudy, 2004). Model comparison to experiment at different rates (Fig. 32*a*) shows accurate reproduction of the increase in CaT at fast rates (a ‘ positive force-frequency ’ relationship) and more rapid rate of relaxation (enhanced lusitropy). The magnitude of the simulated transient at various rates is compared to experiment (Sipido *et al*. 2000) and shows close correlation (Fig. 32*b*). Underlying the increase in CaT magnitude at faster rates is increased CaMKII activity that enhances SR Ca^{2+} uptake by PLB phosphorylation (Fig. 32*d*), resulting in increased Ca^{2+} loading. CaMKII also increases peak $I_{Ca(L)}$, the trigger for SR release, and enhances Ca^{2+} release via RyR. The result is an increased excitation-contraction coupling (ECC) gain at fast rate (Fig. 32*c*) and a greater CaT. When CaMKII is inhibited in the model, the rate dependence of CaT becomes negative (‘negative force-frequency’) for pacing rates >1 Hz (Fig. 32*b*), because increased ECC gain (Fig. 32*c*) mediated by CaMKII, no longer occurs.

This result implies that existence of the positive force-frequency relationship is dependent on the CaMKII signaling cascade, and enforces the notion that cell signaling plays an integral role in cell excitation and contraction.

5.2 The β-adrenergic signaling cascade

β-adrenergic stimulation directly increases the force of contraction in isolated ventricular myocytes by increasing Ca^{2+} influx through $I_{Ca(L)}$, which results in elevated $[Ca^{2+}]_i$ that signals stronger contraction. This increase in a depolarizing current can also lead to prolonged APs that are susceptible to arrythmogenic EADs (Priori & Corr, 1990;Zeng & Rudy, 1995). One way in which the myocyte stabilizes the AP to counter EAD formation is increasing repolarizing current, primarily I_{Ks}, in response to β-adrenergic stimulus (Walsh & Kass, 1988). However, if I_{Ks} availability were reduced by mutation (LQT1), or if it were unable to respond to β-adrenergic stimulation, this important anti-arrhythmic mechanism (termed ‘RR’) would be compromised and cells would be more susceptible to EAD generation and triggered activity. In support of this hypothesis, patients with I_{Ks} mutations and the LQT1 syndrome are prone to arrhythmias and sudden cardiac death in situations where β-adrenergic tone is elevated (Priori *et al*. 2003).

The interaction between β-adrenergic stimulation and I_{Ks} was recently shown to involve association of cAMP-dependent PKA and PP1 with the C-terminal domain of KCNQ1 (the α-subunit of I_{Ks}) (Marx *et al*. 2002). This finding shows that the β-adrenergic signaling cascade is actually a part of the I_{Ks} channel complex, directly participating in the generation of the AP. Additional experiments with accompanying simulations have shown that this interaction enhances I_{Ks} participation in the AP by increasing the rate of I_{Ks} activation and slowing the rate of deactivation, resulting in I_{Ks} accumulation and more open channels throughout the course of the AP (Terrenoire *et al*. 2005).

The effects described above reflect the steady-state consequences of β-adrenergic stimulation, however the time-dependence of substrate phosphorylation may also affect the cellular phenotype. A β-adrenergic model that accounts for time-dependence of substrate phosphorylation (for timescales that are faster than 10 min and slower than 0.1 s) has been formulated based on data primarily from the rat (Saucerman *et al*. 2003) (schematic shown in Fig. 33*a*). This model simulates agonist stimulation of the β_1-adrenergic receptor (β_1AR) (Post *et al*. 1995) and subsequent activation of the stimulatory G protein subunit (G_s) (Brandt & Ross, 1986;Frace *et al*. 1993), which increases adenylyl cyclase (AC) activity (Dessauer *et al*. 1997). In the model, the β_1AR can be inhibited by β-adrenergic receptor kinase (βARK) (Freedman *et al*. 1995) and by the catalytic subunit of PKA (Fishman *et al*. 1991;Freedman *et al*. 1995). Dissociation of the PKA catalytic subunit from the holoenzyme (Smith *et al*. 1981), which consists of two regulatory and two catalytic subunits, occurs when cAMP (synthesized by AC) binds to the regulatory subunits (Beavo *et al*. 1974;Hofmann *et al*. 1975). The concentration of free cAMP is determined by the rate of synthesis by AC (Dessauer *et al*. 1997), degradation by phosphodiesterase (Reeves *et al*. 1987), and by sequestration due to its binding to the PKA regulatory subunits (Beavo *et al*. 1974;Hofmann *et al*. 1975). Two types of PKA have been identified in myocytes and were included in the model: type I, which is predominant in rat ventricular myocytes and diffuses through the cytosol (Corbin *et al*. 1977;Taylor *et al*. 1990), and type II, which is typically anchored to the membrane by an A kinase-anchoring protein (AKAP) (Bers, 2001). Both types I and II PKA catalytic subunits can be inhibited by the heat-stable protein kinase inhibitor (PKI) (Walsh *et al*. 1990;Johnson *et al*. 2001). PKA type I phosphorylation targets include PLB (inhibitory effect) (Gibson & Taylor, 1997) and protein phosphatase inhibitor-1 (I1) (stimulatory effect) (Cohen *et al*. 1977), while PKA type II is responsible for $I_{Ca(L)}$ channel phosphorylation (increased current) (Bers, 2001). PLB inhibits uptake of Ca^{2+} into the SR by SERCA2a, therefore inhibiting PLB activity via PKA phosphorylation results in increased uptake. Stimulation of I1, which is itself inhibited by protein phosphatase-2A (PP2A) (Takai *et al*. 2000), has similar consequences (increased Ca^{2+} uptake by SERCA2a) because it inhibits a PLB agonist, protein phosphatase-1 (PP1) (Takai *et al*. 2000). PP1 and PP2A can also be co-localized to the membrane where they serve as $I_{Ca(L)}$ inhibitors (Bers, 2001).

To study the cellular level electrophysiological effects of the β-adrenergic signaling cascade, this model was expanded to include PKA phosphorylation of the L-type calcium channel, PLB, I1, RyR, troponin I (Saucerman & McCulloch, 2004) and KCNQ1 (Saucerman *et al*. 2004), and was incorporated into a model of the rabbit ventricular AP (Puglisi & Bers, 2001). Since the model was formulated to reproduce data from the rat, protein expression levels of the β_1AR, PDE, PKA and PLB were adjusted to reproduce cAMP and PKA dependence on time and isoproterenol in the rabbit (Saucerman *et al*. 2004).

Using this model to simulate control conditions in normal cells, β-adrenergic stimulation resulted in AP shortening (Saucerman *et al*. 2004). However, in the presence of a simulated KCNQ1-G589D mutation, which prevents PKA-mediated I_{Ks} increase (Kass & Moss, 2003), APD prolonged significantly. Incorporation of the mutant cell model into a transmural rabbit ventricular tissue model that included endocardial, mid-myocardial and epicardial cell types,

resulted in β-adrenergic-mediated repolarization abnormalities and APD prolongation that was most significant in the endocardial layer (Fig. 33*b, c*). Since APD prolongation was spatially nonuniform in the tissue, it resulted in increased transmural dispersion of repolarization (TDR), a substrate that is prone to the development of re-entrant arrhythmias (Verrier & Antzelevitch, 2004) (Fig. 33*d*). These results indicate that interruption of β-adrenergic effects on I_{Ks} is likely to generate arrhythmic behavior via repolarization abnormalities and increased spatial dispersion of repolarization.

The CaMKII and β-adrenergic simulations presented above underscore the importance of accounting for cell signaling effects in models of cardiac cell electrophysiology and calcium cycling. These models are first examples of this integrated modeling approach, and reflect our current (but still evolving) understanding of the signaling pathways. As experiments provide better characterization of substrates and help resolve existing controversies, these models will have to be revisited and refined.

6. Epilogue

‘The earth is like a single cell. ’ Lewis Thomas, *The Lives of the Cell*

Mechanistic understanding of the cardiac excitatory process is a prerequisite for correct diagnosis and effective treatment of cardiac arrhythmias. Such understanding requires integration of processes at various levels, from the ion channel, to the whole cell, to the multicellular tissue, to the heart as a whole organ. Traditionally, the reductionist approach has been applied to cardiac research, collecting data from isolated building blocks of the highly integrated cardiac system. Such data are usually acquired under conditions that do not mimic the physiological (or pathophysiological) environment. In this review we describe and provide examples of the use of computational biology (mathematical modeling) in the integration of individual components into the physiologically functioning system of the cardiac cell. As demonstrated here, even the single cell is a highly complex, nonlinear and interactive system. In this system, ion channels interact with a dynamic ionic environment, with the membrane voltage, and with a variety of regulatory molecules to generate and modulate the cardiac AP; the outcome of these interactions usually defies intuition.

This article focuses on integration from the molecular properties of ion channels to the whole-cell electrophysiological function, thus defining the single cardiac cell as the complex system of interest [simulations of the interactions between ion channels and the multicellular tissue during AP propagation were described in a recent review article (Kleber & Rudy, 2004)]. The simulations presented here demonstrate that the role of ion channels in shaping and controlling the cardiac AP is defined by their molecular properties and transitions between kinetic states during the AP time-course. Similarly, the effect of an ion-channel mutation depends on the mutation-induced changes in channel kinetics and, in particular, when during the AP the mutation exerts its effect. Thus, the ‘ gain of function/loss of function ’ rule is not always sufficient to predict the effect of a given mutation on the cardiac AP. The fact that cardiac cells are heterogeneous adds another level of complexity because, as demonstrated by the dual phenotype simulations of the SCN5A 1795insD mutation, the electrophysiological consequences of ion-channel abnormality depend on the ionic profile of the cell. This profile is not only heterogeneous but also dynamic, as ion-channel expression levels change due to remodeling processes induced by pathology and aging. At a higher level of complexity yet, these processes are modulated by interactions with regulatory pathways and the calcium subsystem of the cell.

Computational biology is a powerful approach that can help identify and elucidate mechanistic interactions between various components of the cell and predict their effect on the whole-cell behavior. Given the explosion of genetic and molecular data, we believe that this approach will

continue to evolve and provide a framework for interpretation and integration of experimental information not only in the cardiac system, but in other systems as well.

Acknowledgements

We dedicate this paper to the memory of Professor Silvio Weidmann who passed away on 11 July 2005 in Bern, Switzerland. Professor Weidmann was the first to record a cardiac AP and to show that cardiac cells communicate electrically through conductive pathways (gap junctions). The field of cardiac electrophysiology would not have been where it is today without his pioneering ideas, insights, and ingenious experiments. We thank members of the 'Rudy lab' : Keith Decker, Greg Faber, Leonid Livshitz and Tom O'Hara for reading the manuscript and providing comments. A special thank you goes to Jennifer Godwin-Wyer for her expert help with the preparation of the manuscript and figures. We are very grateful for the continued support by the NIH – National Heart, Lung and Blood Institute through grant R01-HL49054 and MERIT award R37-HL33343 (to Y. Rudy) and fellowship F31-HL68318 (to J. Silva); Yoram Rudy is the Fred Saigh Distinguished Professor at Washington University in St. Louis.

References

Abbott GW, Sesti F, Splawski I, Buck ME, Lehmann MH, Timothy KW, Keating MT, Goldstein SA. MiRP1 forms IKr potassium channels with HERG and is associated with cardiac arrhythmia. Cell 1999;97:175–187. [PubMed: 10219239]

Abriel H, Cabo C, Wehrens XH, Rivolta I, Motoike HK, Memmi M, Napolitano C, Priori SG, Kass RS. Novel arrhythmogenic mechanism revealed by a long-QT syndrome mutation in the cardiac Na($^{+}$) channel. Circulation Research 2001;88:740–745. [PubMed: 11304498]

Antzelevitch C. The Brugada syndrome: ionic basis and arrhythmia mechanisms. Journal of Cardiovascular Electrophysiology 2001;12:268–272. [PubMed: 11232628]

Antzelevitch, C.; Dumaine, R. Electrical heterogeneity in the heart: physiological, pharmacological and clinical implications. In: Page, E.; Fozzard, H.; Solaro, J., editors. Handbook of Physiology, Section 2 The Cardiovascular System. I. New York: Oxford University Press; 2002. p. 654-692.

Antzelevitch C, Fish J. Electrical heterogeneity within the ventricular wall. Basic Research in Cardiology 2001;96:517–527. [PubMed: 11770069]

Antzelevitch C, Shimizu W, Yan GX, Sicouri S, Weissenburger J, Nesterenko VV, Burashnikov A, Di Diego J, Saffitz J, Thomas GP. The M cell : its contribution to the ECG and to normal and abnormal electrical function of the heart. Journal of Cardiovascular Electrophysiology 1999;10:1124–1152. [PubMed: 10466495]

Armstrong CM, Bezanilla F. Inactivation of the sodium channel. II. Gating current experiments. Journal of General Physiology 1977;70:567–590. [PubMed: 591912]

Backx PH, Marban E. Background potassium current active during the plateau of the action potential in guinea pig ventricular myocytes. Circulation Research 1993;72:890–900. [PubMed: 8443875]

Balke CW, Rose WC, Marban E, Wier WG. Macroscopic and unitary properties of physiological ion flux through T-type Ca^{2+} channels in guinea-pig heart cells. Journal of Physiology 1992;456:247–265. [PubMed: 1338097]

Balser JR. Structure and function of the cardiac sodium channels. Cardiovascular Research 1999;42:327–338. [PubMed: 10533571]

Beavo JA, Bechtel PJ, Krebs EG. Activation of protein kinase by physiological concentrations of cyclic AMP. Proceedings of the National Academy of Sciences USA 1974;71:3580–3583.

Beeler GW, Reuter H. Reconstruction of the action potential of ventricular myocardial fibres. Journal of Physiology 1977;268:177–210. [PubMed: 874889]

Bennett PB, Yazawa K, Makita N, George AL Jr. Molecular mechanism for an inherited cardiac arrhythmia. Nature 1995;376:683–685. [PubMed: 7651517]

Bers, DM. Excitation-Contraction Coupling and Cardiac Contractile Force. 2. Dordrecht, Boston: Kluwer Academic Publishers; 2001.

Bezanilla F, Armstrong CM. Inactivation of the sodium channel. I. Sodium current experiments. Journal of General Physiology 1977;70:549–566. [PubMed: 591911]

Bezzina C, Veldkamp MW, van Den Berg MP, Postma AV, Rook MB, Viersma JW, van Langen IM, Tan-Sindhunata G, Bink-Boelkens MT, van Der Hout AH, Mannens MM, Wilde AA. A single Na

(+) channel mutation causing both long-QT and Brugada syndromes. Circulation Research 1999;85:1206–1213. [PubMed: 10590249]

Bondarenko VE, Szigeti GP, Bett GC, Kim SJ, Rasmusson RL. Computer model of action potential of mouse ventricular myocytes. American Journal of Physiology–Heart and Circulatory Physiology 2004;287:H1378–H1403. [PubMed: 15142845]

Brandt DR, Ross EM. Catecholaminestimulated GTPase cycle. Multiple sites of regulation by beta-adrenergic receptor and Mg^{2+} studied in reconstituted receptor-Gs vesicles. Journal of Biological Chemistry 1986;261:1656–1664. [PubMed: 2868003]

Brugada J, Brugada R, Brugada P. Right bundle-branch block and ST-segment elevation in leads V1 through V3: a marker for sudden death in patients without demonstrable structural heart disease. Circulation 1998;97:457–460. [PubMed: 9490240]

Caroni P, Zurini M, Clark A, Carafoli E. Further characterization and reconstitution of the purified Ca^{2+}-pumping ATPase of heart sarcolemma. Journal of Biological Chemistry 1983;258:7305–7310. [PubMed: 6223026]

Chanda B, Asamoah OK, Bezanilla F. Coupling interactions between voltage sensors of the sodium channel as revealed by site-specific measurements. Journal of General Physiology 2004;123:217–230. [PubMed: 14981134]

Chandra R, Starmer CF, Grant AO. Multiple effects of KPQ deletion mutation on gating of human cardiac Na^+ channels expressed in mammalian cells. American Journal of Physiology 1998;274:H1643–H1654. [PubMed: 9612375]

Chen H, Kim LA, Rajan S, Xu S, Goldstein SA. Charybdotoxin binding in the I(Ks) pore demonstrates two MinK subunits in each channel complex. Neuron 2003;40:15–23. [PubMed: 14527430]

Chen J, Zou A, Splawski I, Keating MT, Sanguinetti MC. Long QT syndromeassociated mutations in the Per-Arnt-Sim (PAS) domain of HERG potassium channels accelerate channel deactivation. Journal of Biological Chemistry 1999;274:10113–10118. [PubMed: 10187793]

Clancy CE, Kass RS. Inherited and acquired vulnerability to ventricular arrhythmias: cardiac Na^+ and K^+ channels. Physiological Reviews 2005;85:33–47. [PubMed: 15618477]

Clancy CE, Rudy Y. Linking a genetic defect to its cellular phenotype in a cardiac arrhythmia. Nature 1999;400:566–569. [PubMed: 10448858]

Clancy CE, Rudy Y. Cellular consequences of HERG mutations in the long QT syndrome: pre-cursors to sudden cardiac death. Cardiovascular Research 2001;50:301–313. [PubMed: 11334834]

Clancy CE, Rudy Y. Na(+) channel mutation that causes both Brugada and long-QT syndrome phenotypes: a simulation study of mechanism. Circulation 2002;105:1208–1213. [PubMed: 11889015]

Clancy CE, Tateyama M, Liu H, Wehrens XH, Kass RS. Non-equilibrium gating in cardiac Na^+ channels: an original mechanism of arrhythmia. Circulation 2003;107:2233–2237. [PubMed: 12695286]

Cohen P, Rylatt DB, Nimmo GA. The hormonal control of glycogen metabolism: the amino acid sequence at the phosphorylation site of protein phosphatase inhibitor-1. FEBS Letters 1977;76:182–186. [PubMed: 193727]

Corbin JD, Sugden PH, Lincoln TM, Keely SL. Compartmentalization of adenosine 3′: 5′ monophosphate and adenosine 3′: 5′-monophosphatedependent protein kinase in heart tissue. Journal of Biological Chemistry 1977;252:3854–3861. [PubMed: 16921]

Courtemanche M, Ramirez RJ, Nattel S. Ionic mechanisms underlying human atrial action potential properties: insights from a mathematical model. American Journal of Physiology 1998;275:H301–H321. [PubMed: 9688927]

Cui J, Kline RP, Pennefather P, Cohen IS. Gating of IsK expressed in *Xenopus* oocytes depends on the amount of mRNA injected. Journal of General Physiology 1994;104:87–105. [PubMed: 7964597]

Dessauer CW, Scully TT, Gilman AG. Interactions of forskolin and ATP with the cytosolic domains of mammalian adenylyl cyclase. Journal of Biological Chemistry 1997;272:22272–22277. [PubMed: 9268376]

DiFrancesco D, Noble D. A model of cardiac electrical activity incorporating ionic pumps and concentration changes. Philosophical Transactions of the Royal Society B: Biological Sciences 1985;307:353–398.

Dokos S, Lovell NH. Comment on ' limit cycle oscillations in pacemaker cells '. IEEE Transactions on Biomedical Engineering 2001;48:499–500. [PubMed: 11322539]

Droogmans G, Nilius B. Kinetic properties of the cardiac T-type calcium channel in the guinea-pig. Journal of Physiology 1989;419:627–650. [PubMed: 2559976]

Duggal P, Vesely MR, Wattanasirichaigoon D, Villafane J, Kaushik V, Beggs AH. Mutation of the gene for IsK associated with both Jervell and Lange-Nielsen and Romano-Ward forms of Long-QT syndrome. Circulation 1998;97:142–146. [PubMed: 9445165]

Dumaine R, Towbin JA, Brugada P, Vatta M, Nesterenko DV, Nesterenko VV, Brugada J, Brugada R, Antzelevitch C. Ionic mechanisms responsible for the electrocardiographic phenotype of the Brugada syndrome are temperature dependent. Circulation Research 1999;85:803–809. [PubMed: 10532948]

Dumaine R, Wang Q, Keating MT, Hartmann HA, Schwartz PJ, Brown AM, Kirsch GE. Multiple mechanisms of Na^+ channel-linked long-QT syndrome. Circulation Research 1996;78:916–924. [PubMed: 8620612]

Ehara T, Noma A, Ono K. Calcium-activated non-selective cation channel in ventricular cells isolated from adult guinea-pig hearts. Journal of Physiology 1988;403:117–133. [PubMed: 2473193]

Endresen LP, Hall K, Hoye JS, Myrheim J. A theory for the membrane potential of living cells. European Biophysics Journal 2000;29:90–103. [PubMed: 10877018]

Faber GM, Rudy Y. Action potential and contractility changes in [Na(+)](i) overloaded cardiac myocytes: a simulation study. Biophysical Journal 2000;78:2392–2404. [PubMed: 10777735]

Fabiato A. Two kinds of calcium-induced release of calcium from the sarcoplasmic reticulum of skinned cardiac cells. Advances in Experimental Medicine and Biology 1992;311:245–262. [PubMed: 1529757]

Fishman PH, Nussbaum E, Duman RS. Characterization and regulation of beta 1-adrenergic receptors in a human neuroepithelioma cell line. Journal of Neurochemistry 1991;56:596–602. [PubMed: 1671088]

Fodstad H, Swan H, Laitinen P, Piippo K, Paavonen K, Viitasalo M, Toivonen L, Kontula K. Four potassium channel mutations account for 73% of the genetic spectrum underlying long-QT syndrome (LQTS) and provide evidence for a strong founder effect in Finland. Annals of Internal Medicine 2004;36 (Suppl 1):53–63.

Fox JJ, McHarg JL, Gilmour RF Jr. Ionic mechanism of electrical alternans. American Journal of Physiology–Heart and Circulatory Physiology 2002;282:H516–H530. [PubMed: 11788399]

Frace AM, Mery PF, Fischmeister R, Hartzell HC. Rate-limiting steps in the beta-adrenergic stimulation of cardiac calcium current. Journal of General Physiology 1993;101:337–353. [PubMed: 8386216]

Francis J, Sankar V, Nair VK, Priori SG. Catecholaminergic polymorphic ventricular tachycardia. Heart Rhythm 2005;2:550–554. [PubMed: 15840485]

Freedman NJ, Liggett SB, Drachman DE, Pei G, Caron MG, Lefkowitz RJ. Phosphorylation and desensitization of the human beta 1-adrenergic receptor. Involvement of G proteincoupled receptor kinases and cAMP-dependent protein kinase. Journal of Biological Chemistry 1995;270:17953–17961. [PubMed: 7629102]

George AL Jr, Varkony TA, Drabkin HA, Han J, Knops JF, Finley WH, Brown GB, Ward DC, Haas M. Assignment of the human heart tetrodotoxin-resistant voltage-gated Na^+ channel alpha-subunit gene (SCN5A) to band 3p21. Cytogenetics and Cell Genetics 1995;68:67–70. [PubMed: 7956363]

Gibson RM, Taylor SS. Dissecting the cooperative reassociation of the regulatory and catalytic subunits of cAMP-dependent protein kinase. Role of Trp-196 in the catalytic subunit. Journal of Biological Chemistry 1997;272:31998–32005. [PubMed: 9405392]

Gima K, Rudy Y. Ionic current basis of electrocardiographic waveforms: a model study. Circulation Research 2002;90:889–896. [PubMed: 11988490]

Grant AO. Molecular biology of sodium channels and their role in cardiac arrhythmias. American Journal of the Medical Sciences 2001;110:296–305.

Guan S, Lu Q, Huang K. A discussion about the DiFrancesco–Noble model. Journal of Theoretical Biology 1997;189:27–32. [PubMed: 9398500]

Hagemann D, Kuschel M, Kuramochi T, Zhu W, Cheng H, Xiao RP. Frequency-encoding Thr17 phospholamban phosphorylation is independent of Ser16 phosphorylation in cardiac myocytes. Journal of Biological Chemistry 2000;275:22532–22536. [PubMed: 10825152]

Hanson PI, Meyer T, Stryer L, Schulman H. Dual role of calmodulin in autophosphorylation of multifunctional CaM kinase may underlie decoding of calcium signals. Neuron 1994;12:943–956. [PubMed: 8185953]

Hartmann HA, Tiedeman AA, Chen SF, Brown AM, Kirsch GE. Effects of III-IV linker mutations on human heart Na^+ channel inactivation gating. Circulation Research 1994;75:114–122. [PubMed: 8013069]

Hille, B. Ion Channels of Excitable Membranes. 3. Sunderland, MA: Sinauer; 2001.

Hodgkin AL, Huxley AF. Action potentials recorded from inside a nerve fibre. Nature 1939;144:710–711.

Hodgkin AL, Huxley AF. A quantitative description of membrane current and its application to conduction and excitation in nerve. Journal of Physiology 1952;117:500–544. [PubMed: 12991237]

Hodgkin AL, Huxley AF, Katz B. Measurement of current-voltage relations in the membrane of the giant axon of *Loligo*. Journal of Physiology 1952;116:424–448. [PubMed: 14946712]

Hofmann F, Beavo JA, Bechtel PJ, Krebs EG. Comparison of adenosine 3′: 5′-monophosphatedependent protein kinases from rabbit skeletal and bovine heart muscle. Journal of Biological Chemistry 1975;250:7795–7801. [PubMed: 170270]

Hund TJ, Kucera JP, Otani NF, Rudy Y. Ionic charge conservation and long-term steady state in the Luo-Rudy dynamic cell model. Biophysical Journal 2001;81:3324–3331. [PubMed: 11720995]

Hund TJ, Rudy Y. Rate dependence and regulation of action potential and calcium transient in a canine cardiac ventricular cell model. Circulation 2004;110:3168–3174. [PubMed: 15505083]

Hund, TJ.; Rudy, Y. A role for calcium/calmodulin- dependent protein kinase II in cardiac disease and arrhythmia. In: Kass, RS.; Clancy, CE., editors. Basis and Treatment of Cardiac Arrhythmias (Handbook of Experimental Pharmacology). 171. Heidelberg: Springer-Verlag; 2006. p. 201-220.

Iyer V, Mazhari R, Winslow RL. A computational model of the human left-ventricular epicardial myocyte. Biophysical Journal 2004;87:1507–1525. [PubMed: 15345532]

January CT, Riddle JM. Early afterdepolarizations: mechanism of induction and block. A role for L-type Ca^{2+} current. Circulation Research 1989;64:977–990. [PubMed: 2468430]

January CT, Riddle JM, Salata JJ. A model for early afterdepolarizations : induction with the Ca^{2+} channel agonist Bay K 8644. Circulation Research 1988;62:563–571. [PubMed: 2449297]

Johnson DA, Akamine P, Radzio-Andzelm E, Madhusudan M, Taylor SS. Dynamics of cAMP-dependent protein kinase. Chemistry Review 2001;101:2243–2270.

Kakei M, Noma A, Shibasaki T. Properties of adenosine-triphosphate-regulated potassium channels in guinea-pig ventricular cells. Journal of Physiology 1985;363:441–462. [PubMed: 2410608]

Kameyama M, Kakei M, Sato R, Shibasaki T, Matsuda H, Irisawa H. Intracellular Na+ activates a K^+ channel in mammalian cardiac cells. Nature 1984;309:354–356. [PubMed: 6328309]

Kass RS, Moss AJ. Long QT syndrome: novel insights into the mechanisms of cardiac arrhythmias. Journal of Clinical Investigation 2003;112:810–815. [PubMed: 12975462]

Kay NG, Plumb VJ, Arciniegas JG, Henthorn RW, Waldo AL. Torsade de pointes: the long-short initiating sequence and other clinical features: Observations in 32 patients. Journal of the American College of Cardiology 1983;2:806–817. [PubMed: 6630761]

Keating MT, Sanguinetti MC. Molecular genetic insights into cardiovascular disease. Science 1996;272:681–685. [PubMed: 8614827]

Kiehn J, Lacerda AE, Brown AM. Pathways of HERG inactivation. American Journal of Physiology 1999;277:H199–H210. [PubMed: 10409198]

Kleber AG, Rudy Y. Basic mechanisms of cardiac impulse propagation and associated arrhythmias. Physiological Reviews 2004;84:431–488. [PubMed: 15044680]

Koren G, Liman ER, Logothetis DE, NadalGinard B, Hess P. Gating mechanism of a cloned potassium channel expressed in frog oocytes and mammalian cells. Neuron 1990;4:39–51. [PubMed: 2310574]

Krogh-Madsen T, Schaffer P, Skriver AD, Taylor LK, Pelzmann B, Koidl B, Guevara MR. An ionic model for rhythmic activity in small clusters of embryonic chick ventricular cells. American Journal of Physiology–Heart and Circulatory Physiology 2005;289:H398–H413. [PubMed: 15708964]

Kupershmidt S, Yang IC, Sutherland M, Wells KS, Yang T, Yang P, Balser JR, Roden DM. Cardiac-enriched LIM domain protein fhl2 is required to generate I(Ks) in a heterologous system. Cardiovascular Research 2002;56:93–103. [PubMed: 12237170]

Kurachi Y. Voltage-dependent activation of the inward-rectifier potassium channel in the ventricular cell membrane of guinea-pig heart. Journal of Physiology 1985;366:365–385. [PubMed: 2414434]

Kurata Y, Hisatome I, Matsuda H, Shibamoto T. Dynamical mechanisms of pacemaker generation in IK1-downregulated human ventricular myocytes : insights from bifurcation analyses of a mathematical model. Biophysical Journal 2005;89:2865–2887. [PubMed: 16040746]

Lahat H, Pras E, Eldar M. RYR2 and CASQ2 mutations in patients suffering from catecholaminergic polymorphic ventricular tachycardia. Circulation 2003;107:e29. [PubMed: 12551888]author reply e29.

Le Peuch CJ, Haiech J, Demaille JG. Concerted regulation of cardiac sarcoplasmic reticulum calcium transport by cyclic adenosine monophosphate dependent and calcium–calmodulin-dependent phosphorylations. Biochemistry 1979;18:5150–5157. [PubMed: 227448]

Lees-Miller JP, Duan Y, Teng GQ, Thorstad K, Duff HJ. Novel gain-of-function mechanism in K(+) channel-related long-QT syndrome: altered gating and selectivity in the HERG1 N629D mutant. Circulation Research 2000;86:507–513. [PubMed: 10720411]

Liu DW, Antzelevitch C. Characteristics of the delayed rectifier current (IKr and IKs) in canine ventricular epicardial, midmyocardial, and endocardial myocytes. A weaker IKs contributes to the longer action potential of the M cell. Circulation Research 1995;76:351–365. [PubMed: 7859382]

Liu DW, Gintant GA, Antzelevitch C. Ionic bases for electrophysiological distinctions among epicardial, midmyocardial, and endocardial myocytes from the free wall of the canine left ventricle. Circulation Research 1993;72:671–687. [PubMed: 8431990]

Loussouarn G, Park KH, Bellocq C, Baro I, Charpentier F, Escande D. Phosphatidylinositol-4,5-bisphosphate, PIP2, controls KCNQ1/KCNE1 voltage-gated potassium channels: a functional homology between voltage-gated and inward rectifier K^+ channels. EMBO Journal 2003;22:5412–5421. [PubMed: 14532114]

Lu Z, Kamiya K, Opthof T, Yasui K, Kodama I. Density and kinetics of I(Kr) and I(Ks) in guinea pig and rabbit ventricular myocytes explain different efficacy of I(Ks) blockade at high heart rate in guinea pig and rabbit : implications for arrhythmogenesis in humans. Circulation 2001;104:951–956. [PubMed: 11514385]

Luk HN, Carmeliet E. Na(+)-activated K^+ current in cardiac cells : rectification, open probability, block and role in digitalis toxicity. Pügers Archiv: European Journal of Physiology 1990;416:766–768.

Luo CH, Rudy Y. A model of the ventricular cardiac action potential. Depolarization, repolarization, and their interaction. Circulation Research 1991;68:1501–1526. [PubMed: 1709839]

Luo CH, Rudy Y. A dynamic model of the cardiac ventricular action potential. I. Simulations of ionic currents and concentration changes. Circulation Research 1994a;74:1071–1096. [PubMed: 7514509]

Luo CH, Rudy Y. A dynamic model of the cardiac ventricular action potential. II. Afterdepolarizations, triggered activity, and potentiation. Circulation Research 1994b;74:1097–1113. [PubMed: 7514510]

Maier LS, Bers DM. Calcium, calmodulin, and calcium-calmodulin kinase II : heartbeat to heartbeat and beyond. Journal of Molecular and Cellular Cardiology 2002;34:919–939. [PubMed: 12234763]

Marx SO, Kurokawa J, Reiken S, Motoike H, D'Armiento J, Marks AR, Kass RS. Requirement of a macromolecular signaling complex for beta adrenergic receptor modulation of the KCNQ1-KCNE1 potassium channel. Science 2002;295:496–499. [PubMed: 11799244]

Matsuoka S, Sarai N, Kuratomi S, Ono K, Noma A. Role of individual ionic current systems in ventricular cells hypothesized by a model study. Japanese Journal of Physiology 2003;53:105–123. [PubMed: 12877767]

McAllister RE, Noble D, Tsien RW. Reconstruction of the electrical activity of cardiac Purkinje fibres. Journal of Physiology 1975;251:1–59. [PubMed: 1185607]

McPhee JC, Ragsdale DS, Scheuer T, Catterall WA. A mutation in segment IVS6 disrupts fast inactivation of sodium channels. Proceedings of the National Academy of Sciences USA 1994;91:12346–12350.

McPhee JC, Ragsdale DS, Scheuer T, Catterall WA. A critical role for transmembrane segment IVS6 of the sodium channel alpha subunit in fast inactivation. Journal of Biological Chemistry 1995;270:12025–12034. [PubMed: 7744852]

McPhee JC, Ragsdale DS, Scheuer T, Catterall WA. A critical role for the S4-S5 intracellular loop in domain IV of the sodium channel alpha-subunit in fast inactivation. Journal of Biological Chemistry 1998;273:1121–1129. [PubMed: 9422778]

Meissner, G. Sarcoplasmic reticulum ion channels. In: Zipes, DP.; Jalife, J., editors. Cardiac Electrophysiology : From Cell to Bedside. Philadelphia: Saunders; 1995. p. 51-58.

Moorman JR, Kirsch GE, Brown AM, Joho RH. Changes in sodium channel gating produced by point mutations in a cytoplasmic linker. Science 1990;250:688–691. [PubMed: 2173138]

Motoike HK, Liu H, Glaaser IW, Yang AS, Tateyama M, Kass RS. The Na^+ channel inactivation gate is a molecular complex: a novel role of the COOH-terminal domain. Journal of General Physiology 2004;123:155–165. [PubMed: 14744988]

Nakajima T, Furukawa T, Tanaka T, Katayama Y, Nagai R, Nakamura Y, Hiraoka M. Novel mechanism of HERG current suppression in LQT2: shift in voltage dependence of HERG inactivation. Circulation Research 1998;83:415–422. [PubMed: 9721698]

Nerbonne JM, Kass RS. Molecular physiology of cardiac repolarization. Physiological Reviews 2005;85:1205–1253. [PubMed: 16183911]

Nichols CG, Ripoll C, Lederer WJ. ATPsensitive potassium channel modulation of the guinea pig ventricular action potential and contraction. Circulation Research 1991;68:280–287. [PubMed: 1984868]

Noble D, Varghese A, Kohl P, Noble P. Improved guinea-pig ventricular cell model incorporating a diadic space, IKr and IKs, and length- and tensiondependent processes. Canadian Journal of Cardiology 1998;14:123–134. [PubMed: 9487284]

Noma A. ATP-regulated K^+ channels in cardiac muscle. Nature 1983;305:147–148. [PubMed: 6310409]

Nuyens D, Stengl M, Dugarmaa S, Rossenbacker T, Compernolle V, Rudy Y, Smits JF, Flameng W, Clancy CE, Moons L, Vos MA, Dewerchin M, Benndorf K, Collen D, Carmeliet E, Carmeliet P. Abrupt rate accelerations or premature beats cause life-threatening arrhythmias in mice with long-QT3 syndrome. Nature Medicine 2001;7:1021–1027.

Nygren A, Fiset C, Firek L, Clark JW, Lindblad DS, Clark RB, Giles WR. Mathematical model of an adult human atrial cell : the role of K+ currents in repolarization. Circulation Research 1998;82:63–81. [PubMed: 9440706]

Odermatt A, Kurzydlowski K, MacLennan DH. The vmax of the Ca^{2+}-ATPase of cardiac sarcoplasmic reticulum (SERCA2a) is not altered by Ca^{2+}/ calmodulin-dependent phosphorylation or by interaction with phospholamban. Journal of Biological Chemistry 1996;271:14206–14213. [PubMed: 8662932]

Ohyama H, Kajita H, Omori K, Takumi T, Hiramoto N, Iwasaka T, Matsuda H. Inhibition of cardiac delayed rectifier K^+ currents by an antisense oligodeoxynucleotide against IsK (minK) and over-expression of IsK mutant D77N in neonatal mouse hearts. Pügers Archiv: European Journal of Physiology 2001;442:329–335.

Pandit SV, Giles WR, Demir SS. A mathematical model of the electrophysiological alterations in rat ventricular myocytes in type-I diabetes. Biophysical Journal 2003;84:832–841. [PubMed: 12547767]

Piippo K, Swan H, Pasternack M, Chapman H, Paavonen K, Viitasalo M, Toivonen L, Kontula K. A founder mutation of the potassium channel KCNQ1 in long QT syndrome: implications for estimation of disease prevalence and molecular diagnostics. Journal of the American College of Cardiology 2001;37:562–568. [PubMed: 11216980]

Plonsey, R.; Barr, RC. Bioelectricity : A Quantitative Approach. 2. New York: Kluwer Academic/Plenum Publishers; 2000.

Post SR, Hilal-Dandan R, Urasawa K, Brunton LL, Insel PA. Quantification of signalling components and amplification in the beta-adrenergicreceptor- adenylate cyclase pathway in isolated adult rat ventricular myocytes. Biochemical Journal 1995;311:75–80. [PubMed: 7575483]

Priebe L, Beuckelmann DJ. Simulation study of cellular electric properties in heart failure. Circulation Research 1998;82:1206–1223. [PubMed: 9633920]

Priori SG, Barhanin J, Hauer RN, Haverkamp W, Jongsma HJ, Kleber AG, McKenna WJ, Roden DM, Rudy Y, Schwartz K, Schwartz PJ, Towbin JA, Wilde AM. Genetic and molecular basis of cardiac

arrhythmias : impact on clinical management part III. Circulation 1999a;99:674–681. [PubMed: 9950666]

Priori SG, Barhanin J, Hauer RN, Haverkamp W, Jongsma HJ, Kleber AG, McKenna WJ, Roden DM, Rudy Y, Schwartz K, Schwartz PJ, Towbin JA, Wilde AM. Genetic and molecular basis of cardiac arrhythmias : impact on clinical management parts I and II. Circulation 1999b;99:518–528. [PubMed: 9927398]

Priori SG, Corr PB. Mechanisms underlying early and delayed afterdepolarizations induced by catecholamines. American Journal of Physiology 1990;258:H1796–H1805. [PubMed: 2163219]

Priori SG, Schwartz PJ, Napolitano C, Bloise R, Ronchetti E, Grillo M, Vicentini A, Spazzolini C, Nastoli J, Bottelli G, Folli R, Cappelletti D. Risk stratification in the long-QT syndrome. New England Journal of Medicine 2003;348:1866–1874. [PubMed: 12736279]

Puglisi JL, Bers DM. LabHEART: an interactive computer model of rabbit ventricular myocyte ion channels and Ca transport. American Journal of Physiology–Cell Physiology 2001;281:C2049–C2060. [PubMed: 11698264]

Pusch M. Increase of the single-channel conductance of KvLQT1 potassium channels induced by the association with minK. Pügers Archiv : European Journal of Physiology 1998;437:172–174.

Pusch M, Bertorello L, Conti F. Gating and flickery block differentially affected by rubidium in homomeric KCNQ1 and heteromeric KCNQ1/ KCNE1 potassium channels. Biophysical Journal 2000;78:211–226. [PubMed: 10620287]

Pusch M, Ferrera L, Friedrich T. Two open states and rate-limiting gating steps revealed by intracellular Na^+ block of human KCNQ1 and KCNQ1/ KCNE1 K^+ channels. Journal of Physiology 2001;533:135–143. [PubMed: 11351022]

Ramirez RJ, Nattel S, Courtemanche M. Mathematical analysis of canine atrial action potentials: rate, regional factors, and electrical remodeling. American Journal of Physiology–Heart and Circulatory Physiology 2000;279:H1767–H1785. [PubMed: 11009464]

Rasmusson RL, Clark JW, Giles WR, Robinson K, Clark RB, Shibata EF, Campbell DL. A mathematical model of electrophysiological activity in a bullfrog atrial cell. American Journal of Physiology 1990;259:H370–H389. [PubMed: 2386218]

Reeves ML, Leigh BK, England PJ. The identification of a new cyclic nucleotide phosphodiesterase activity in human and guinea-pig cardiac ventricle. Implications for the mechanism of action of selective phosphodiesterase inhibitors. Biochemical Journal 1987;241:535–541. [PubMed: 3036066]

Rice JJ, Jafri MS, Winslow RL. Modeling short-term interval-force relations in cardiac muscle. American Journal of Physiology–Heart and Circulatory Physiology 2000;278:H913–H931. [PubMed: 10710361]

Rocchetti M, Besana A, Gurrola GB, Possani LD, Zaza A. Rate dependency of delayed rectifier currents during the guinea-pig ventricular action potential. Journal of Physiology 2001;534:721–732. [PubMed: 11483703]

Roden DM. Drug-induced prolongation of the QT interval. New England Journal of Medicine 2004;350:1013–1022. [PubMed: 14999113]

Roden DM, Balser JR. A plethora of mechanisms in the HERG-related long QT syndrome. Genetics meets electrophysiology. Cardiovascular Research 1999;44:242–246. [PubMed: 10690299]

Rosen, MR. The concept of afterdepolarizations. In: Rosen, MR.; Janse, MJ.; Wit, AL., editors. Cardiac Electrophysiology : A Textbook. Mount Kisco, NY: Futura; 1990. p. 267-271.

Rudy, Y. The cardiac ventricular action potential. In: Page, E.; Fozzard, HA.; Solaro, RJ., editors. The Cardiovascular System Volume 1, The Heart. New York: Oxford University Press; 2002. p. 531-547.published for the American Physiological Society

Rudy Y. Modelling and imaging cardiac repolarization abnormalities. Journal of Internal Medicine 2006;259:91–106. [PubMed: 16336517]

Saucerman JJ, Brunton LL, Michailova AP, McCulloch AD. Modeling beta-adrenergic control of cardiac myocyte contractility in silico. Journal of Biological Chemistry 2003;278:47997–48003. [PubMed: 12972422]

Saucerman JJ, Healy SN, Belik ME, Puglisi JL, McCulloch AD. Proarrhythmic consequences of a KCNQ1 AKAP-binding domain mutation : computational models of whole cells and heterogeneous tissue. Circulation Research 2004;95:1216–1224. [PubMed: 15528464]

Saucerman JJ, McCulloch AD. Mechanistic systems models of cell signaling networks: a case study of myocyte adrenergic regulation. Progress in Biophysics & Molecular Biology 2004;85:261–278. [PubMed: 15142747]

Schwartz PJ, Priori SG, Locati EH, Napolitano C, Cantu F, Towbin JA, Keating MT, Hammoude H, Brown AM, Chen LS. Long QT syndrome patients with mutations of the SCN5A and HERG genes have differential responses to Na^+ channel blockade and to increases in heart rate. Implications for gene-specific therapy. Circulation 1995;92:3381–3386. [PubMed: 8521555]

Schwarz W, Palade PT, Hille B. Local anesthetics. Effect of pH on use-dependent block of sodium channels in frog muscle. Biophysical Journal 1977;20:343–368. [PubMed: 21711]

Sesti F, Goldstein SA. Single-channel characteristics of wild-type IKs channels and channels formed with two minK mutants that cause long QT syndrome. Journal of General Physiology 1998;112:651–663. [PubMed: 9834138]

Shannon TR, Wang F, Puglisi J, Weber C, Bers DM. A mathematical treatment of integrated Ca dynamics within the ventricular myocyte. Biophysical Journal 2004;87:3351–3371. [PubMed: 15347581]

Shaw RM, Rudy Y. Electrophysiologic effects of acute myocardial ischemia: a theoretical study of altered cell excitability and action potential duration. Cardiovascular Research 1997a;35:256–272. [PubMed: 9349389]

Shaw RM, Rudy Y. Ionic mechanisms of propagation in cardiac tissue. Roles of the sodium and L-type calcium currents during reduced excitability and decreased gap junction coupling. Circulation Research 1997b;81:727–741. [PubMed: 9351447]

Shimizu W, Antzelevitch C. Sodium channel block with mexiletine is effective in reducing dispersion of repolarization and preventing torsade des pointes in LQT2 and LQT3 models of the long-QT syndrome. Circulation 1997;96:2038–2047. [PubMed: 9323097]

Sicouri S, Antzelevitch C. A subpopulation of cells with unique electrophysiological properties in the deep subepicardium of the canine ventricle. The M cell. Circulation Research 1991;68:1729–1741. [PubMed: 2036721]

Silva J, Rudy Y. Subunit interaction determines IKs participation in cardiac repolarization and repolarization reserve. Circulation 2005;112:1384–1391. [PubMed: 16129795]

Silverman WR, Roux B, Papazian DM. Structural basis of two-stage voltage-dependent activation in K^+ channels. Proceedings of the National Academy of Sciences USA 2003;100:2935–2940.

Sipido KR, Volders PG, de Groot SH, Verdonck F, Van de Werf F, Wellens HJ, Vos MA. Enhanced Ca (2+) release and Na/Ca exchange activity in hypertrophied canine ventricular myocytes: potential link between contractile adaptation and arrhythmogenesis. Circulation 2000;102:2137–2144. [PubMed: 11044433]

Smith PL, Baukrowitz T, Yellen G. The inward rectification mechanism of the HERG cardiac potassium channel. Nature 1996;379:833–836. [PubMed: 8587608]

Smith SB, White HD, Siegel JB, Krebs EG. Cyclic AMP-dependent protein kinase I : cyclic nucleotide binding, structural changes, and release of the catalytic subunits. Proceedings of the National Academy of Sciences USA 1981;78:1591–1595.

Splawski I, Tristani-Firouzi M, Lehmann MH, Sanguinetti MC, Keating MT. Mutations in the hminK gene cause long QT syndrome and suppress IKs function. Nature Genetics 1997;17:338–340. [PubMed: 9354802]

Stengl M, Volders PG, Thomsen MB, Spatjens RL, Sipido KR, Vos MA. Accumulation of slowly activating delayed rectifier potassium current (IKs) in canine ventricular myocytes. Journal of Physiology 2003;551:777–786. [PubMed: 12819301]

Tada, M.; Shigekawa, M.; Kadoma, M.; Nimura, Y. Uptake of calcium by sarcoplasmic reticulum and its regulation and functional consequences. In: Sperelakis, N., editor. Physiology and Pathophysiology of the Heart. Boston: Kluwer Academic Publishers; 1989. p. xv+-1009.

Takai A, Tsuboi K, Koyasu M, Isobe M. Effects of modification of the hydrophobic C-1-C-16 segment of tautomycin on its affinity to type-1 and type- 2A protein phosphatases. Biochemical Journal 2000;350:81–88. [PubMed: 10926829]

Taylor, SS.; Beuchler, JA.; Knighton, DR. cAMP-Dependent protein kinase: mechanism for atp : protein phosphotransfer. In: Kemp, BE., editor. Peptides and Protein Phosphorylation. Boca Raton: CRC Press; 1990. p. 43-83.

Terrenoire C, Clancy CE, Cormier JW, Sampson KJ, Kass RS. Autonomic control of cardiac action potentials: role of potassium channel kinetics in response to sympathetic stimulation. Circulation Research 2005;96:e25–e34. [PubMed: 15731462]

Toyofuku T, Curotto Kurzydlowski K, Narayanan N, MacLennan DH. Identification of Ser38 as the site in cardiac sarcoplasmic reticulum Ca(2+)- ATPase that is phosphorylated by Ca^{2+}/calmodulindependent protein kinase. Journal of Biological Chemistry 1994;269:26492–26496. [PubMed: 7929371]

Tristani-Firouzi M, Sanguinetti MC. Voltage-dependent inactivation of the human K^+ channel KvLQT1 is eliminated by association with minimal K^+ channel (minK) subunits. Journal of Physiology 1998;510:37–45. [PubMed: 9625865]

Varghese A, Sell GR. A conservation principle and its effect on the formulation of Na-Ca exchanger current in cardiac cells. Journal of Theoretical Biology 1997;189:33–40. [PubMed: 9398501]

Vassort G, Alvarez J. Cardiac T-type calcium current: pharmacology and roles in cardiac tissues. Journal of Cardiovascular Electrophysiology 1994;5:376–393. [PubMed: 7912618]

Veldkamp MW, Viswanathan PC, Bezzina C, Baartscheer A, Wilde AA, Balser JR. Two distinct congenital arrhythmias evoked by a multidysfunctional Na(+) channel. Circulation Research 2000;86:E91–E97. [PubMed: 10807877]

Verrier RL, Antzelevitch C. Autonomic aspects of arrhythmogenesis : the enduring and the new. Current Opinion in Cardiology 2004;19:2–11. [PubMed: 14688627]

Virag L, Iost N, Opincariu M, Szolnoky J, Szecsi J, Bogats G, Szenohradszky P, Varro A, Papp JG. The slow component of the delayed rectifier potassium current in undiseased human ventricular myocytes. Cardiovascular Research 2001;49:790–797. [PubMed: 11230978]

Viswanathan PC, Rudy Y. Pause induced early afterdepolarizations in the long QT syndrome: a simulation study. Cardiovascular Research 1999;42:530–542. [PubMed: 10533588]

Viswanathan PC, Rudy Y. Cellular arrhythmogenic effects of congenital and acquired long- QT syndrome in the heterogeneous myocardium. Circulation 2000;101:1192–1198. [PubMed: 10715268]

Viswanathan PC, Shaw RM, Rudy Y. Effects of IKr and IKs heterogeneity on action potential duration and its rate dependence: a simulation study. Circulation 1999;99:2466–2474. [PubMed: 10318671]

Volders PG, Stengl M, van Opstal JM, Gerlach U, Spatjens RL, Beekman JD, Sipido KR, Vos MA. Probing the contribution of IKs to canine ventricular repolarization: key role for betaadrenergic receptor stimulation. Circulation 2003;107:2753–2760. [PubMed: 12756150]

Walsh, DA.; Angelos, KL.; Van Patten, SM.; Glass, DB.; Garretto, LP. The inhibitor protein of the cAMP-dependent protein kinase. In: Kemp, BE., editor. Peptides and Protein Phosphorylation. Boca Raton: CRC Press; 1990. p. 43-83.

Walsh KB, Kass RS. Regulation of a heart potassium channel by protein kinase A and C. Science 1988;242:67–69. [PubMed: 2845575]

Wang DW, Makita N, Kitabatake A, Balser JR, George AL Jr. Enhanced Na(+) channel intermediate inactivation in Brugada syndrome. Circulation Research 2000;87:e37–e43. [PubMed: 11029409]

Wang DW, Yazawa K, Makita N, George AL Jr, Bennett PB. Pharmacological targeting of long QT mutant sodium channels. Journal of Clinical Investigation 1997;99:1714–1720. [PubMed: 9120016]

Wang DY, Chae SW, Gong QY, Lee CO. Role of aiNa in positive force-frequency staircase in guinea pig papillary muscle. American Journal of Physiology 1988;255:C798–C807. [PubMed: 3202149]

Wang Q, Curran ME, Splawski I, Burn TC, Millholland JM, VanRaay TJ, Shen J, Timothy KW, Vincent GM, de Jager T, Schwartz PJ, Toubin JA, Moss AJ, Atkinson DL, Landes GM, Connors TD, Keating MT. Positional cloning of a novel potassium channel gene: KVLQT1 mutations cause cardiac arrhythmias. Nature Genetics 1996;12:17–23. [PubMed: 8528244]

Wang W, Xia J, Kass RS. MinK-KvLQT1 fusion proteins, evidence for multiple stoichiometries of the assembled IsK channel. Journal of Biological Chemistry 1998;273:34069–34074. [PubMed: 9852064]

Wang Z, Kimitsuki T, Noma A. Conductance properties of the Na(+)-activated K^+ channel in guineapig ventricular cells. Journal of Physiology 1991;433:241–257. [PubMed: 1841940]

Wegener AD, Simmerman HK, Lindemann JP, Jones LR. Phospholamban phosphorylation in intact ventricles. Phosphorylation of serine 16 and threonine 17 in response to beta-adrenergic stimulation. Journal of Biological Chemistry 1989;264:11468–11474. [PubMed: 2544595]

Wehrens XH, Abriel H, Cabo C, Benhorin J, Kass RS. Arrhythmogenic mechanism of an LQT-3 mutation of the human heart Na(+) channel alpha-subunit : a computational analysis. Circulation 2000;102:584–590. [PubMed: 10920073]

West JW, Patton DE, Scheuer T, Wang Y, Goldin AL, Catterall WA. A cluster of hydrophobic amino acid residues required for fast Na(+)-channel inactivation. Proceedings of the National Academy of Sciences USA 1992;89:10910–10914.

Witcher DR, Kovacs RJ, Schulman H, Cefali DC, Jones LR. Unique phosphorylation site on the cardiac ryanodine receptor regulates calcium channel activity. Journal of Biological Chemistry 1991;266:11144–11152. [PubMed: 1645727]

Yan GX, Antzelevitch C. Cellular basis for the Brugada syndrome and other mechanisms of arrhythmogenesis associated with ST-segment elevation. Circulation 1999;100:1660–1666. [PubMed: 10517739]

Yang T, Kupershmidt S, Roden DM. Anti-minK antisense decreases the amplitude of the rapidly activating cardiac delayed rectifier K^+ current. Circulation Research 1995;77:1246–1253. [PubMed: 7586238]

Yang Y, Sigworth FJ. Single-channel properties of IKs potassium channels. Journal of General Physiology 1998;112:665–678. [PubMed: 9834139]

Yehia AR, Jeandupeux D, Alonso F, Guevara MR. Hysteresis and bistability in the direct transition from 1 : 1 to 2 : 1 rhythm in periodically driven single ventricular cells. Chaos 1999;9:916–931. [PubMed: 12779889]

Yuan W, Bers DM. Ca-dependent facilitation of cardiac Ca current is due to Ca-calmodulindependent protein kinase. American Journal of Physiology 1994;267:H982–H993. [PubMed: 8092302]

Yue DT, Burkhoff D, Franz MR, Hunter WC, Sagawa K. Postextrasystolic potentiation of the isolated canine left ventricle. Relationship to mechanical restitution. Circulation Research 1985;56:340–350. [PubMed: 2578901]

Yue DT, Marban E. A novel cardiac potassium channel that is active and conductive at depolarized potentials. Pügers Archiv: European Journal of Physiology 1988;413:127–133.

Zagotta WN, Hoshi T, Aldrich RW. Shaker potassium channel gating. III : Evaluation of kinetic models for activation. Journal of General Physiology 1994a;103:321–362. [PubMed: 8189208]

Zagotta WN, Hoshi T, Dittman J, Aldrich RW. Shaker potassium channel gating. II : Transitions in the activation pathway. Journal of General Physiology 1994b;103:279–319. [PubMed: 8189207]

Zeng J, Laurita KR, Rosenbaum DS, Rudy Y. Two components of the delayed rectifier K^+ current in ventricular myocytes of the guinea pig type. Theoretical formulation and their role in repolarization. Circulation Research 1995;77:140–152. [PubMed: 7788872]

Zeng J, Rudy Y. Early afterdepolarizations in cardiac myocytes: mechanism and rate dependence. Biophysical Journal 1995;68:949–964. [PubMed: 7538806]

Zhang M, Liu J, Tseng GN. Gating charges in the activation and inactivation processes of the HERG channel. Journal of General Physiology 2004;124:703–718. [PubMed: 15545400]

Zhang R, Khoo MS, Wu Y, Yang Y, Grueter CE, Ni G, Price EE Jr, Thiel W, Guatimosim S, Song LS, Madu EC, Shah AN, Vishnivetskaya TA, Atkinson JB, Gurevich VV, Salama G, Lederer WJ, Colbran RJ, Anderson ME. Calmodulin kinase II inhibition protects against structural heart disease. Nature Medicine 2005;11:409–417.

Zhou Z, Gong Q, Epstein ML, January CT. HERG channel dysfunction in human long QT syndrome. Intracellular transport and functional defects. Journal of Biological Chemistry 1998;273:21061–21066. [PubMed: 9694858]

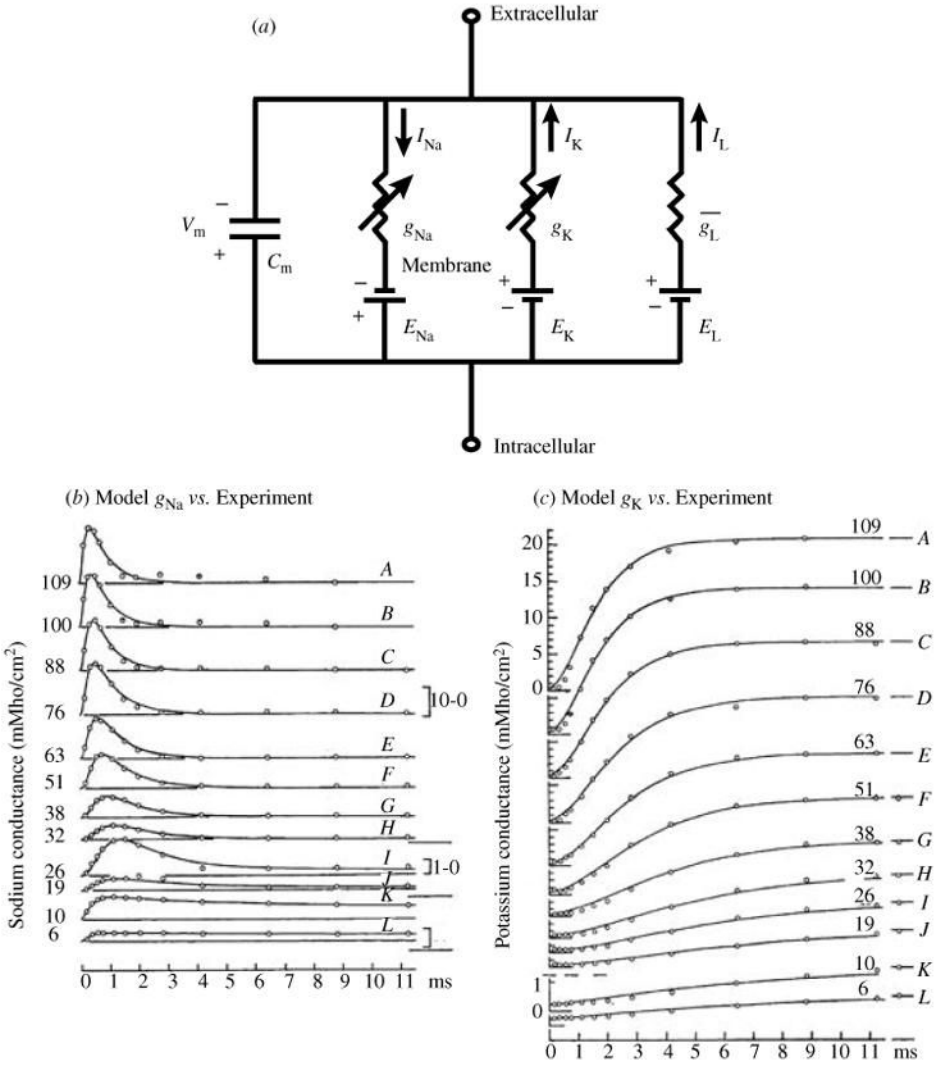

Fig 1.

(*a*) Circuit diagram of the Hodgkin–Huxley membrane model. Two voltage-dependent conductances (g_{Na}, sodium and g_K, potassium) and one voltage-independent conductance ($\overline{g_L}$) in parallel with a capacitor describe the electrical properties of the membrane. The driving force for each current is the difference between the transmembrane potential, V_m, and the equilibrium potential, E, for the charge-carrying ion, for example, the driving force for I_{Na} is ($V_m - E_{Na}$). The equilibrium potential is calculated with the Nernst equation. (*b*, *c*). Voltage and time dependence of ionic conductances; comparison of the Hodgkin–Huxley model with experiment. (*b*) Model-simulated sodium conductance, g_{Na} (solid line) is superimposed on experimental data (open circles). V_m values (mV) are indicated by numbers on each trace; conductance scales (mMho/cm^2) are provided on the right. (*c*) Same as (*b*) for potassium conductance, g_K. V_m values (mV) are indicated by numbers above tracings and conductance scales (mMho/cm^2) are on the left. (From Hodgkin & Huxley, 1952, with permission.)

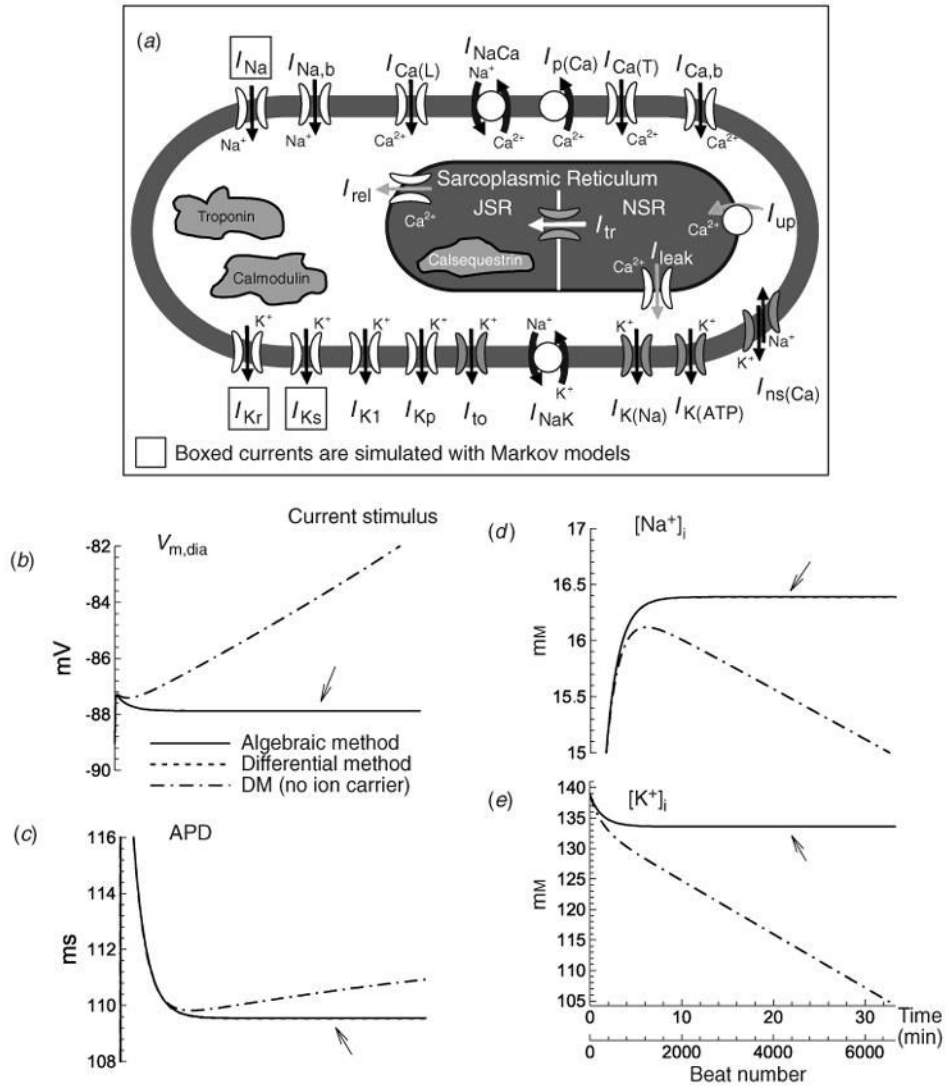

Fig 2.

A schematic of the Luo–Rudy dynamic (LRd) ventricular cell model. The model is based mostly on data from the guinea pig. Dynamics of intracellular Na^+, K^+, and Ca^{2+} are accounted for in the model. Dynamic changes of intracellular Ca^{2+} are determined by transmembrane fluxes, release and uptake by a two compartment sarcoplasmic reticulum (SR), and Ca^{2+} interactions with buffers. Boxed ionic currents are simulated with recently published Markov formulations (other currents follow the Hodgkin–Huxley formulation). Definitions: I_{Na}, fast sodium current; $I_{Ca(L)}$, calcium current through L-type calcium channels; $I_{Ca(T)}$, calcium current through T-type calcium channels (Droogmans & Nilius, 1989;Balke *et al*. 1992;Vassort & Alvarez, 1994); I_{Kr}, rapid delayed rectifier potassium current (Clancy & Rudy, 2001;Silva & Rudy, 2005); I_{Ks}, slow delayed rectifier potassium current (Silva & Rudy, 2005); $I_K{}^1$, inward rectifier potassium current (Kurachi, 1985); I_{Kp}, plateau potassium current (Yue & Marban, 1988;Backx & Marban, 1993); $I_{Na,b}$, sodium background current; $I_{Ca,b}$, calcium background current; I_{NaK}, sodium–potassium pump current; I_{NaCa}, sodium–calcium exchange current; $I_{p(Ca)}$ calcium pump in the sarcolemma (Caroni *et al*. 1983); I_{up}, calcium uptake from the myoplasm to network sarcoplasmic reticulum (NSR) (Tada *et al*. 1989); I_{rel}, calcium release from junctional sarcoplasmic reticulum (JSR) (Meissner, 1995); I_{leak}, calcium leakage from

NSR to myoplasm; I_{tr}, calcium translocation from NSR to JSR (Yue *et al*. 1985). The following currents (shaded in the figure) are included under pathological conditions: $I_{K(ATP)}$, ATP-sensitive potassium current, activated under conditions of ATP depletion (ischemia) (Kakei *et al*. 1985;Nichols *et al*. 1991;Noma, 1983;Shaw & Rudy, 1997a); $I_{K(Na)}$, sodium-activated potassium current, activated under conditions of sodium overload (Kameyama *et al*. 1984;Luk & Carmeliet, 1990;Wang *et al*. 1991;Faber & Rudy, 2000); $I_{ns(Ca)}$, non-specific calcium-activated current, activated under conditions of calcium overload (Ehara *et al*. 1988;Luo & Rudy, 1994b); Calmodulin and troponin represent calcium buffers in the myoplasm. Calsequestrin is a calcium buffer in the JSR. I_{to} the transient outward current is not present in guinea pig ventricular myocytes; it is included in certain simulations that examine its possible effects on the AP (Dumaine *et al*. 1999). Details of the LRd model can be found in the literature (Luo & Rudy, 1991;Luo & Rudy, 1994a;Zeng *et al.* 1995;Shaw & Rudy, 1997b;Viswanathan & Rudy, 1999;Viswanathan *et al*. 1999;Faber & Rudy, 2000;Hund *et al*. 2001;Rudy, 2002) and at http://rudylab.wustl.edu where the model code is also provided. (*b*)–(*e*). Stability of dynamic cell models (‘second-generation models’); effect of stimulus charge carrier. (*b*) V_m during the diastolic interval ($V_{m,dia}$); (*c*) action potential duration (APD); (*d*) $[Na^+]_i$, and (*e*) $[K^+]_i$ as a function of time during pacing with a current stimulus at a cycle length (CL) of 300 ms using the algebraic method (solid line) and the differential method (dashed line indicated with arrow); note that the two are indistinguishable. In both cases, the stimulus current carries K^+ ions into the cell and contributes directly to computed changes in intracellular ion concentrations. Note the stability (lack of drift) and identical results for both methods. An additional simulation is shown using the differential method and a current stimulus formulation that does not account for the charge carrying ion species (dash-dot line). Notice that computed parameters drift if ions carried by the stimulus current are not taken into account in the computation of ion concentration changes, which violates conservation laws. (From Hund *et al*. 2001, with permission.)

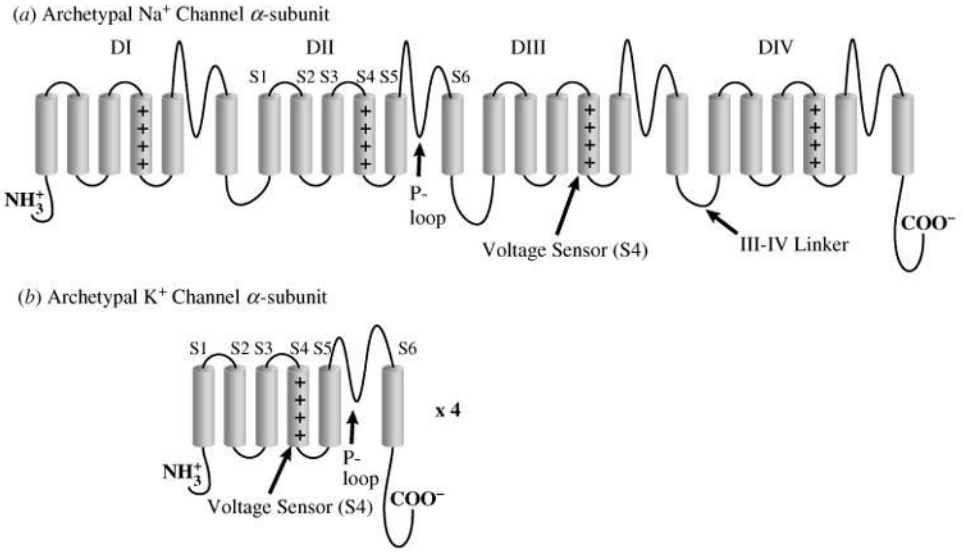

Fig 3.

Archetypal Na^+ and K^+ channel subunits. (*a*) The homomeric Na^+ channel is typically composed of a single four-domain α-subunit. Each domain consists of six transmembrane spanning segments (S1–S6). The fourth segment (S4) contains positively charged amino acids that confer voltage sensitivity on the channel. The S5–S6 linker forms a hairpin that enters the membrane to partially form the channel pore (P-loop), and determines ion selectivity. Several amino acids in the III–IV linker (labeled) have been linked to sodium channel fast inactivation. (*b*) Homomeric K^+ channels are typically composed of four identical α-subunits. Each subunit bears some functional resemblance to the domains of the Na^+ channel.

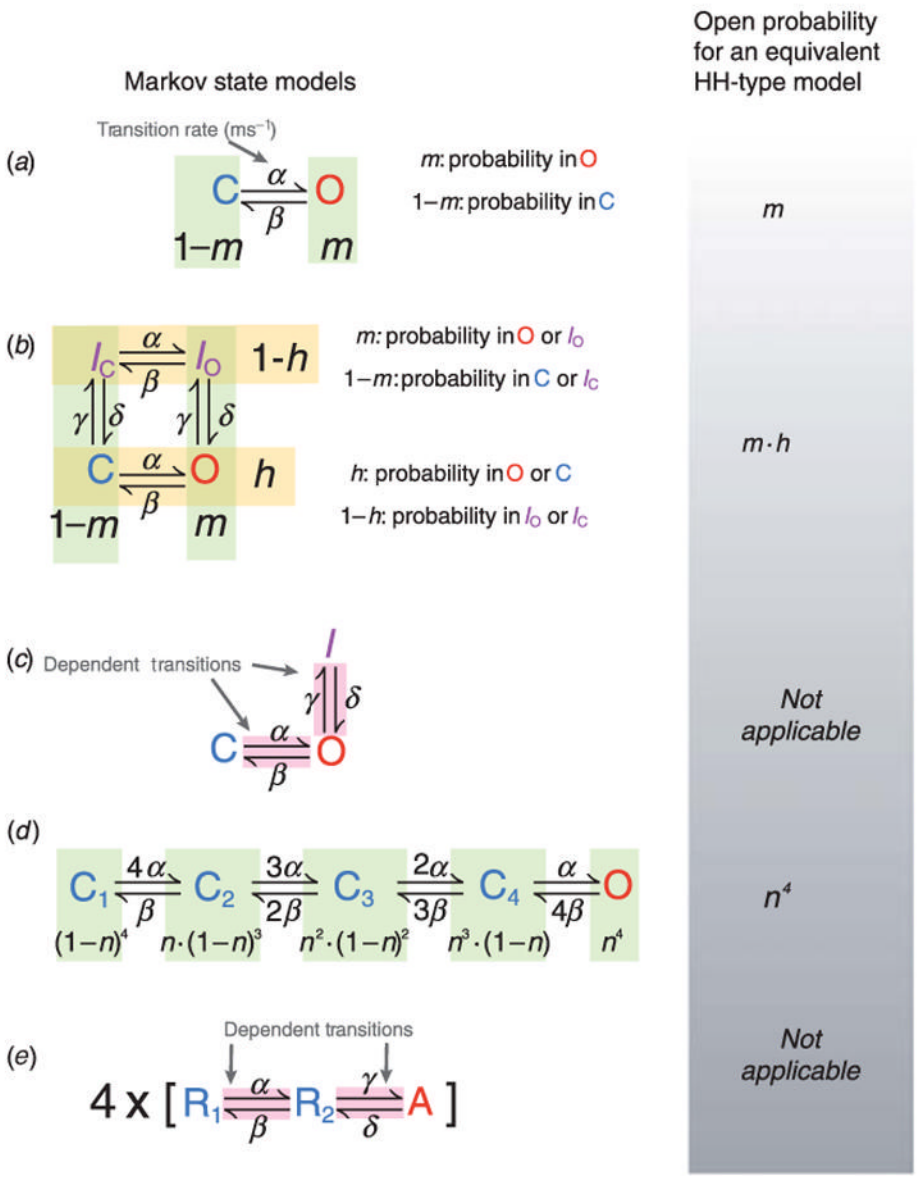

Fig 4.

Examples of Markov and equivalent Hodgkin–Huxley (HH) models of ionic currents. (*a*) A two-state closed (C) – open (O) model with α and β as forward and reverse transition rates. In the equivalent HH-type formulation, current activation is described by a single gating variable, such as *m*. (*b*) A four-state model with two independent transitions. C, Closed; O, open; I_C, closed-inactivated I_O, open-inactivated. The transition rates α, β between I_C and I_O and between C and O are identical, as are transition rates γ, δ between C and I_C and between O and I_O. Thus activation and inactivation transitions are independent in this model. Independent transitions are readily modeled using the HH formulation. The probability for current activation is *m* and the probability that it is not inactivated is *h*; the open probability is $m \cdot h$. (*c*) A three-state model with dependent transitions from C to O and O to I. There is no HH equivalent because of the dependent transitions. (*d*) K^+ channels have four identical subunits, suggesting four independent identical transitions to the activated state. When all subunits are activated, the channel is open. Assigning an activation gate *n*, the probability of all four subunits being in

the activated position, and thus the probability of the channel being open, is n^4. (*e*) Biophysical analysis has shown that each of the four voltage sensors in certain K^+ channels undergoes two transitions before channel opening. A model describing this gating property is shown; R_1 is the rest state, R_2 is an intermediate state, and A is the activated state. The channel is open when all four sensors are in the activated (A) position. Because transitions from R_2 to A depend on transitions from R_1 to R_2, a HH analog of the Markov model does not exist.

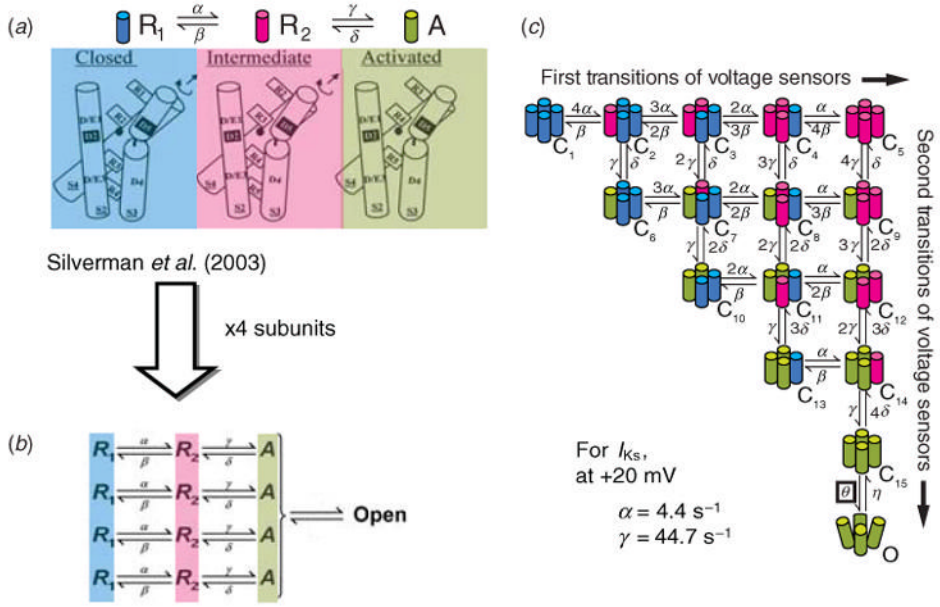

Fig 5.

Conformational changes of K^+ channels during activation. (*a*) Structural basis for two voltage-sensor transitions before channel opening (modified from Silverman *et al*. 2003, with permission). (*b*) Kinetic representation of the two voltage-sensor transitions in panel (*a*); all four α-subunits that form the channel undergo a first transition from a resting state (R_1) to an intermediate state (R_2) and a second transition from R_2 to an activated state (A). Once all voltage sensors are in the activated state, the channel can open. (*c*) Total number of combinations of voltage-sensor positions in the four subunits is 15 and can be represented by 15 closed states before channel opening. Blue, red, green indicate a voltage sensor in position R_1, R_2 or A, respectively. (From Rudy, 2006, with permission.) Panel (*a*) is based on data from ether-à-go-go (eag) and *Shaker* K^+ channels and is adapted from Silverman *et al*. 2003, with permission.

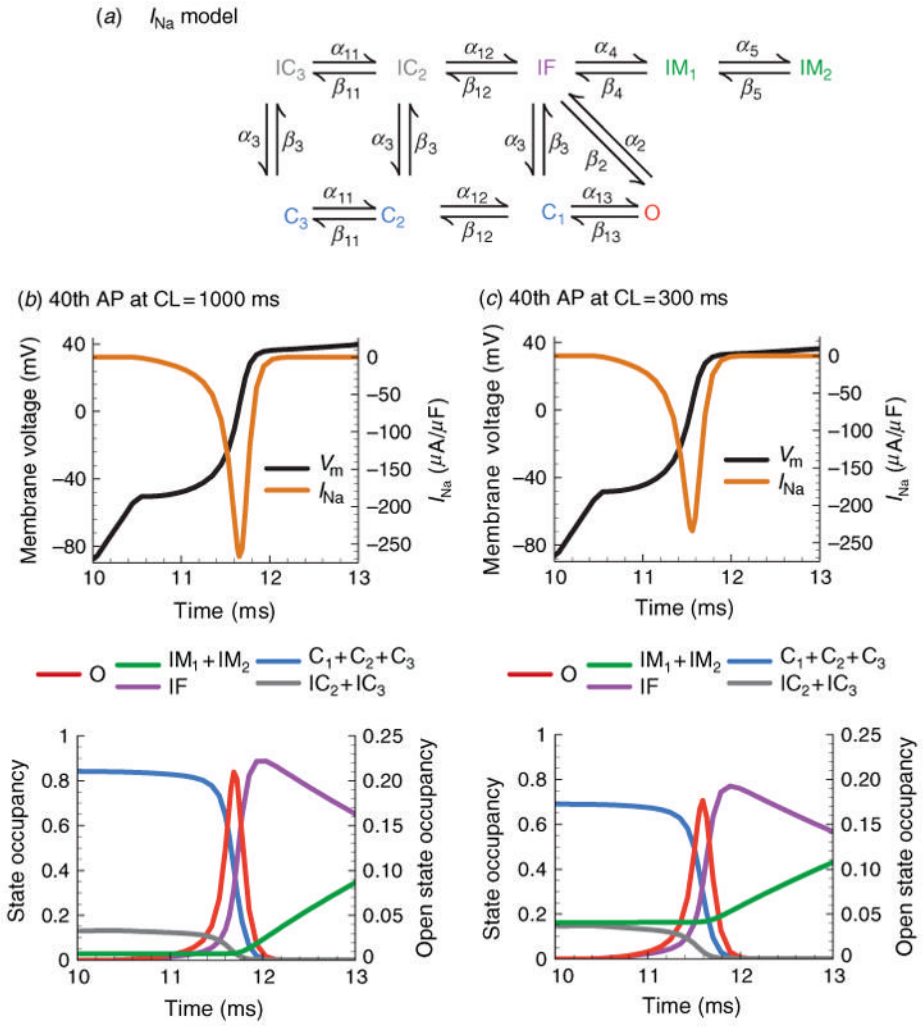

Fig 6.

Kinetic transitions of Na^+ channels during the AP at slow and fast rate. (*a*) Markov model of the Na^+ channel (Clancy & Rudy, 2002). States are color coded according to their type: closed-inactivated (gray), fast-inactivated (purple), slow inactivated (green), closed (blue), open (red). (*b*) I_{Na}, V_m and channel state occupancies during first 3 ms of the 40th AP at slow rate, CL = 1000 ms. The channel state occupancies during the same time period (bottom panel) show a rapid transition out of the closed states into the open state. The time required for inactivation after channel opening determines peak I_{Na} = –270 μA/μF. While V_m remains at depolarized potentials, channels enter the slow inactivated states. At slow rate, few channels are inactivated at the initiation of the AP. (*c*) I_{Na}, V_m and channel state occupancies during first 3 ms of the 40th AP at fast rate, CL = 300 ms. Accumulation of channels in the slow inactivated states (green) at fast rate results in reduction of I_{Na} during the upstroke and consequently a slower dV_m/dt_{max}.

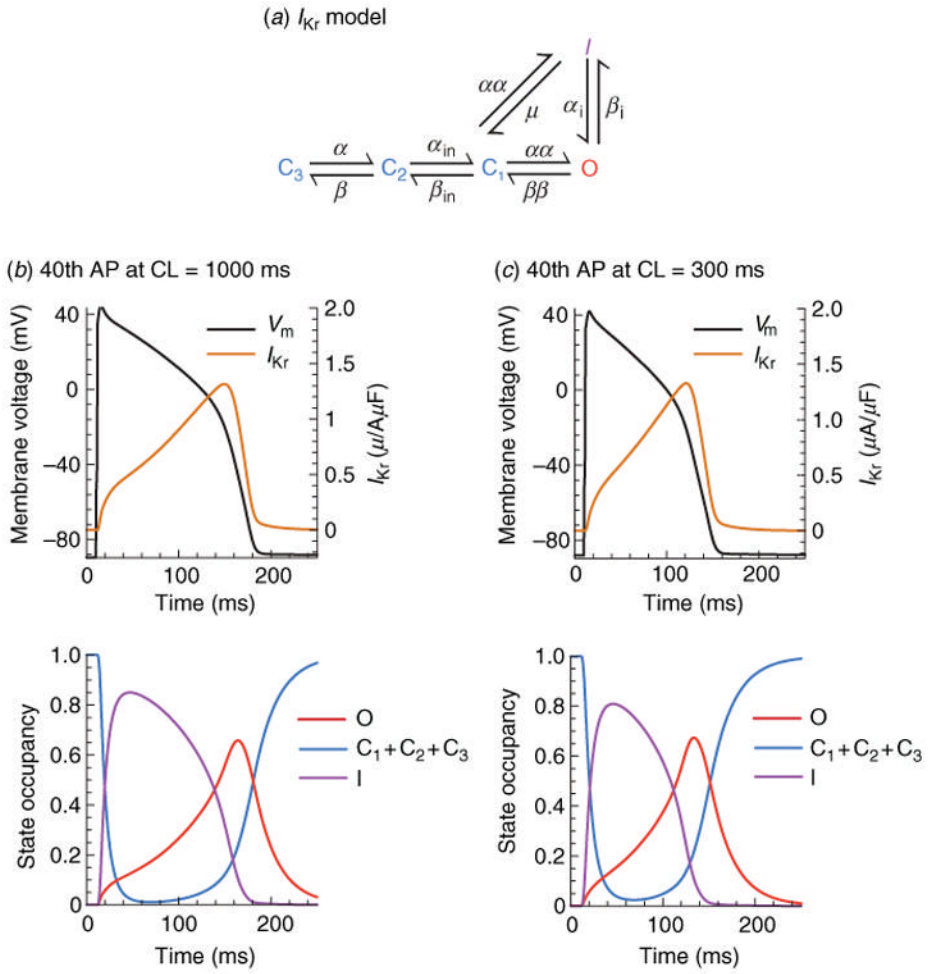

Fig 7.

Kinetic transitions of I_{Kr} channels during the AP at slow and fast rate. (*a*) Markov model of the I_{Kr} channel (Clancy & Rudy, 2001;Silva & Rudy, 2005). States are color coded according to their type: closed (blue), inactivated (purple), open (red). (*b*) I_{Kr}, V_m, and channel state occupancies during the 40th AP at slow rate, CL = 1000 ms. Even though I_{Kr} activates nearly instantaneously, few channels move into the open state because of rapid inactivation. Then, as V_m decreases, channels begin to recover from inactivation generating a pronounced peak of open-state occupancy and peak current during the late phase of the AP. (*c*) I_{Kr}, V_m, and channel state occupancies during the 40th AP at fast rate, CL = 300 ms. Surprisingly, peak I_{Kr} is not changed significantly at fast rate. Examination of the state occupancies (bottom panel) reveals that conditions at AP initiation are identical at fast and slow rates, preventing any current accumulation. However, faster increase of I_{Kr} at fast rate during the AP contributes to APD shortening.

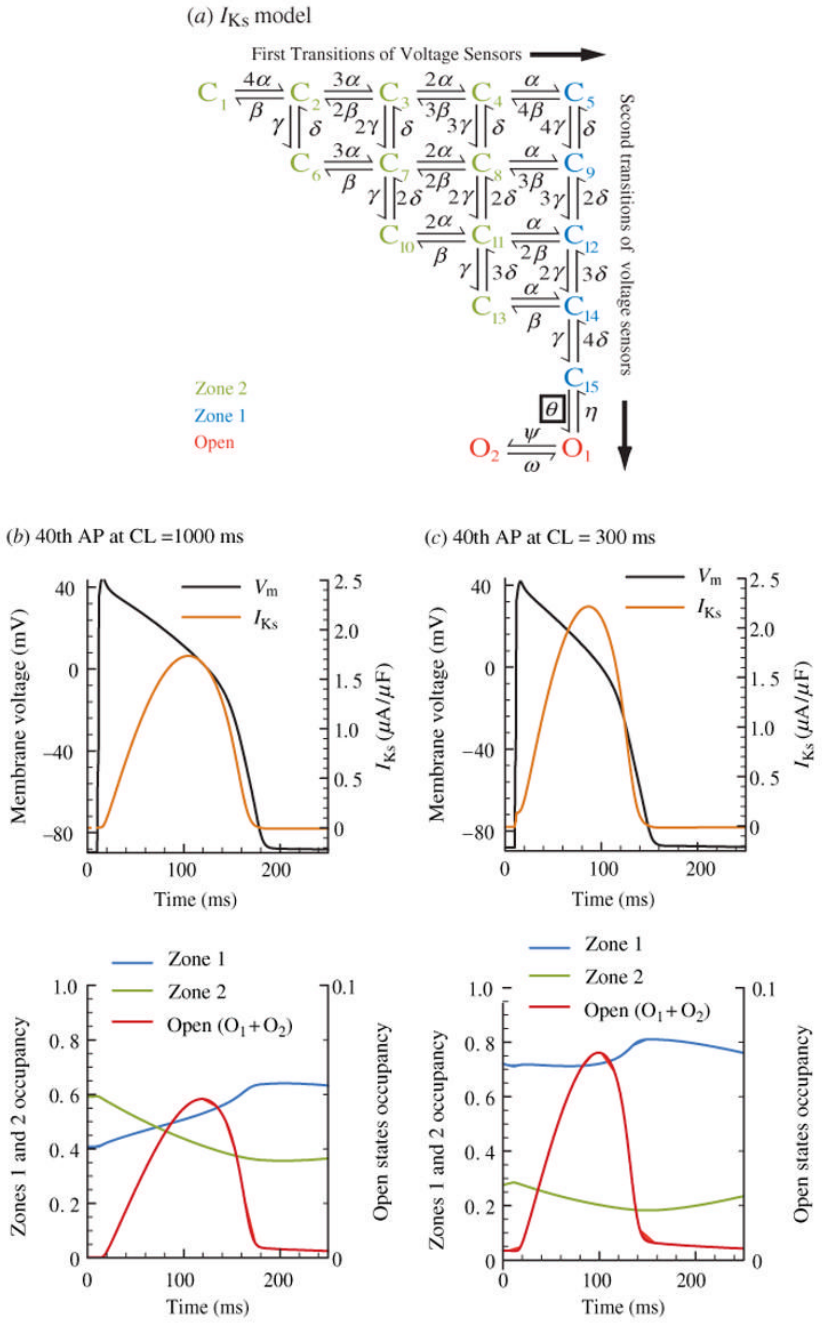

Fig 8.

Kinetic transitions of I_{Ks} channels during the AP at slow and fast rate. (*a*) Markov model of the I_{Ks} channel (Silva & Rudy, 2005). States are color coded according to their type: zone 2, closed states for which not all voltage sensors have completed the first transition (light green). zone 1, closed states for which all four voltage sensors have completed the first transition (blue). Open (red). (*b*) I_{Ks}, V_m and channel state occupancies during the 40th AP at slow rate, CL = 1000 ms. I_{Ks} rises slowly, resulting in peak current at the end of the AP where it most efficiently contributes to repolarization. Only 40% of channels reside in zone 1 at AP onset and can activate rapidly. While V_m remains depolarized, channels continue to transition from zone 2 to zone 1. (*c*) I_{Ks}, V_m, and channel state occupancies during the 40th AP at fast rate, CL = 300 ms. Since

the diastolic interval is shorter at CL = 300 ms, V_m stays at depolarized potentials for a larger percentage of time, which causes accumulation in zone 1 of closed states. At AP onset 75% of channels reside in zone 1, facilitating rapid transitions to the open state. This results in increased I_{Ks} late during the AP and APD shortening. Note that the mechanism for I_{Ks} increase is accumulation in closed states near the open state (zone 1) as opposed to open-state accumulation. The accumulation in zone 1 creates a reserve of channels that are ready to open rapidly, 'on demand' to generate a greater repolarizing current; we call this pool of channels 'available reserve'.

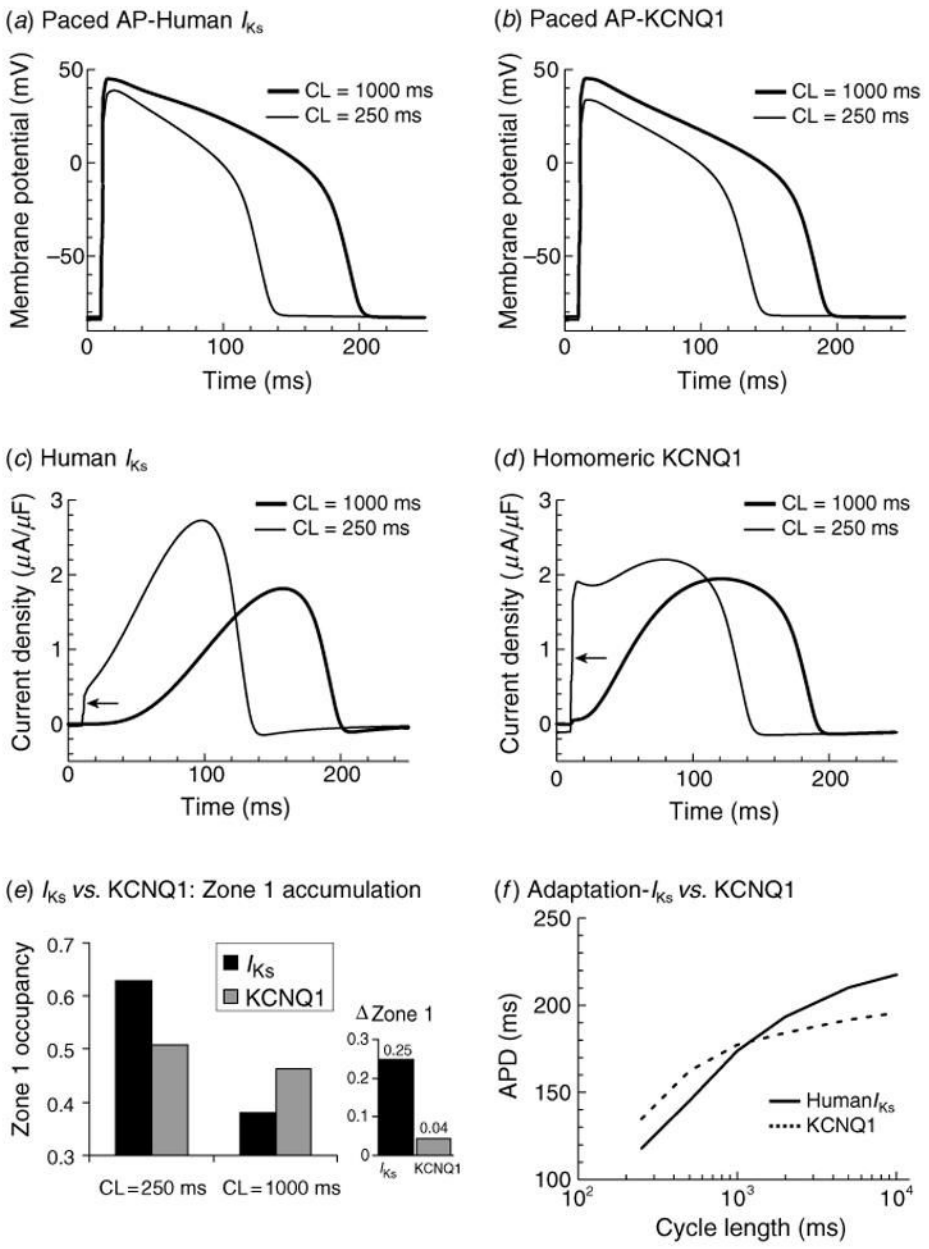

Fig 9.

APD rate-rdaptation with human I_{Ks} *vs*. human KCNQ1. (*a*) 40th AP computed with human I_{Ks} in the cell model at CL = 250 ms (thin line) and CL = 1000 ms (thick line). (*b*) Same as panel (*a*) with KCNQ1 replacing I_{Ks} in the model. (*c*) Human I_{Ks} during the AP at fast and slow rates. Some open-state accumulation at fast rate causes a small instantaneous current upon depolarization (arrow), while closed-state accumulation in zone 1 [see panel (*e*) and Fig. 10*c*] creates a reserve that allows the current to increase to a late peak that shortens APD effectively. (*d*) KCNQ1 during the AP at fast and slow rate. Slow kinetics of deactivation cause large open- state accumulation at fast rate and large instantaneous current upon depolarization (arrow). Note that in the absence of zone 1 reserve [see panel (*e*)], the current stays constant during the AP, lacking the late, repolarizing peak of I_{Ks}. (*e*) Human I_{Ks} (black) and KCNQ1 (gray) zone 1 occupancy at CL = 250 ms and 1000 ms. Accumulation in zone 1

at fast rate allows I_{Ks} to participate in adaptation. In contrast, little accumulation is seen in zone 1 for KCNQ1. ΔZone 1 is increase in zone 1 occupancy between CL = 1000 ms and 250 ms. (*f*) APD adaptation curves for an AP with human I_{Ks} (solid line) and KCNQ1 (dashed line). Lack of accumulation in zone 1 results in less APD shortening at fast rates with KCNQ1 compared to I_{Ks}. (From Silva & Rudy, 2005, with permission.)

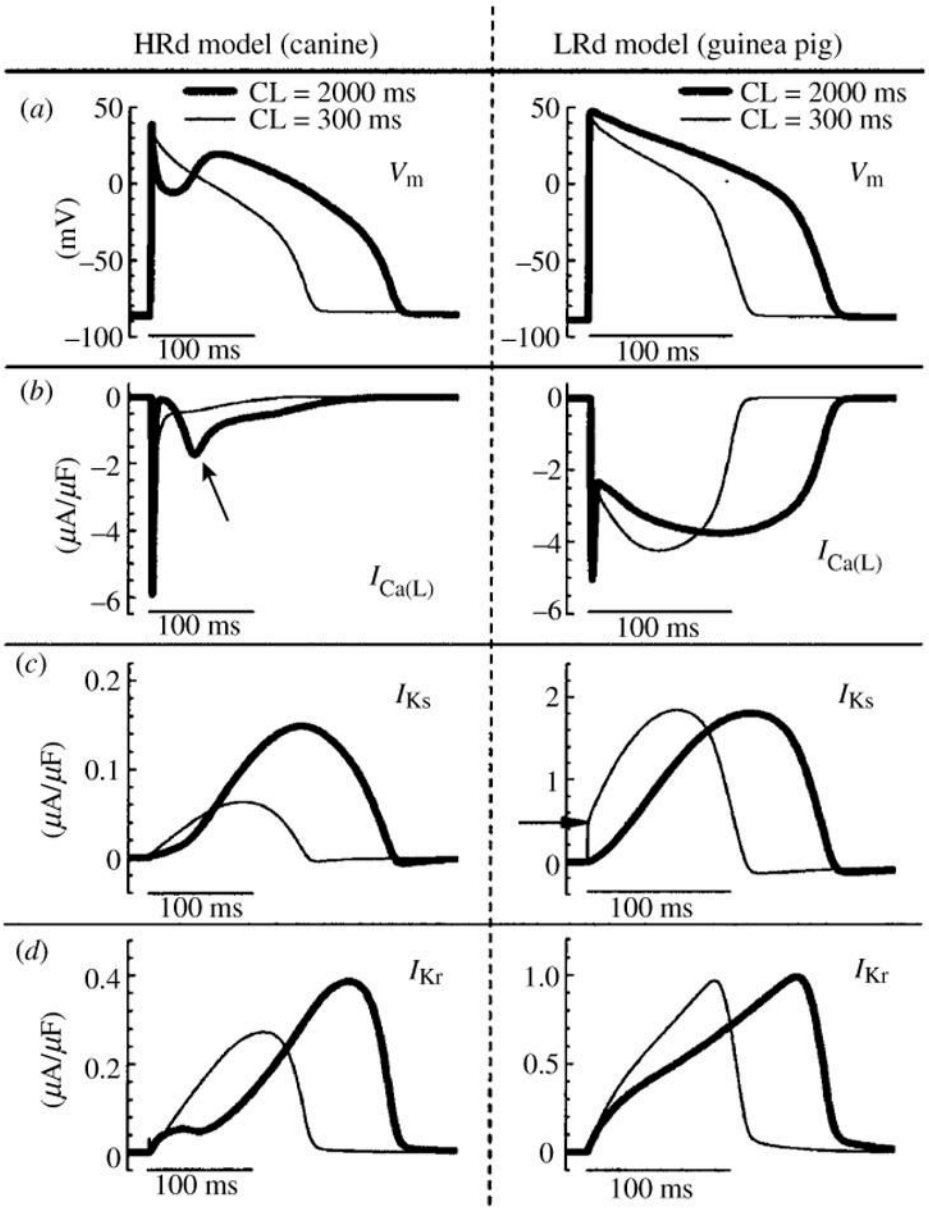

Fig 10.

Role of selected ion-currents in APD rate-adaptation in the canine and the guinea pig. Simulations conducted with HRd canine (Hund & Rudy, 2004) (left panels) and LRd guinea pig (Luo & Rudy, 1994a) (right panels) cell models. Steady-state values are shown at fast rate (CL = 300 ms, thin line) and slow rate (CL = 2000 ms, thick line). (*a*) AP; (*b*), $I_{Ca(L)}$; (*c*), I_{Ks} (arrow indicates I_{Ks} accumulation); (*d*), I_{Kr}. Schematic of the HRd model is provided in Fig. 31. (From Hund & Rudy, 2004, with permission.)

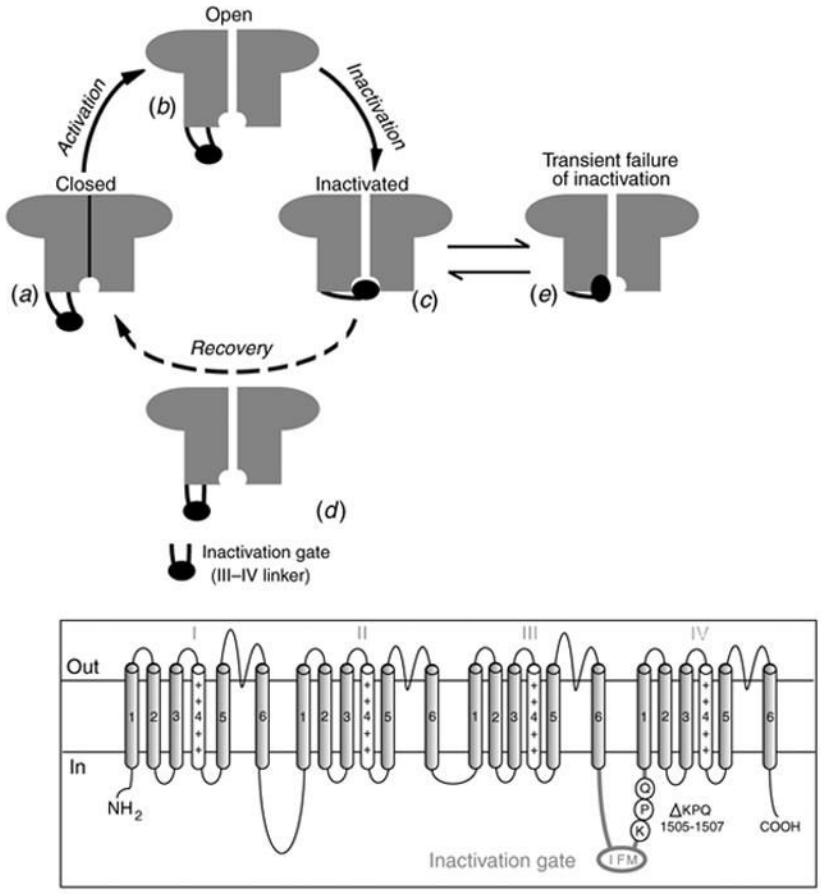

Fig 11.

The excitatory cycle of an ion channel and its alteration by the ΔKPQ deletion mutation of the Na^+ channel. (*a*)–(*e*) Schematic description of ion-channel transitions during the action potential. Because of the ΔKPQ structural defect in the III–IV linker, the 'hinged-lid' mechanism of inactivation fails to plug the channel pore in some channels, some of the time. Thus, ΔKPQ mutant channels experience a transient failure of inactivation [panel (*e*)]. The boxed panel shows the mutant channel, where three amino acids, Lys1505 (K), Pro1506 (P) and Gln1507 (Q) are deleted from the III–IV linker which participates in fast inactivation.

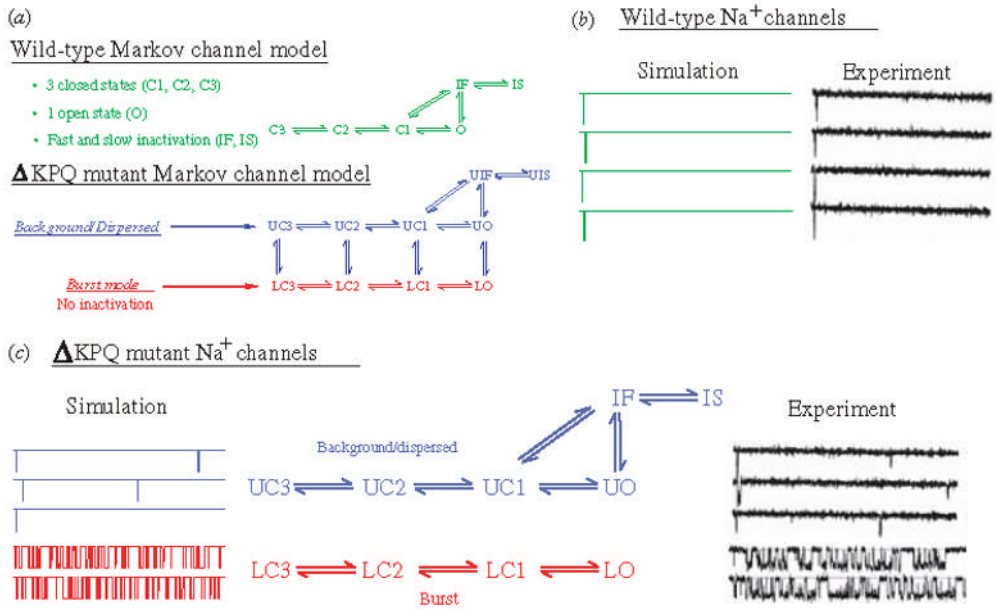

Fig 12.

(*a*) Markov models of the wild-type (WT) and ΔKPQ mutant Na^+ channels. The WT channel (top, green) contains three closed states, an open (conducting) state, and fast and slow inactivated states. The ΔKPQ channel has two modes of gating : the background (or dispersed) mode (blue) that is similar in structure to WT, and a burst mode (red) in which channels fail to inactivate. The U and L prefixes to ΔKPQ states indicate upper mode and lower mode, respectively. (Modified from Clancy & Rudy, 1999, with permission.) (*b*, *c*) WT and ΔKPQ single-channel gating. (*b*) Simulated WT channels (left) show only single openings in response to depolarization, as observed experimentally by Chandra *et al* (right). (*c*) Simulated ΔKPQ channels in the background mode (left, blue) show secondary reopenings beyond the first opening. In the burst mode (red), channels do not inactivate and fluctuate between open and closed states. Similar behavior is observed experimentally. (Modified from Clancy & Rudy, 1999; experimental data are reproduced from Chandra *et al*. 1998, with permission.)

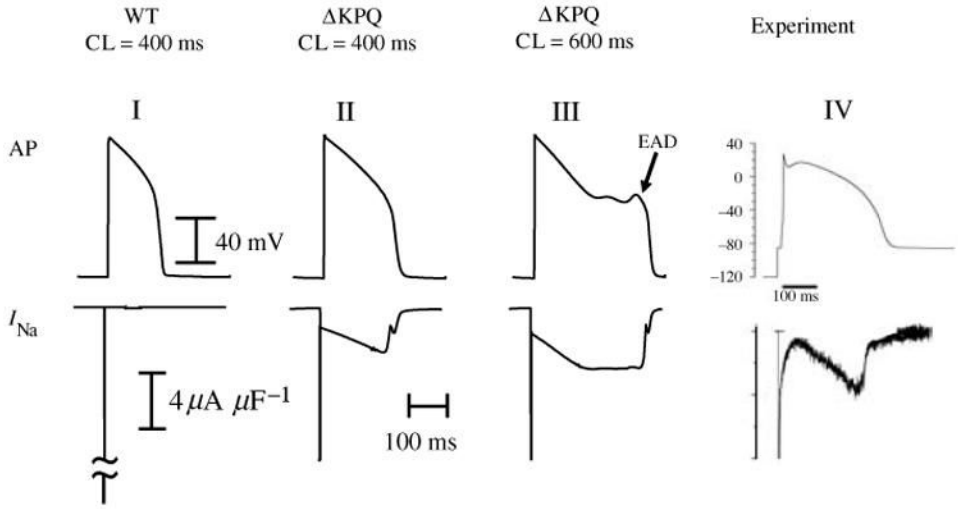

Fig 13.

Effect of ΔKPQ mutation on the whole-cell AP. Simulated AP is shown on top and corresponding I_{Na} on the bottom. ΔKPQ I_{Na} generates a persistent current during the AP plateau that prolongs APD (II) relative to WT (I). As pacing rate is decreased, persistent I_{Na} increases causing greater prolongation of APD and generation of EADs (III). Panel IV shows experimental AP-clamp mutant data from Wang *et al.* (1997); note the similar morphology of persistent I_{Na} to that simulated in panel II. (From Clancy & Rudy, 1999; experimental data are reproduced from Wang *et al*. 1997, with permission.)

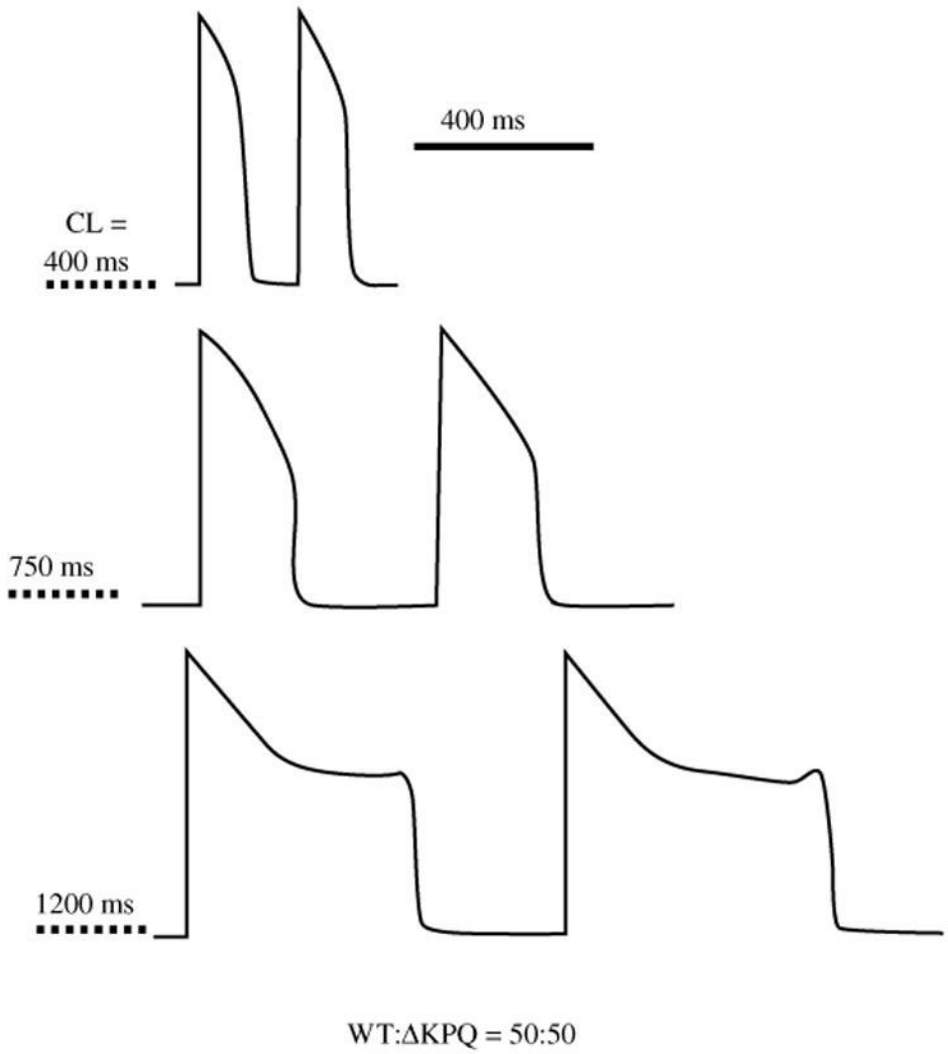

Fig 14.

Effect of ΔKPQ at various pacing cycle lengths (CL). The cell contains equal densities of WT and mutant channels (50%/50%). As pacing rate decreases, APD prolongation becomes more pronounced. At a bradycardia CL of 1200 ms, EADs develop. (From Clancy & Rudy, 1999, with permission.)

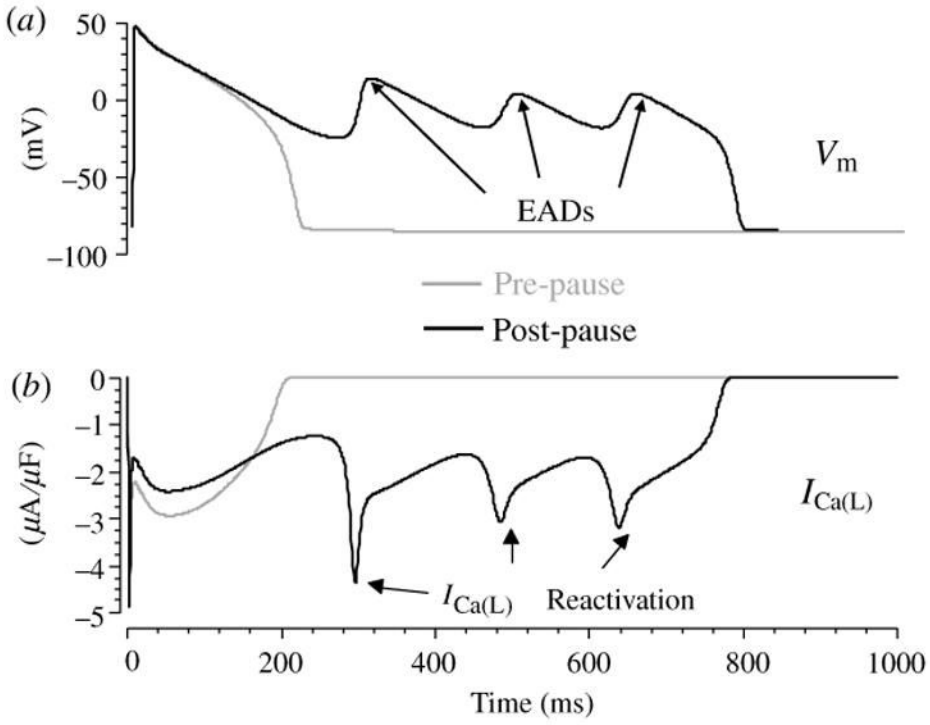

Fig 15.

Ionic mechanism of plateau EADs. (*a*) Pre-pause (gray) and post-pause (black) APs. (*b*) The corresponding $I_{Ca(L)}$ during the AP. Reactivation of $I_{Ca(L)}$ [(*b*), arrows] depolarizes the membrane to generate the EADs [(*a*), arrows]. (Modified from Viswanathan & Rudy, 1999, with permission.)

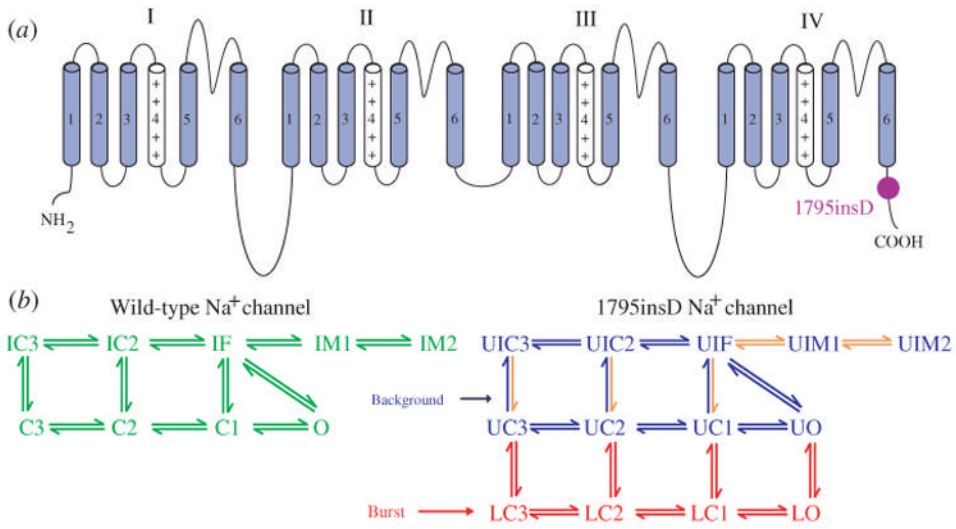

Fig 16.

Markov models of WT and 1795insD mutant Na^+ channels. (*a*) Location of the aspartic acid insertion in the C terminus of the 1795insD mutant channel protein. (*b*) The WT Markov model (left, green) and the 1795insD Markov model (right) with its background mode (blue) and burst mode (red). Orange arrows indicate transitions with rate modified by the mutation (e.g. slower recovery from IC3 to C3; see text). IM1 and IM2 are intermediate inactivation states. (Modified from Clancy & Rudy, 2002, with permission.)

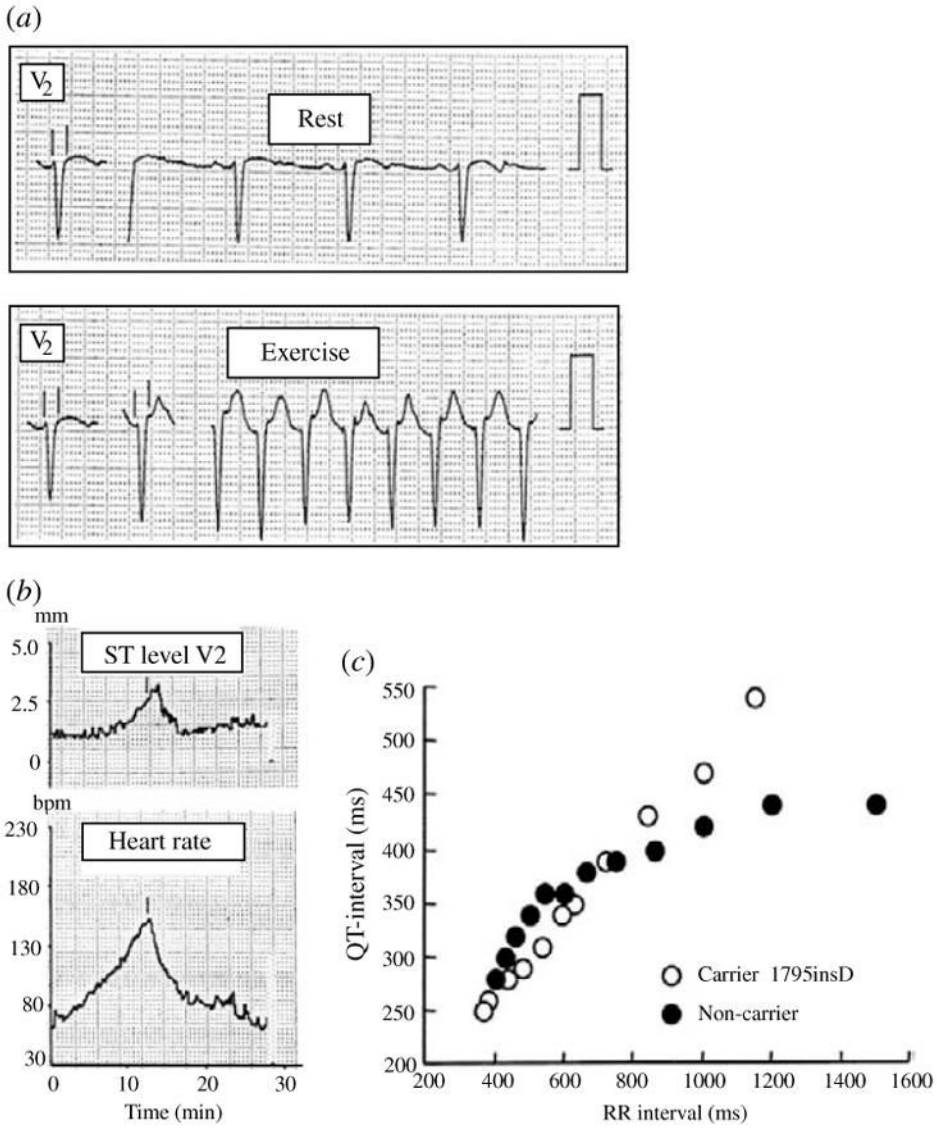

Fig 17.

Clinical data from patients with the 1795insD mutation. (*a*) ST-segment elevation at fast heart rate (Exercise, bottom) compared to control (Rest, top) in lead V_2 of the ECG. (*b*) Indicates that the ST-segment elevation (top) increases with heart rate (bottom). (*c*) Indicates much greater QT prolongation in mutation carriers (○) compared to non-carriers (●) as heart rate decreases. (From Veldkamp *et al*. 2000, with permission.)

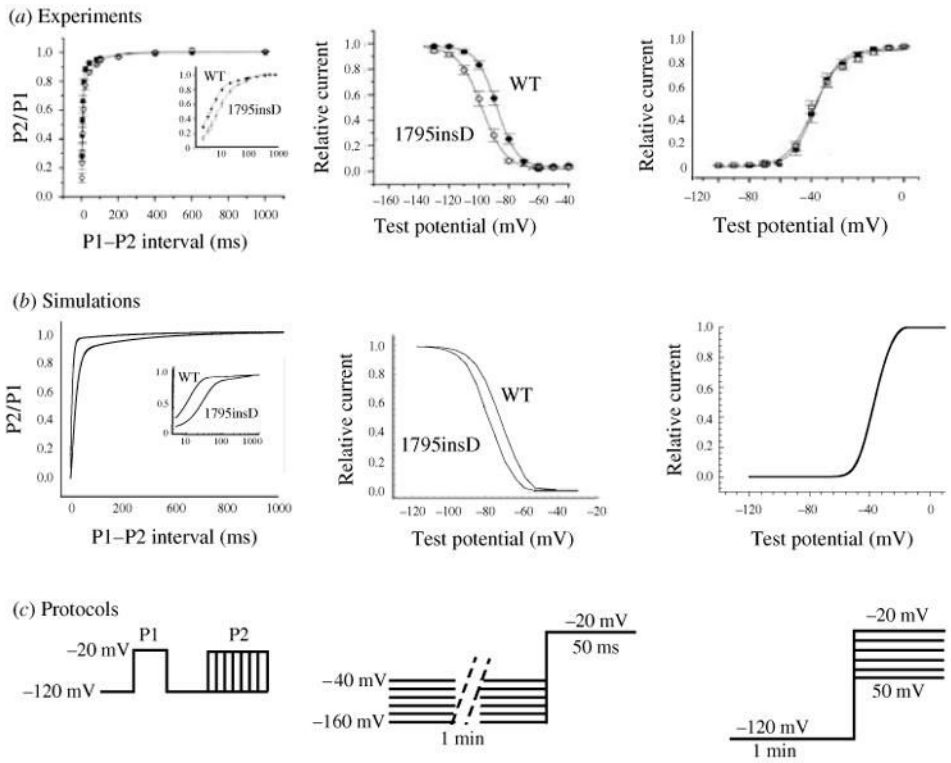

Fig 18.

Properties of WT and 1795insD mutant I_{Na} current. (*a*) Experimental data from Veldkamp *et al*. (2000). (*b*) Simulations of the experimental protocols. (*c*) Diagrams illustrating the protocols. Voltage dependence of activation (right) is indistinguishable between WT and mutant. Channel availability curve (middle) is shifted to the left by the mutation because of increased absorbency of inactivation states; thus, at any given voltage, channel availability is reduced. Mutant channels recover slower from inactivation (left); on an expanded log scale (inset) it is evident that recovery time could be as long as 100 ms, which is on a timescale of the AP duration. (From Clancy & Rudy, 2002; experimental data are reproduced from Veldkamp *et al*. 2000, with permission.)

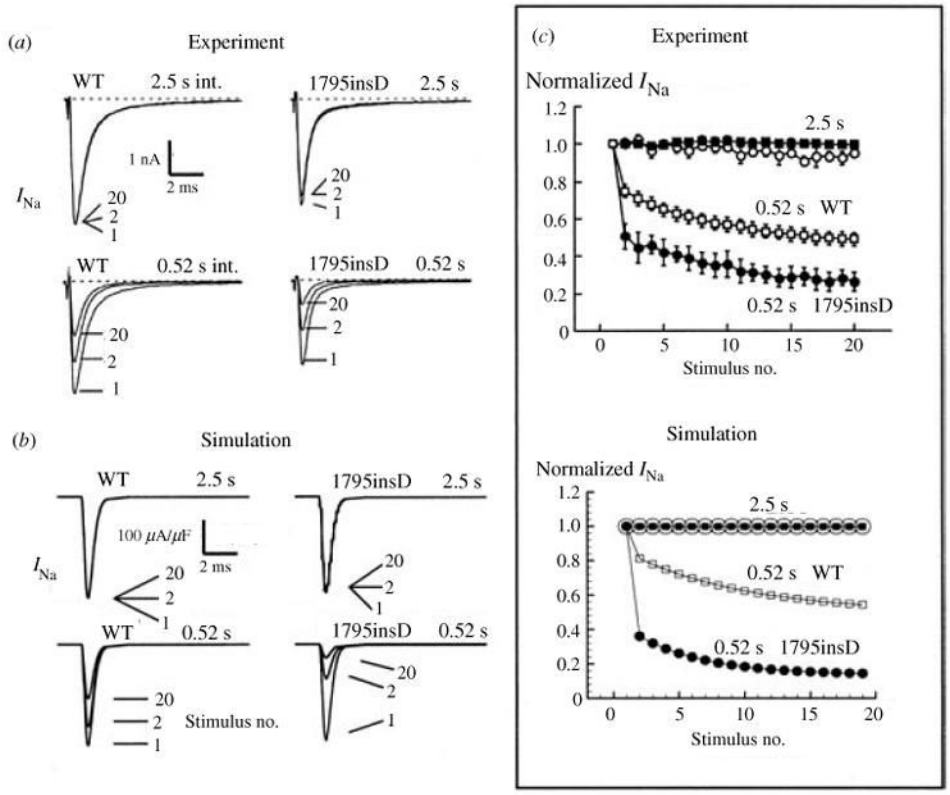

Fig 19.

The 1795insD mutation causes rate-dependent reduction of I_{Na}. A train of 500 ms depolarizing pulses are applied at slow (2·5 s interval) or fast (0·52 s interval) rate. (*a*) I_{Na} for WT (left) and mutant (right) channels at these slow (top) and fast (bottom) rates. At fast rate there is progressive (cumulative) loss of I_{Na} from stimulus 1 to stimulus 2 to stimulus 20. (*b*) Results of the corresponding simulation. (*c*) Summary of the results of panels (*a*) and (*b*) indicating normalized peak I_{Na} for 20 stimuli during the same protocol. At slow rate (2·5 s), there is no loss of current. At fast rate (0·25 s) the mutant loss is greater than WT. Experiment (top) and simulation (bottom) show similar behavior. (From Clancy & Rudy, 2002; experimental data are reproduced from Veldkamp *et al*. 2000.)

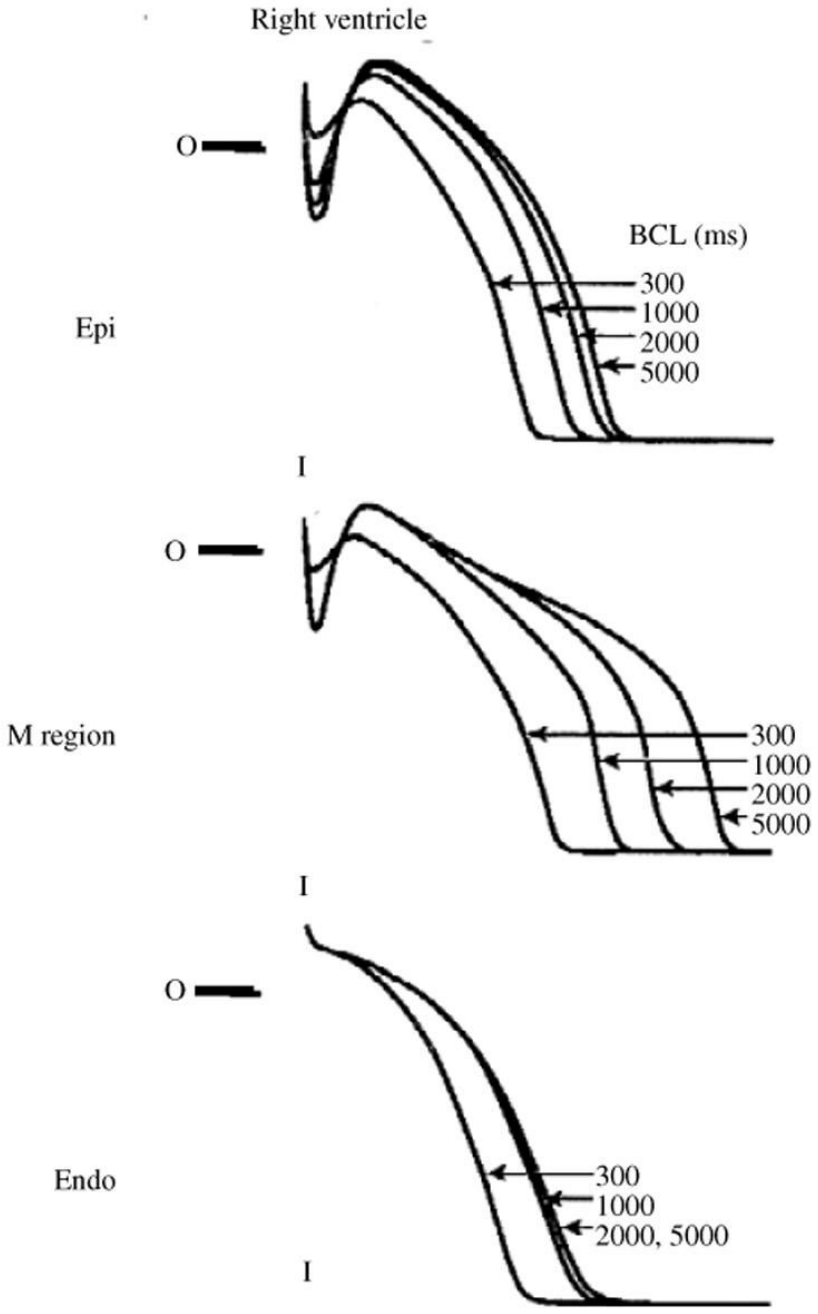

Fig 20.

AP of different right ventricular cell types. Epicardial cells (top) show a distinct ‘spike and dome’ morphology of the AP, with a deep notch separating spike from dome. M cells from the mid-myocardium (middle) typically have a more shallow notch; their I_{to} and I_{Ks} densities are lower than those of epicardial cells and as a result their AP repolarization phase is easily perturbed by mutations or drugs, or by changes of pacing rate (shown in the figure). Endocardial cells (bottom) do not express I_{to} and their AP does not display a notch. (From Sicouri & Antzelevitch, 1991, with permission.)

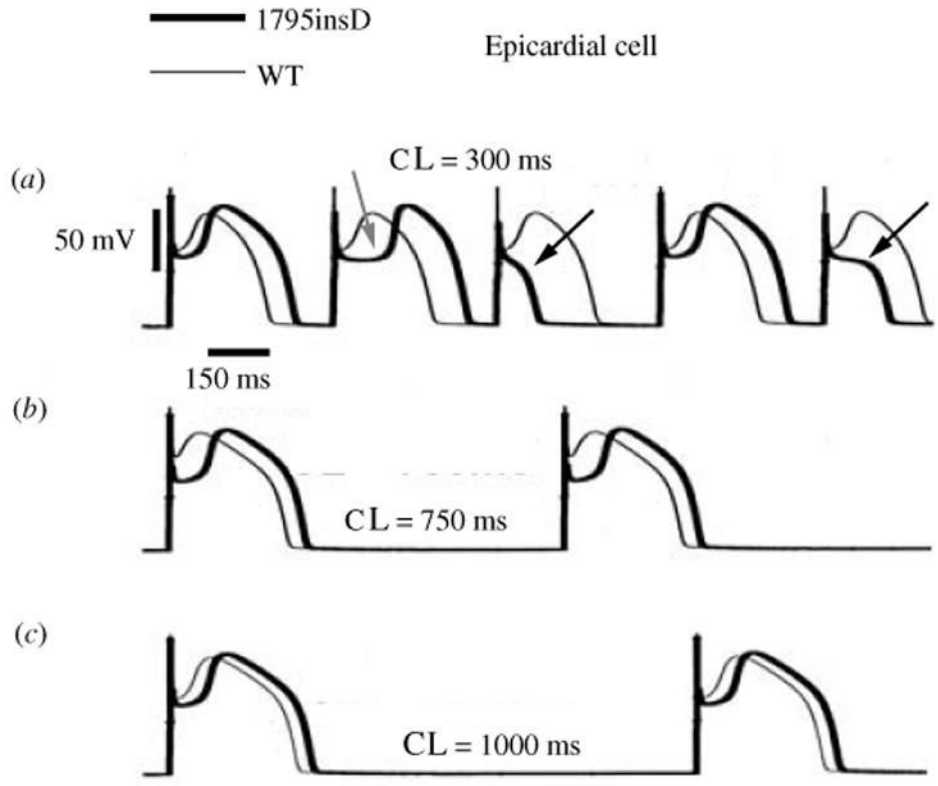

Fig 21.

Rate-dependent effect of 1795insD on epicardial cell AP. At fast pacing (*a*) the AP morphology alternates between 'loss of dome' (black arrows) and a prolonged notch ('coved dome', gray arrow). At intermediate rate (*b*) the AP has a coved-dome morphology on every beat. At slow rate (*c*) WT and mutant AP morphologies are similar. (From Clancy & Rudy, 2002, with permission.)

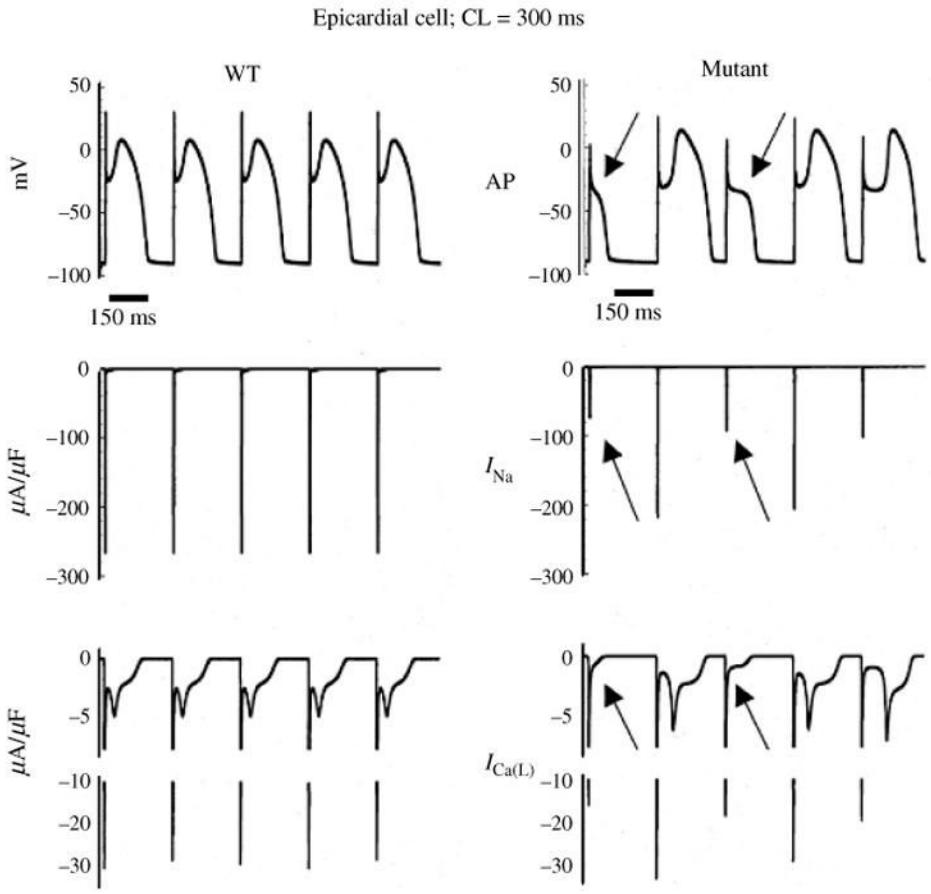

Fig 22.

Mechanism of 1795insD effect on AP of epicardial cell during fast pacing. APs are shown on top, with corresponding I_{Na} and $I_{Ca(L)}$ in middle and bottom panels, respectively. For WT channels (left) I_{Na} is fully recovered between beats. $I_{Ca(L)}$ develops its plateau phase, and the AP is normal on every beat. For mutant channels (right) cumulative loss of I_{Na} (arrows in middle panel) causes premature repolarization, loss of plateau $I_{Ca(L)}$ (arrows in bottom panel) and loss of the AP dome (arrows in top panel). For some beats (e.g. last AP shown) the I_{Na} loss is not sufficient to cause a complete loss of the dome and the notch is greatly prolonged. (From Clancy & Rudy, 2002, with permission.)

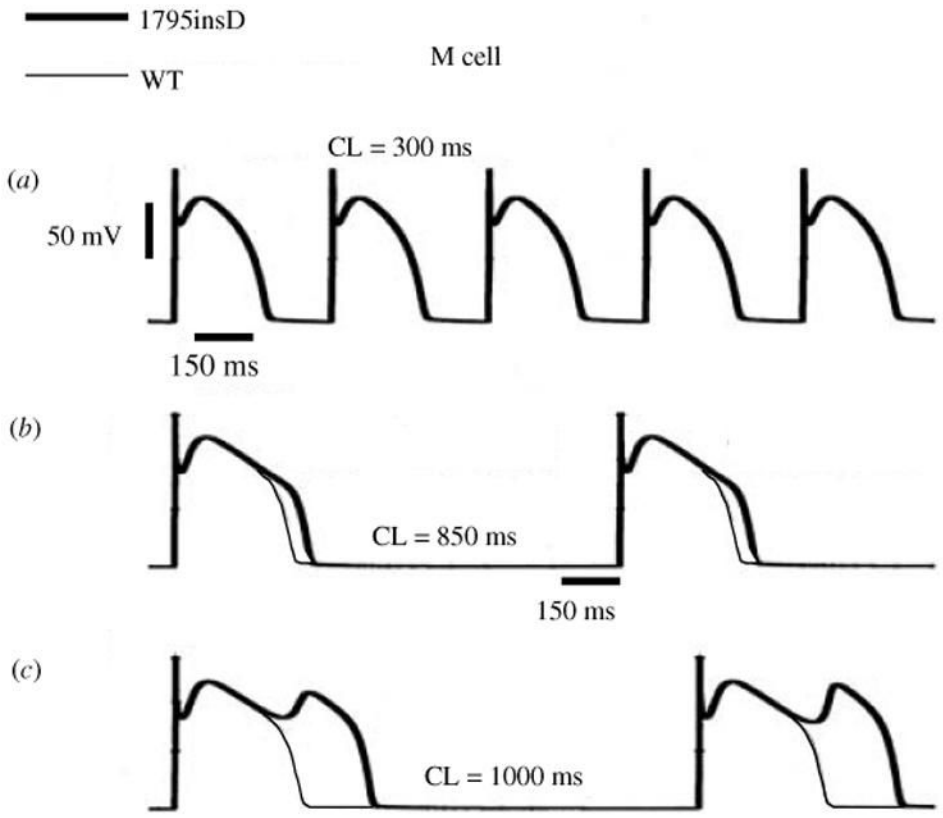

Fig 23.

Rate-dependent effect of 1795insD on M cell AP. At fast rate (*a*) the WT and mutant APs are indistinguishable. At a rate of CL = 850 ms (*b*) mutant AP is prolonged relative to WT. At slow rate (*c*) of CL = 1000 ms, mutant APD is greatly prolonged and arrhythmogenic EADs develop. (From Clancy & Rudy, 2002, with permission.)

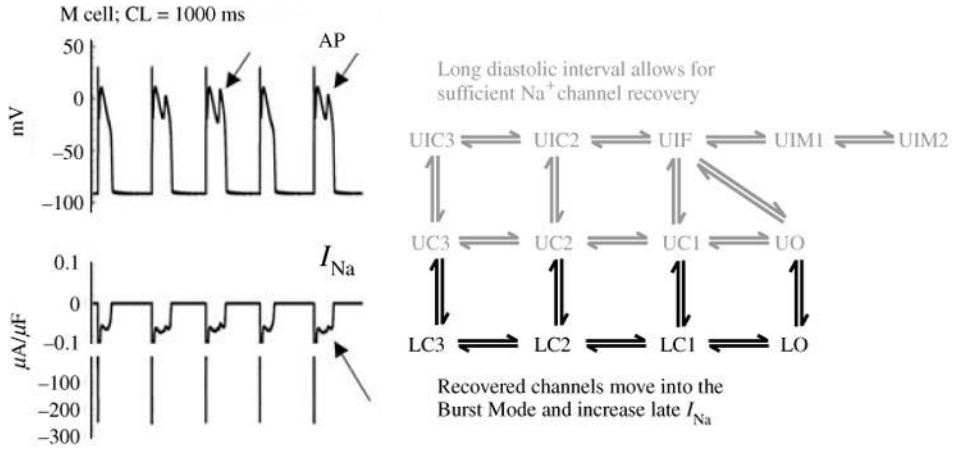

Fig 24.

Mechanism of 1795insD effect on AP of M cell during slow pacing. Left: mutant APs are shown on top, with corresponding I_{Na} on bottom. Mutant I_{Na} generates current during the AP plateau (bottom arrow) that prolongs the APD and results in EAD formation (top arrows). Right: the I_{Na} Markov model identifies the processes that lead to late I_{Na} during the AP plateau. At slow rate, there is sufficient time between beats for channels to recover from inactivation into the closed and open states of the background mode (gray). From these states, they can transition into the burst mode (black) to generate late I_{Na}. (From Clancy & Rudy, 2002, with permission.)

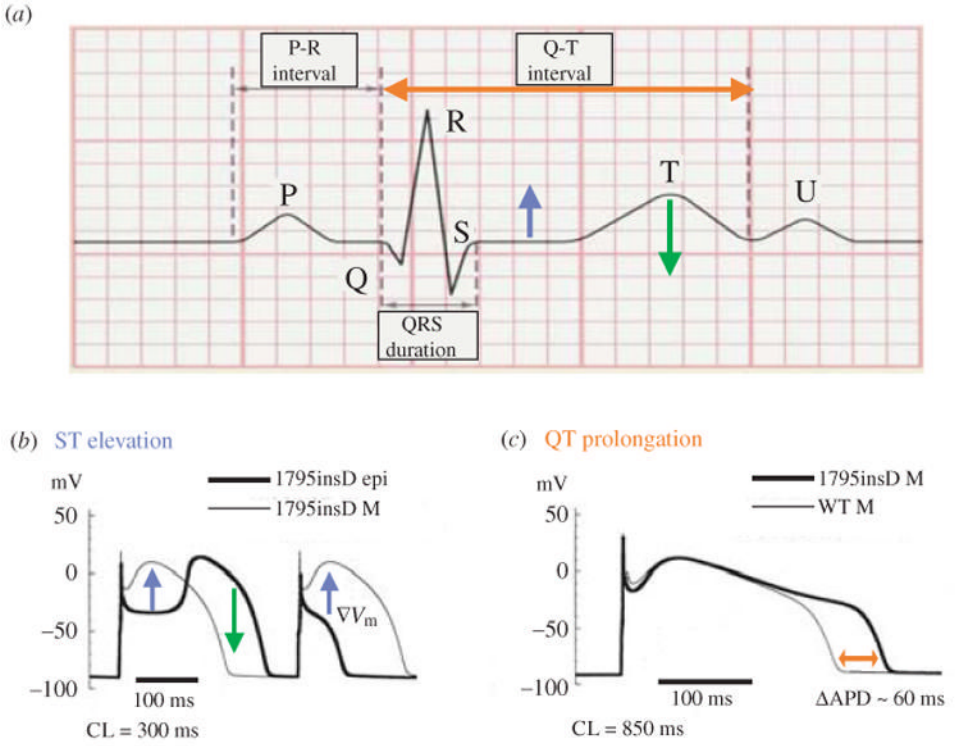

Fig 25.

Mechanisms of ECG changes caused by the 1795insD mutation. (*a*) Stylized ECG defining the different deflections, waves and intervals. (*b*) Cellular mechanism of ST elevation and T-wave inversion. At fast rate, loss of dome or coved dome in epicardial cells creates a voltage gradient (∇V_m, blue arrows) between these cells (bold line) and M cells (thin line) during the AP plateau, leading to ST-segment elevation on the ECG [blue arrow in (*a*)]. Greatly prolonged notch in a coved-dome epicardial AP could delay its repolarization beyond that of M cell, thus reversing the normal gradient (normally, M cells have the longest APD and repolarize last) as indicated by the green arrow in (*b*), possibly leading to T-wave inversion [green arrow in (*a*)]. (*c*) Cellular mechanism of QT prolongation. At slow rate M-cell APD is prolonged by the mutation (red arrow). The delayed repolarization is reflected as QT prolongation on the ECG [red arrow in (*a*)]. [Simulation data in (*b*) and (*c*) are reproduced from Clancy & Rudy, 2002, with permission.]

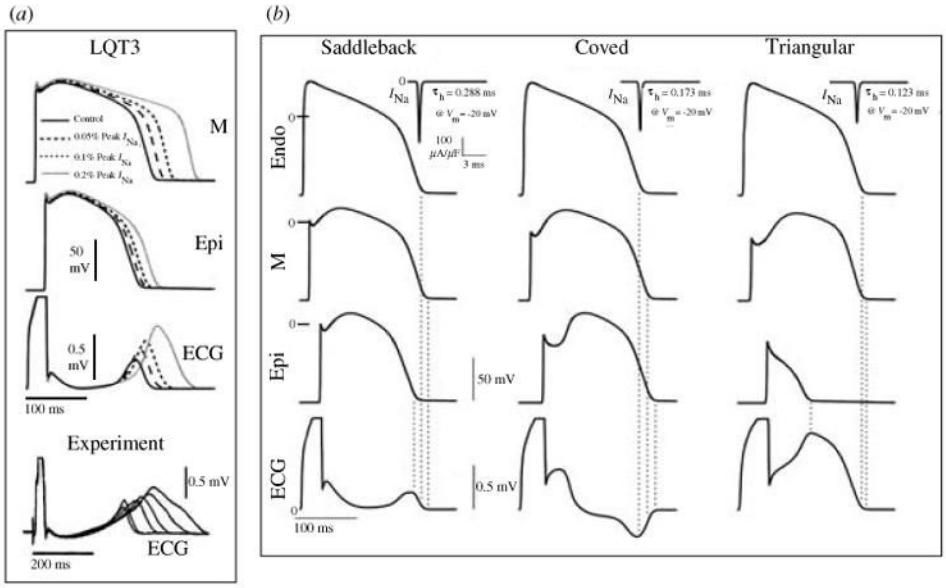

Fig 26.

Simulations of ECG changes in LQT3 and Brugada syndromes. The simulations were conducted in a 1-dimensional fiber containing regions of epicardial (Epi), endocardial (Endo) and M cells. The different cell types AP and ECG are shown. (*a*) LQT3 is simulated, with increasing severity, by incorporating a late I_{Na} component with magnitude of 0.05%, 0.1%, and 0.2% of peak I_{Na}. APD prolongation increases with increasing severity and M cell APD prolongs more than epicardial APD, increasing dispersion of repolarization. These AP changes are reflected as QT prolongation and T-wave widening in the ECG. These simulation results are consistent with experimental data of Shimizu & Antzelevitch, 1997 recorded in a transmural wedge preparation (shown in the bottom panel). (*b*) Brugada syndrome at increasing severity is simulated by accelerating fast inactivation of I_{Na} (progressively decreasing its time constant, τ_h, from left to right). For all degrees of severity, ST-segment elevation is observed on the ECG, with typical ‘saddleback’, ‘coved’, and ‘ triangular ’ morphologies as severity increases. (From Gima & Rudy, 2002; experimental data in panel (*a*) are reproduced from Shimizu & Antzelevitch, 1997, with permission.)

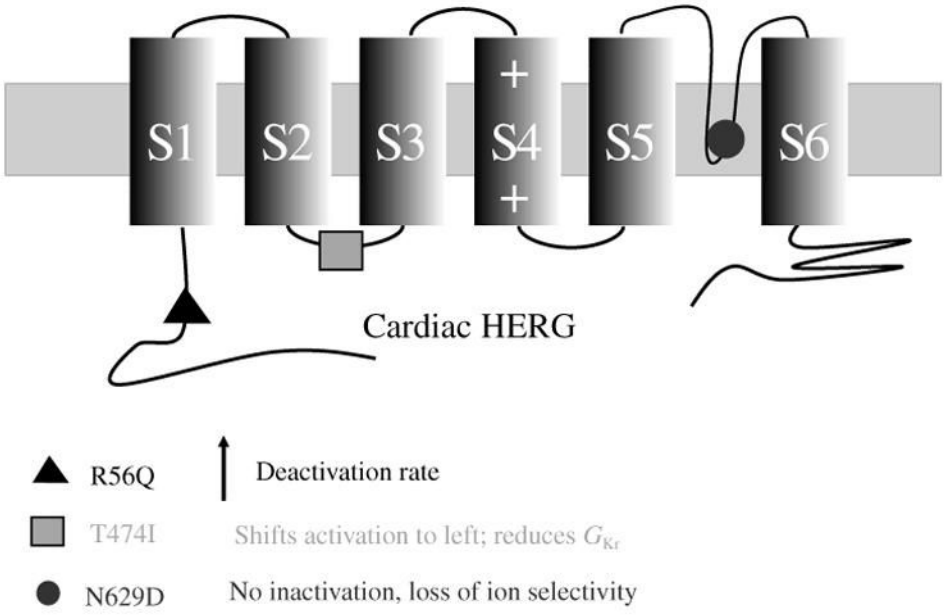

Fig 27.

HERG mutations. Structure of cardiac HERG showing locations of mutations simulated in this study. Kinetic changes caused by the mutations are summarized below the diagram. For Markov model of I_{Kr} see Fig. 7*a* (Clancy & Rudy, 2001;Silva & Rudy, 2005).

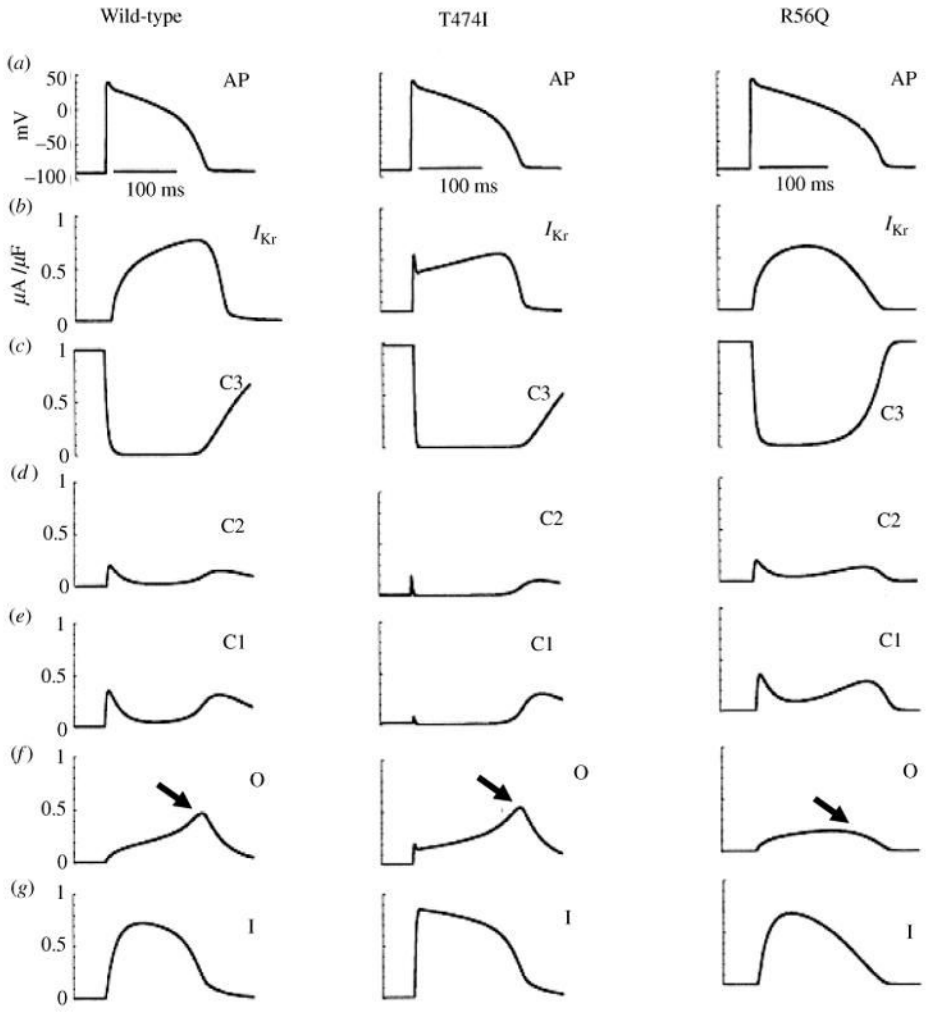

Fig 28.

Effects of HERG mutations on the AP. (*a*) The AP (1000th paced beat) at a cycle length (CL) =750 ms. (*b*) Denotes I_{Kr} during the AP. (*c*)–(*g*) The probabilities of residence in the indicated channel states over the course of the AP. Left column: wild-type; middle column: T474I mutation; right column: R56Q mutation. (From Clancy & Rudy, 2001, with permission.)

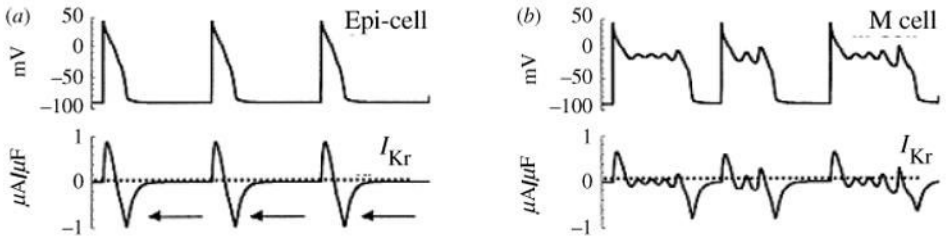

Fig 29.

Simulation of HERG N629D mutation. AP and I_{Kr} during the AP are shown for (*a*) epicardial cell and (*b*) M cell. (Adapted from Clancy & Rudy, 2001, with permission.)

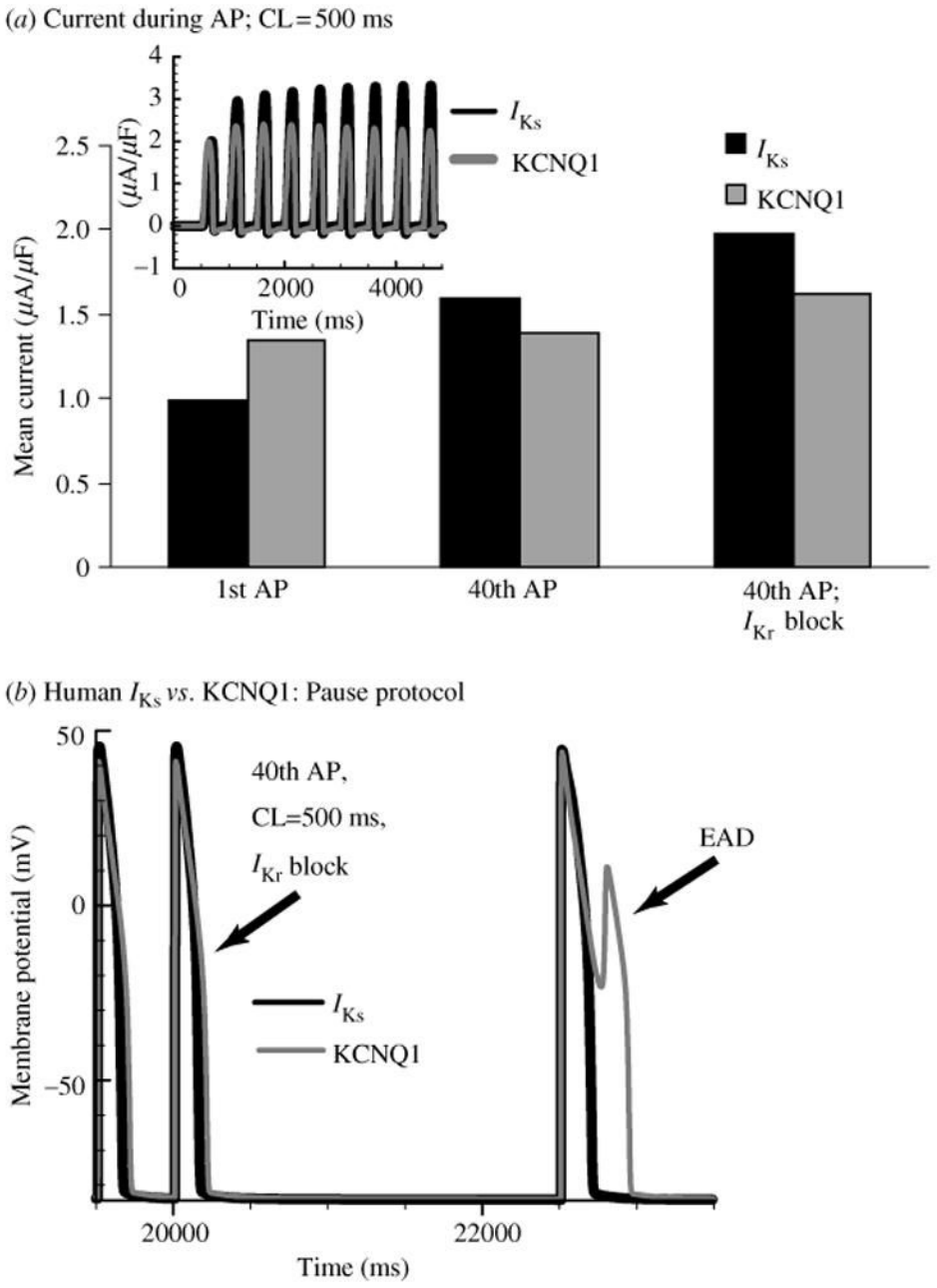

Fig 30.

I_{Ks} as repolarization reserve. (*a*) Mean I_{Ks} during the AP (black) accumulates during pacing, showing significant increase over 40 paced APs. In contrast, KCNQ1 shows only a small increase. When I_{Kr} is blocked (right bars) I_{Ks} increases further, providing a compensating repolarizing current. (*b*) When I_{Kr} is blocked, a post-pause AP develops an EAD with KCNQ1 (gray) but not with I_{Ks} (black). (From Silva & Rudy, 2005, with permission.)

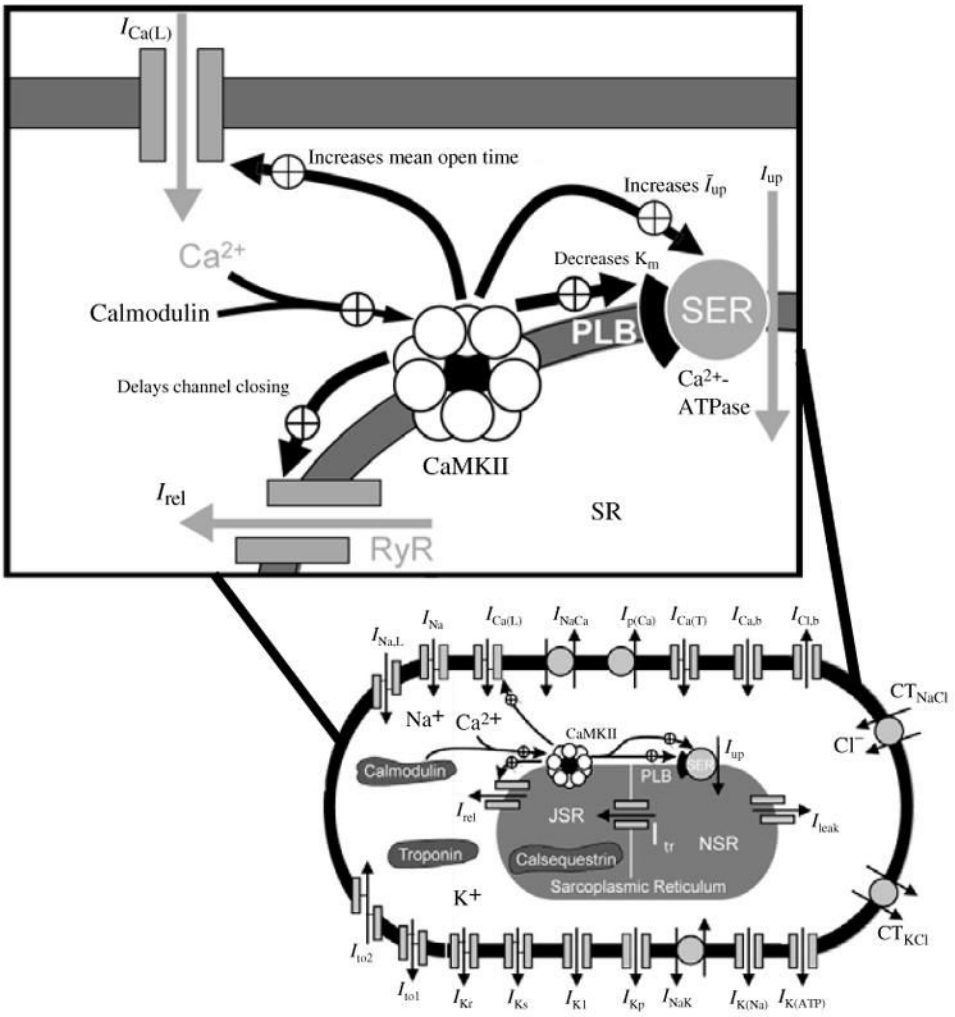

Fig 31.

CaMKII pathway incorporated into a canine ventricular cell model. Bottom: cell model containing the CaMKII pathway. Top: a detailed view of the CaMKII pathway and substrates. Upon Ca_{2+} binding, CaMKII phosphorylates $I_{Ca(L)}$, I_{rel} (the ryanodine receptor, RyR), SERCA2a (SR Ca^{2+}-ATPase; SER in the figure), and phospholamban (PLB). PLB phosphorylation relieves inhibition of SERCA2a Ca^{2+} uptake. Autophosphorylation of CaMKII is also represented in the model, a property which enables detection of Ca^{2+} spike frequency. The model includes a calcium subspace where $I_{Ca(L)}$ and I_{rel} interact. It also includes $I_{to,2}$, an inward chloride current, and intracellular Cl^- regulation by the Na^+-dependent Cl^- co-transporter CT_{NaCl} and the K^+-Cl^- co-transporter CT_{KCl}. (Modified from Hund & Rudy, 2004, with permission.)

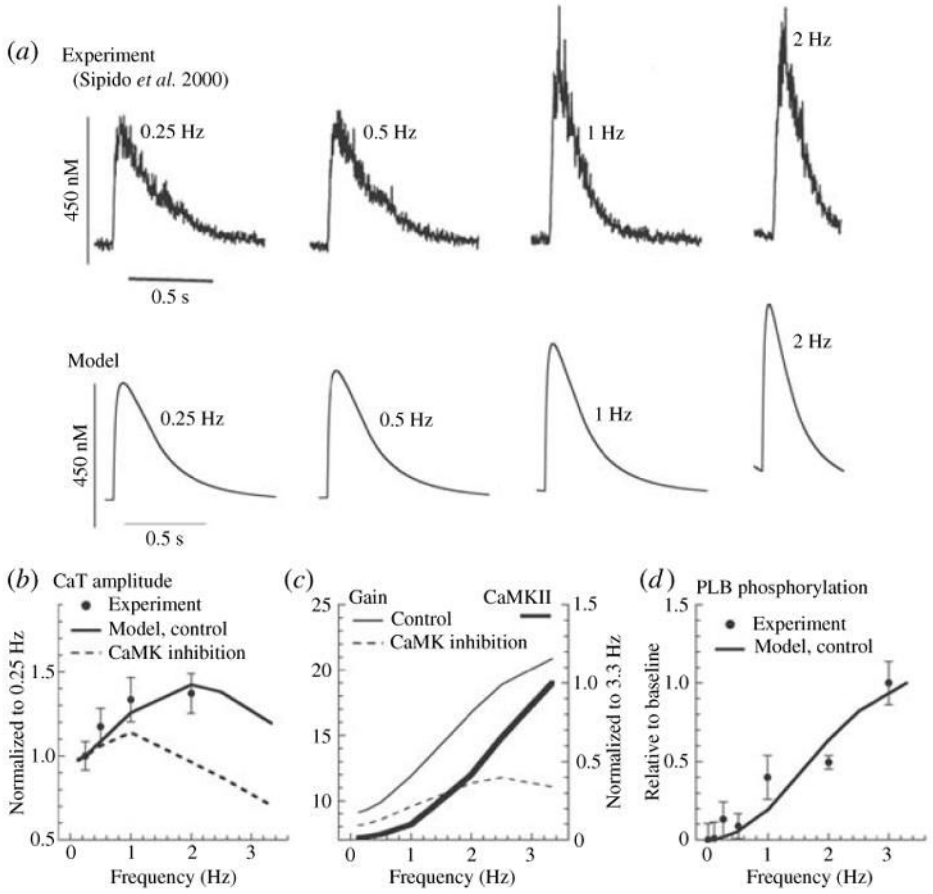

Fig 32.

CaMKII regulation of the Ca^{2+}-transient rate-dependence. (*a*) Simulated (bottom) and measured (top) steady-state Ca^{2+} transient (CaT) for 0.25, 0.5, 1, and 2 Hz pacing. (Experimental tracings are adapted from Sipido *et al*. 2000, with permission.) (*b*) CaT-frequency relation for experiment (circles), model under control conditions (line), and in presence of CaMKII inhibition (dashed line). (*c*) Minimal diastolic CaMKII activity (thick line, normalized to 3.3 Hz) and excitation-contraction coupling (ECC) gain. ECC gain=$\int_A F_{rel}dt/\int_A F_{Ca(L)}dt$, where F_{rel} and $F_{Ca(L)}$ are fluxes through RyR and $I_{Ca(L)}$, respectively, and the integration interval, *A*, is over one cycle. Gain is shown for control model (thin line) and in presence of CaMKII inhibition (dashed line). (*d*) PLB phosphorylation *vs*. pacing frequency compared with experimental data (Hagemann *et al*. 2000). (From Hund & Rudy, 2004, with permission.)

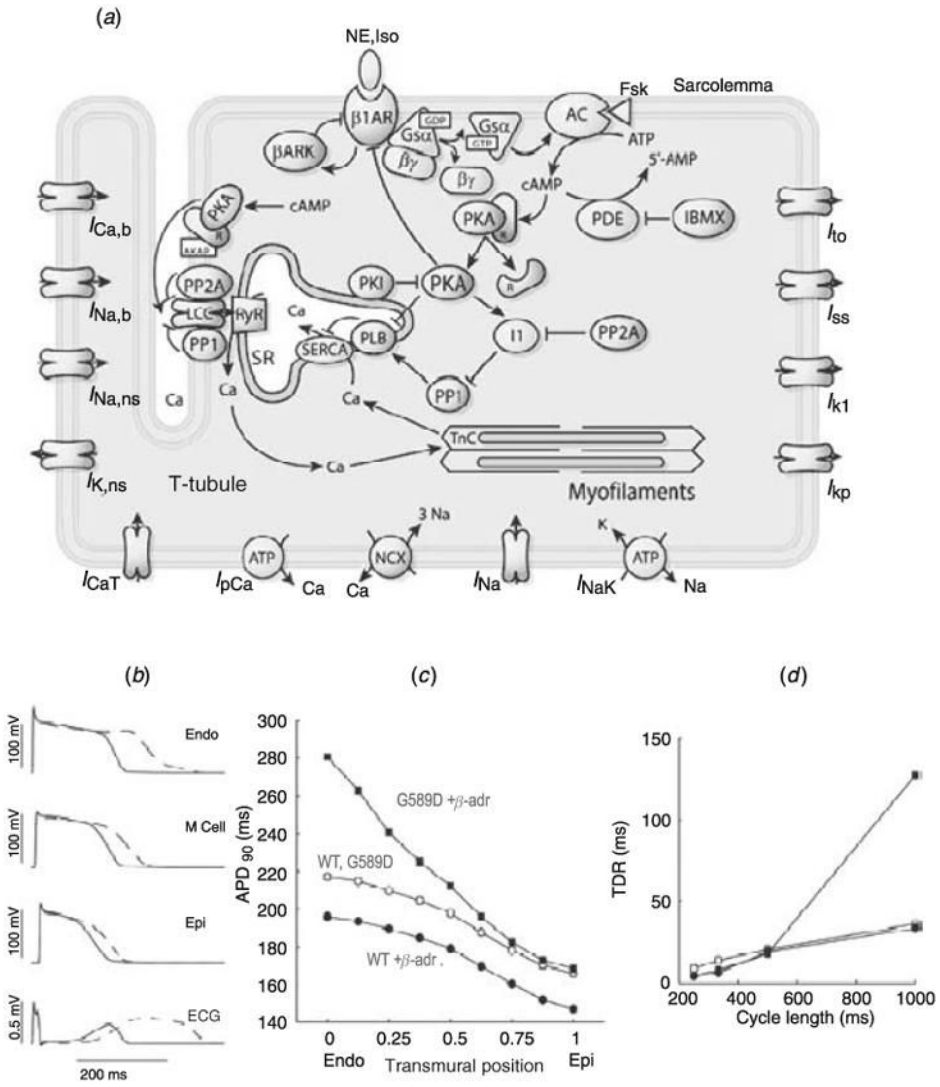

Fig 33.

(*a*) Schematic of the β-adrenergic network and signaling mechanisms in the model of Saucerman *et al*. (2003). Schematic of integrated model components, including the β_1-adrenergic network, calcium handling, and electrophysiology; β-adrenergic model is based on data from rat, while electrophysiology data are from rabbit. NE, norepinephrine; Iso, isoproterenol; β_1AR, β_1-adrenergic receptor; βARK, β-adrenergic receptor kinase; AC, adenylyl cyclase; Fsk, forskolin; PDE, phosphodiesterase; PKA, protein kinase A; PKI, heat-stable protein kinase inhibitor; PP1, protein phosphatase-1; PP2A, protein phosphatase-2A; I1, protein phosphatase inhibitor-1; PLB, phospholamban; LCC, L-type calcium channel; SERCA, sarcoplasmic reticulum Ca^{2+}-ATPase; RyR, ryanodine receptor. (Modified from Saucerman *et al*. 2003, with permission.) (*b*)–(*d*). Simulated effects of G589D mutation and β-adrenergic signaling on action potential in a transmural ventricular tissue model. (*b*) In presence of β-adrenergic stimulation, action potentials prolong in G589D mutants (dashed line) compared with WT (solid line) preferentially in endocardial cells, forming a broad T-wave and prolonged QT interval on the simulated ECG. (*c*) Transmural heterogeneity of APD_{90} in absence (empty markers) and presence of β-adrenergic stimulation (filled markers) for WT (circles) and G589D mutant (squares) tissue models. (*d*) Transmural dispersion of

repolarization (TDR) is particularly elevated in sympathetic-stimulated G589D mutant models (filled squares) at long cycle lengths. (Modified from Saucerman *et al*. 2004, with permission.)